A Reproduced Copy

OF

Reproduced for NASA

by the

NASA Scientific and Technical Information Facility

FOR EARLY DOMESTIC DISSEMINATION

Because of its significant early commercial potential, this information, which has been developed under a U.S. Government program, is being disseminated within the United States in advance of general publication. This information may be duplicated and used by the recipient with the express limitation that it not be published. Release of this information to other domestic parties by the recipient shall be made subject to these limitations. Foreign release may be made only with prior NASA approval and appropriate export licenses. This legend shall be marked on any reproduction of this information in whole or in part.

Date for general release June 1983.

FEDD Removed per NASA LaRC ltr dtd 7-15-83
3/J.G. Ross dtd 11-15-83

N81-77502 #

BOEING

(NASA-CR-165767) FLIGHT TEST EVALUATION OF DRAG EFFECTS ON SURFACE COATINGS ON THE NASA BOEING 737 ICV AIRPLANE An Early Domestic Dissemination Report (Boeing Commercial Airplane Co., Seattle) 150 p AVAIL: NASA [illegible] [illegible]

SBI-77502

[illegible]

FLIGHT TEST EVALUATION OF DRAG EFFECTS OF SURFACE COATINGS ON THE NASA BOEING 737 TCV AIRPLANE

D6-37256

CONTRACT NAS1-15325
TASK ASSIGNMENT 06

JUNE 1981

Prepared by: Dezso George-Falvy
Dezso George-Falvy

Danny A. Sikavi
Danny A. Sikavi

Approved by:
A. L. Nagel
R. L. Kreitinger
L. B. Gratzer
P. O. Saelid
M. E. Kirchner
G. W. Hanks

FOREWORD

The flight tests described herein were conducted under the Energy Efficient Transport (EET) program, Contract NAS1-15325. Mr. D. B. Middleton of the EET Project Office at Langley Research Center was the technical monitor. The Terminal Configured Vehicle (TCV) Program Office coordinated the experiment and provided the test aircraft. Principal participants were:

R. L. Kreitinger	Project Manager
J. R. Hall (NASA-TCVPO)	Experiment Manager
D. George-Falvy	Principal Investigator
H. R. Gelbach	Instrumentation
L. R. Elvigan	Coating Applications
D. A. Sikavi	Data Analysis
J. Weber	Data Processing
R. M. Winebarger (NASA-FLTMD)	Flight Operations
W. F. White (NASA-TCVPO)	Instrumentation
J. A. Boeck (NASA-TCVPO)	Instrumentation
P. Baldasare (NASA-TCVPO)	Data Processing
I. M. Stewart (NASA-FLTMD)	Airplane Modification

NOTE:

Certain commercial materials are identified in this paper in order to specify adequately which materials were investigated in the research effort. In no case does such identification imply recommendation or endorsement of the product by NASA or Boeing, nor does it imply that the materials are necessarily the only ones or the best ones available for the purpose.

CONTENTS

FIGURES

1.0 SUMMARY

A flight test program was conducted in which the effects of various surface coatings on aerodynamic drag were investigated; results of this program are described in this report. The tests were conducted at NASA-Langley Research Center on the terminal configured vehicle (TCV) Boeing 737 research airplane. The Boeing Company, as contractor with NASA under the Energy Efficient Transport (EET) program (Contract NAS1-15325), planned and evaluated the experiment. The NASA-TCV Program Office coordinated the experiment and performed the flight tests.

The principal objective of the test was to evaluate the drag reduction potential of an elastomeric polyurethane surface coating, CAAPCO B-274, which also has been considered for application on transport airplanes to protect leading edges from erosion. The smooth surface achievable with this type of coating held some promise of reducing the skin friction drag as compared to conventional production type aircraft surfaces, which are usually anodized bare metal or coated with corrosion protective paint. Requirements for high-precision measurements were the principal considerations in the experiment.

Figure 1 shows the test plan summary. The drag increments between various surface coatings were evaluated from boundary layer measurements made at the downstream end of a 2m (80 in) wide test surface on the inboard portion of the wing. Measurements were taken simultaneously on both the left and right wing panels. The various surface coatings were applied to the left wing test section in a series of test flights, while the right wing test section remained bare metal, stripped of paint, to provide a constant basis of comparison.

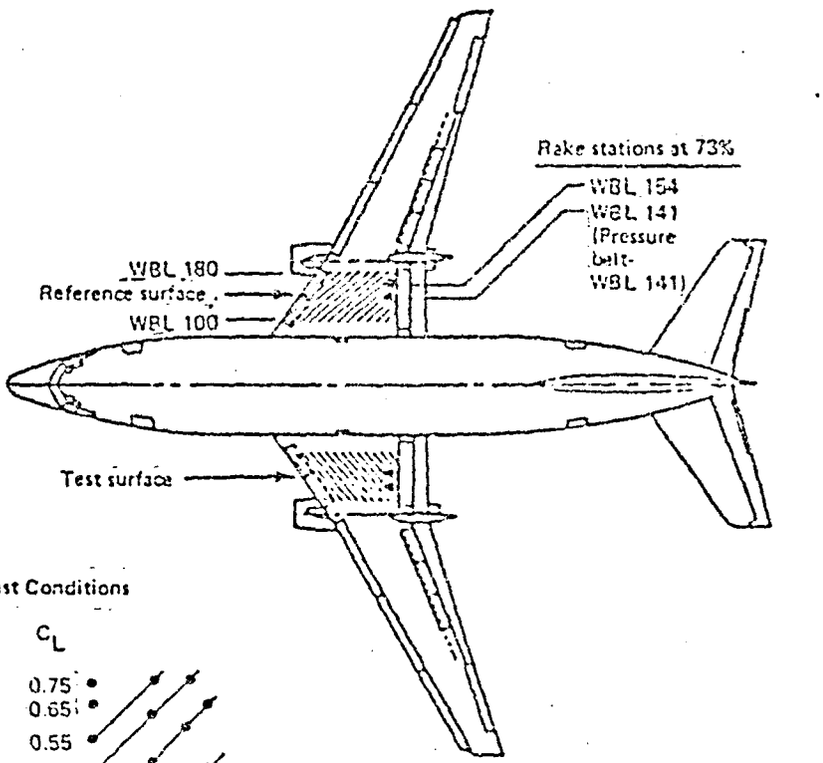

Test Conditions

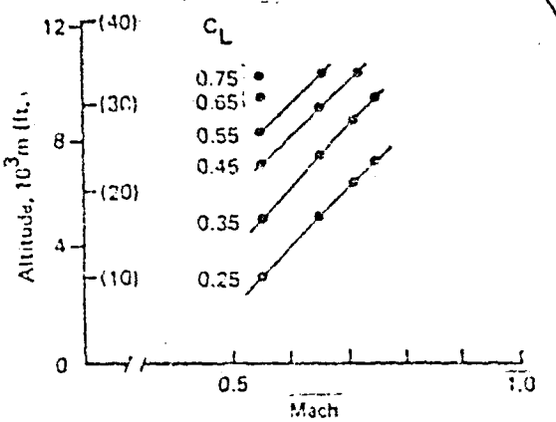

- Instrumentation
  - Four 25-probe rakes
  - Two 18-port static pressure belts

Schedule and Configuration

Flight		Test surfaces		Data source
No.	Date	Left wing	Right wing	
1	12-11-80	Existing paint	Bare metal	Boundary layer rakes
2	1-20-81	Bare	Bare metal	Pressure belts
3a	1-23-81	Bare—leading-edge grit	Bare metal	Boundary layer rakes
3	1-23-81	Bare	Bare metal	Boundary layer rakes
4	1-27-81	Corogard	Bare metal	Boundary layer rakes
5	2-03-81	CAAPCO	Bare metal	Boundary layer rakes

Figure 1. Test Plan Summary

The boundary layer measurements were made by fixed pitot rakes (two on each side) located near the midspan of the test area. Pressure distributions along the test section were also measured during a separate flight using a belt of plastic tubing (Strip-a-tube).

The test program consisted of five flights in the sequence indicated in figure 1. During the first flight, the existing enamel paint (which was not factory applied and somewhat weathered) was retained on the left wing test section; the right wing test section was stripped of paint to the bare metal. During the second and third flights, static pressure and boundary layer surveys were made, respectively, to obtain baseline measurements of bare metal surfaces on both sides of the airplane. During the fourth flight, the left wing test surface was coated with Corogard, which is used on production airplanes over the inspar area for corrosion protection. The CAAPCO B-274 coating was tested during the fifth flight. A supplementary experiment was performed during flight 3, in which a strip of metallic grit was applied to the leading-edge region to simulate a badly eroded leading edge.

Each test flight included 15 test conditions selected to provide systematic variations of Mach number and lift coefficient covering the cruise regime of the test airplane. During each condition, at least two sets of boundary layer profiles were recorded.

The principal results of the test are summarized in figure 2. The percentage section profile drag increments (or decrements) due to the various surface configurations, relative to the bare metal reference surface, are shown as a function of the unit Reynolds number, which is the dominant variable according to classical roughness drag correlations.

In Section 5.3 of this document, figures 37 and 38 show the projected drag increments (or decrements) for each surface configuration expressed in terms of section profile drag and airplane total drag.

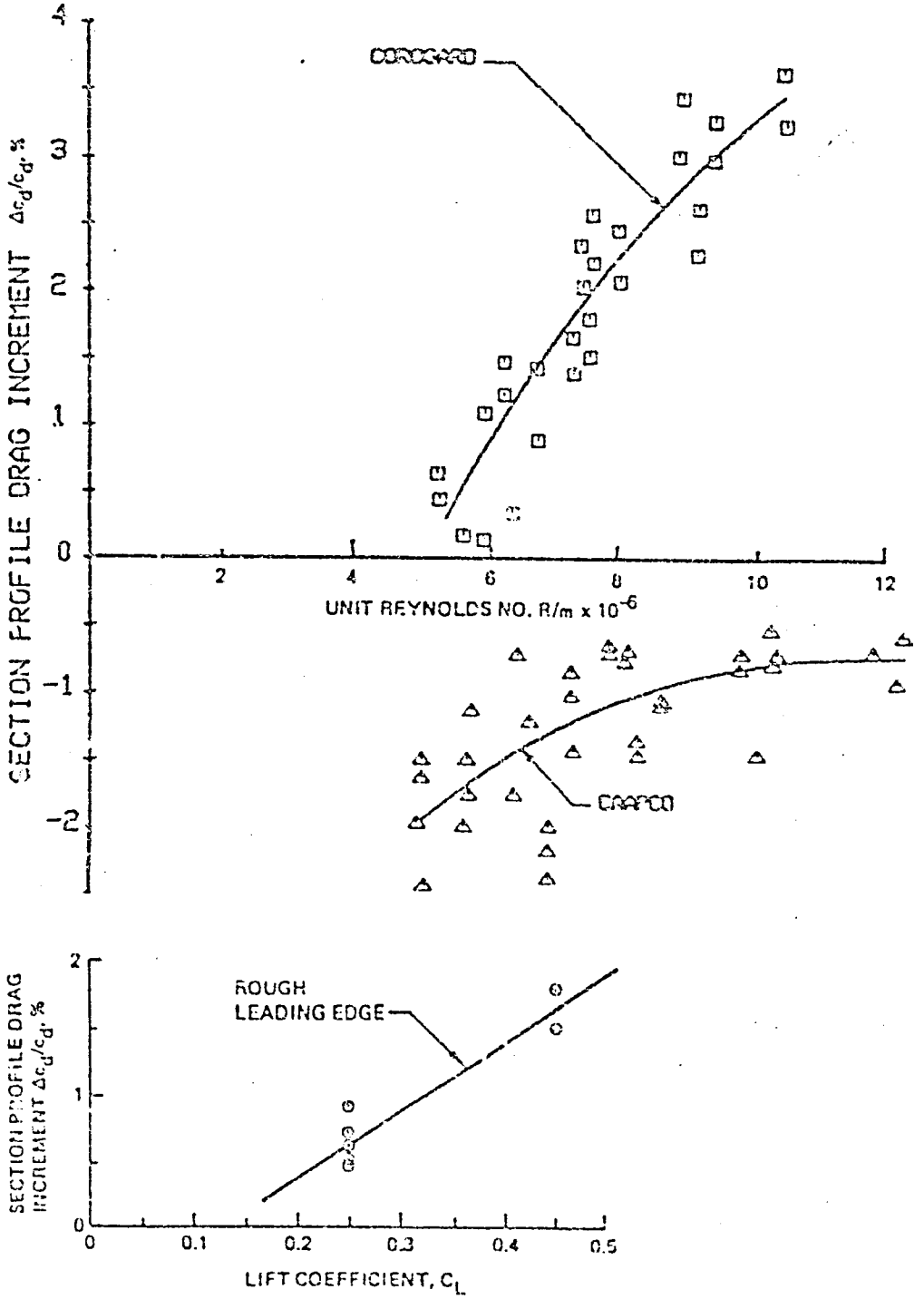

Figure 2. Summary of Principal Test Results

CAAPCO Coating--This coating showed a 0.75% to 2.0% reduction in section profile drag relative to the bare surface. The drag decrement was consistent throughout the entire range of the test and was somewhat larger at low Reynolds numbers; i.e., higher airplane lift coefficients (C_L). At typical cruise conditions, i.e., at a unit Reynolds number of R_1 = 6.5 million/m (2 million/ft), the section profile drag decrement was about 1.4% (mean value of the data band).

Corogard Surface--This surface showed a clear trend of increasing drag with increasing unit Reynolds number (R_1), varying from essentially zero at the low end of the Reynolds number range of the test (high altitudes) to about 3.5% at the high end (low altitudes). At typical cruise conditions, i.e., R_1 = 6.5 million/m (2 million/ft), the increment in section profile drag was about 1.2%.

The average roughness of the Corogard paint tested was characterized by a profilometer gage reading of $r_a \cong 160$ μin, a value somewhat higher than the average roughness of Corogard paint on Boeing production airplanes.

Roughened Leading Edge--This caused a small but clearly measurable drag increment relative to the bare surface, ranging from 0.5% to 1.6% of the section profile drag.

Existing Paint--The existing paint appeared to have slightly higher drag than the bare surface. The increments, however, are of the same magnitude as the experimental data scatter.

To accurately determine total airplane drag increments, similar measurements should be made at other spanwise locations. However, if it is assumed that the same local section drag increments apply at all spanwise stations and that for Corogard, which behaves as a distributed roughness, the increments are proportional to the coated area, then the following airplane drag increments are obtained for typical cruise conditions:

CAAPCO	0.2% decrease
Corogard	0.2% increase
Rough L.E.	0.3% increase

Based on these test results, it is concluded that the CAAPCO coating offers some small drag benefits, particularly in comparison with the Corogard coated surface tested. However, before CAAPCO (or any similar coating such as Chemglaze or Astrocoat) could be considered for application to the inspar area on production airplanes, it would have to be shown, through laboratory tests and service evaluation, that the coating provides corrosion protection equivalent to that of Corogard paint. Initial laboratory tests for corrosion protection are in progress under the EET program.

2.0 INTRODUCTION

Tests by Beasley and McGhee (ref. 1), on a wing section covered with a smooth film to reduce profile drag, were reported in 1977. It was found that at high Reynolds numbers the specially prepared surface showed a reduction in section profile drag of about 12%. This stimulated an industry interest to determine if some of this improvement could be realized from coatings or films applied to commercial transport wings.

An investigation (ref. 2) under Contract NAS1-14742 eliminated films from consideration because of difficulties in applying them to large surfaces with compound curvature and/or movable control surfaces. The investigation, however, identified certain types of elastomeric polyurethanes as having such desirable characteristics as smooth surface; durability, especially in areas of high erosion; and feasibility to apply and maintain. Three commercially available products--CAAPCO B-274, Chemglaze M313, and Astrocoat--were cited as potential candidates for application. The investigation described in reference 2 included a cost/benefit analysis for various configurations of these three coatings applied to a medium-range transport aircraft. It showed that a small reduction in airplane drag due to the coatings would offset the cost of coating application and maintenance. It was essential, therefore, that reliable experimental data be obtained on the effect of surface coatings on aerodynamic drag before recommendations could be made as to the application of such coatings on commercial transport airplanes for fuel savings. Subsequently, an experimental program was initiated under the current NASA-EET program (Contract NAS1-15325) to investigate the potentials for drag reduction due to surface coatings. Only CAAPCO was evaluated in this experiment. The surface smoothness of the other two materials is very similar to that of CAAPCO, and it is believed that testing all three of the materials would not have contributed significantly to the results.

It was believed that the effects of surface coatings on wing section drag could be evaluated with sufficient accuracy from boundary layer measurements made on a representative airplane surface. Because the differences in skin friction drag between various surface configurations would be very small, the proposed experiment had to be conducted with extreme care and high precision. Extrapolation to total airplane drag increments would be approximate because of varying geometry and aerodynamic conditions along the span.

Plans for the test program were formulated under NASA Contract NAS1-15325-06 and are described in detail in references 3 and 4. The NASA TCV (Boeing 737) research aircraft met the cost, performance, and availability requirements and was selected as the test vehicle. The NASA-Langley TCV Program Office participated in the planning and coordination of the experiment. The formal agreement for the test was concluded in July 1980, and assembly of the experimental hardware was begun shortly thereafter. The flight test program started in December 1980 and was concluded in early February 1981.

This report contains the test results, a summary description of the test apparatus and measurement techniques (also documented in ref. 4), and the analysis method. Section 4.0 cortains a description of the test, including the experimental layou., surface configurations tested, instrumentation, test procedure, and test analysis. The test results grouped according to the various surface configurations tested are in Section 5.0. Results and conclusions are summarized in Section 6.0.

3.0 ABBREVIATIONS AND SYMBOLS

3.1 GENERAL ABBREVIATIONS

A_{exp}	exposed wing planform area
b	wing span
c	chord length
c_d	section drag coefficient
C_D	airplane drag coefficient
C_L	airplane lift coefficient
c_p	local pressure coefficient
EET	Energy Efficient Transport
GW	gross weight
h_p	pressure altitude
H	boundary layer shape parameter, δ^*/Θ
I.D.	inside diameter
L.E.	leading edge
m	magnification factor
M	Mach number
O.D.	outside diameter
P_o	sea level static pressure in standard atmosphere
P_T	total pressure
P_S	static pressure
q	dynamic pressure
q_c	impact pressure, total pressure minus static pressure

r_a	measure of surface roughness (profilometer gage reading)
R	Reynolds number
R_1	Unit Reynolds number, U_∞/ν
S_{REF}	reference wing area
TCV	Terminal Configured Vehicle
T_T	total temperature
u	local velocity within the boundary layer
U_e	local velocity at the outer edge of the boundary layer
U	freestream velocity
V	airspeed
w_b	body width
W	airplane gross weight
W_F	remaining fuel weight
WBL	wing buttock line
x	streamwise coordinate
y	distance from the surface (rake probe location)
z	spanwise coordinate

3.2 SUBSCRIPTS

c	chord
e	conditions at edge of boundary layer
I	indicated (airspeed)
m	measurement location
T	true (airspeed)
w	conditions at the wall
y	height above the surface
∞	freestream conditions

3.3 SYMBOLS

α	airplane angle of attack
β	airplane yaw angle
γ	airplane pitch angle
δ	atmospheric pressure ratio, P/P_0, or boundary layer thickness
δ^*	boundary layer displacement thickness
Θ	boundary layer momentum thickness
ρ	density of air
ν	kinematic viscosity of air
τ	wall shear stress

4.0 TEST DESCRIPTION

This section contains a description of the test setup, the surface configurations tested, the instrumentation, the test procedure, the philosophy of test analysis, and the data processing.

4.1 TEST AIRPLANE AND EXPERIMENTAL LAYOUT

The principal requirements for a suitable test vehicle were (1) the capability of achieving flight conditions; i.e., speed, altitude, Mach numbers, and Reynolds numbers typical of today's jet transport airplanes; (2) external surface characteristics representative of transport airplanes; (3) proper instruments for high-precision data recording; and (4) availability for a series of tests that could take at least a month. The NASA TCV (Boeing 737) research aircraft (fig. 3) met these requirements and thus was a suitable choice for these experiments.

Figure 4 shows overall layout of the experiment depicting the location of the test surface on the airplane and the principal instrumentation used. The various surface coatings were applied to a 2.03m (80 in) wide strip on the inboard left wing, extending from the 18% span station (wing buttock line [WBL] 100) to the 32% span station (WBL 180), and terminating at the hinge line of the inboard spoiler. The same area of the right wing panel was stripped of paint to the bare metal surface and was retained in that condition throughout the test to provide a constant baseline reference surface. Evaluation of the various surface coatings was made principally by a side-to-side comparison from measurements taken simultaneously on the test surface and the reference surface. This arrangement ensured that comparison of the two surfaces was made at exactly the same flight conditions. To further validate the evaluation, the left side test surface was also tested in the "bare" condition. The test arrangement also permitted flight-to-flight comparisons between the various surface configurations. However, these comparisons cannot be considered as straightforward as the side-to-side comparisons because flight conditions, particularly the Reynolds number, cannot be duplicated exactly on different flights.

Figure 3. Test Airplane: NASA TCV B-737 Research Aircraft

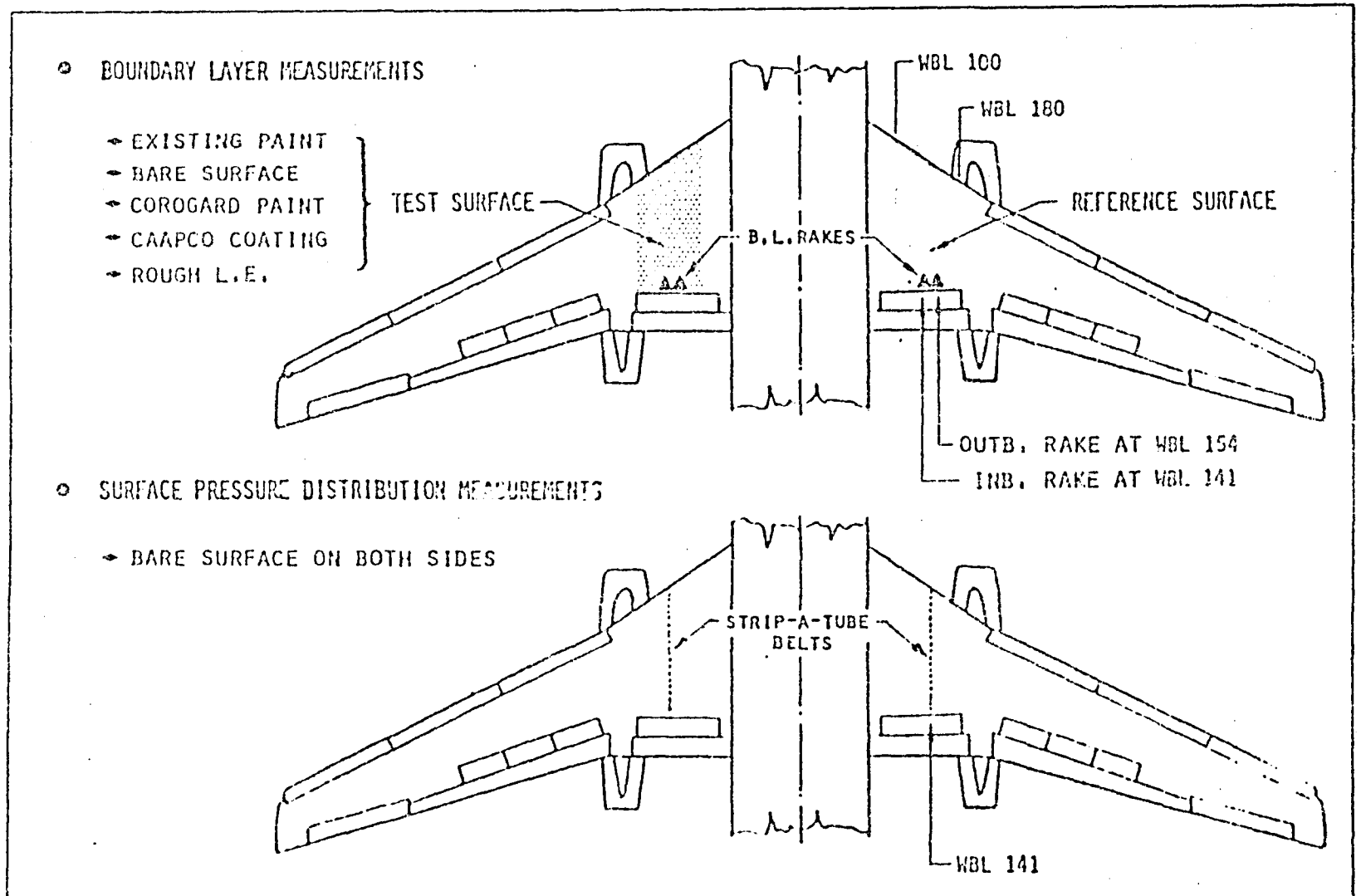

Figure 4. Experiment Layout

The principal instrumentation in this experiment consisted of a pair of boundary layer rakes mounted on the wing near the downstream edge of the test surface (73% of the local wing chord). Two rakes were used on each side--one at WBL 141 (25% semispan) and the other at WBL 154 (28% semispan). The rake at WBL 141 was the primary data source, while the second rake provided backup data.

Chordwise pressure distributions along the main test section (WBL 141) were measured during flight 2, using a strip of multitube plastic belts (Strip-a-tube) bonded to the wing surface. These measurements provided an experimental data base for the calculation of boundary layer growth along the test surface.

4.2 SURFACE CONFIGURATIONS TESTED

Boundary layer measurements were made on five surface configurations: the painted surface, which existed prior to the test; the bare surface; the bare surface with rough leading edge; Corogard paint; and CAAPCO coating.

Existing Paint--The existing paint on the test airplane was a nonstandard enamel coating, applied by a NASA contractor, and was several years old. At certain locations, particularly on the lower surface, it was in a somewhat deteriorated condition. Although there were no major discrepancies on the upper surface test section, there were numerous small lumps and specks. In general, the surface condition was typical of a medium-time airplane in airline service.

Bare Metal Surface--This surface was very smooth on a microscopic scale (readings of the profilometer gage indicated a surface roughness index of $r_a \lesssim 30$ μin). However, numerous rows of rivets run across the test surface (fig. 5a), and individual rivet heads protruding from the surface up to about 0.1 mm (0.004 in) were not uncommon. In addition, spanwise skin butt joints across the test section had small gaps 1 to 3 mm (0.04 to 0.12 in) wide, with aerodynamic putty in the larger ones. There were occasional mismatches of up to 0.25 mm (0.01 in). Because the size of these minute surface imperfections is comparable to the thickness of the viscous sublayer, it can be expected that they produced some incremental drag above the profile drag of the perfectly smooth wing. This, in essence, means that the bare surface, chosen for this experiment as a baseline configuration, should not be assumed to be an ideal, hydraulically smooth surface, but one that has a certain level of discrete roughness elements.

Roughened Leading Edge--The roughened leading edge (fig. 5b) was included among the test configurations as an additional item to obtain data on the effects of an eroded leading edge on drag. The simulation of an eroded leading edge was accomplished by applying metallic grit to the leading edge on the left wing test surface (which otherwise was bare). The roughened strip was about 76 mm (3 in) wide. The grit size was No. 50, 0.33 mm (0.013 in), with a nominal density of about 15 particles/cm^2 (100 particles/in^2). The grit was removed by washing the surface with a solvent after measurements were taken.

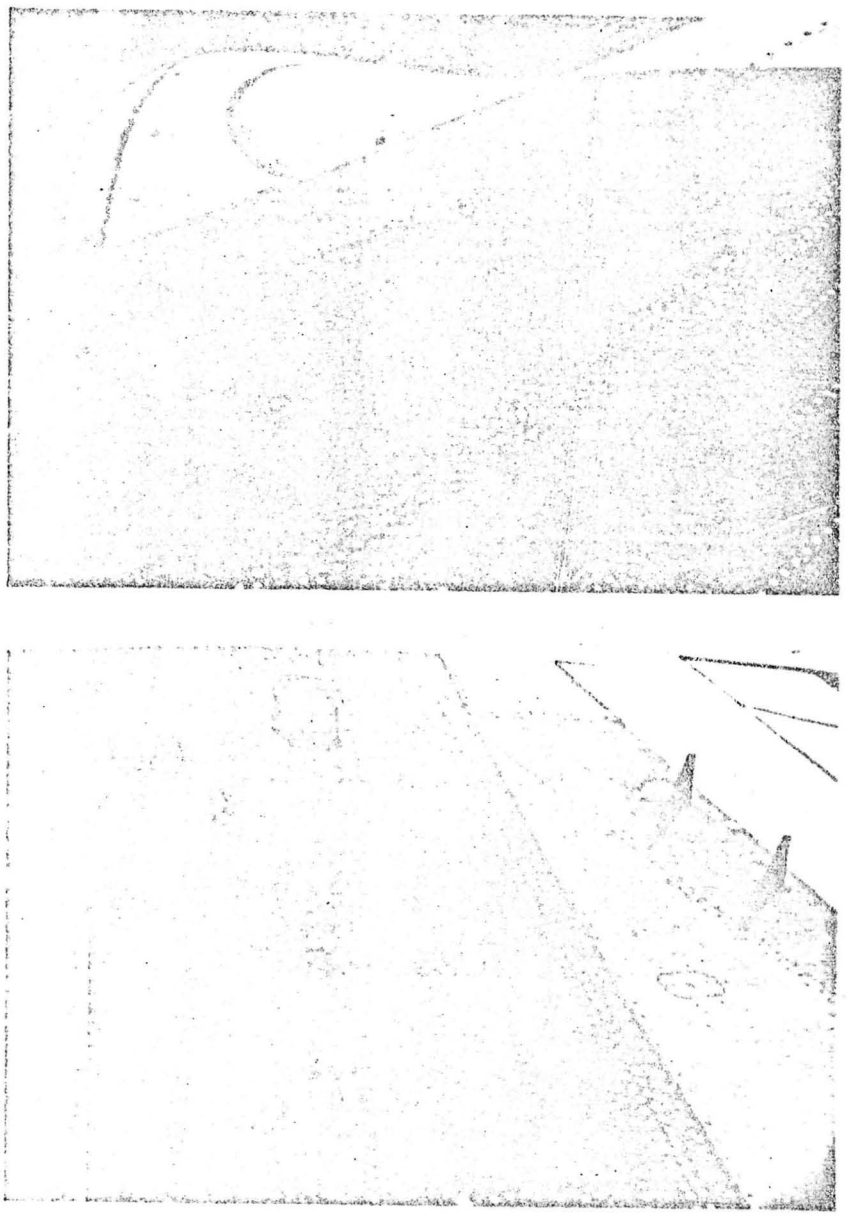

(a) Bare Metal Surface

Figure 5. Test Surfaces

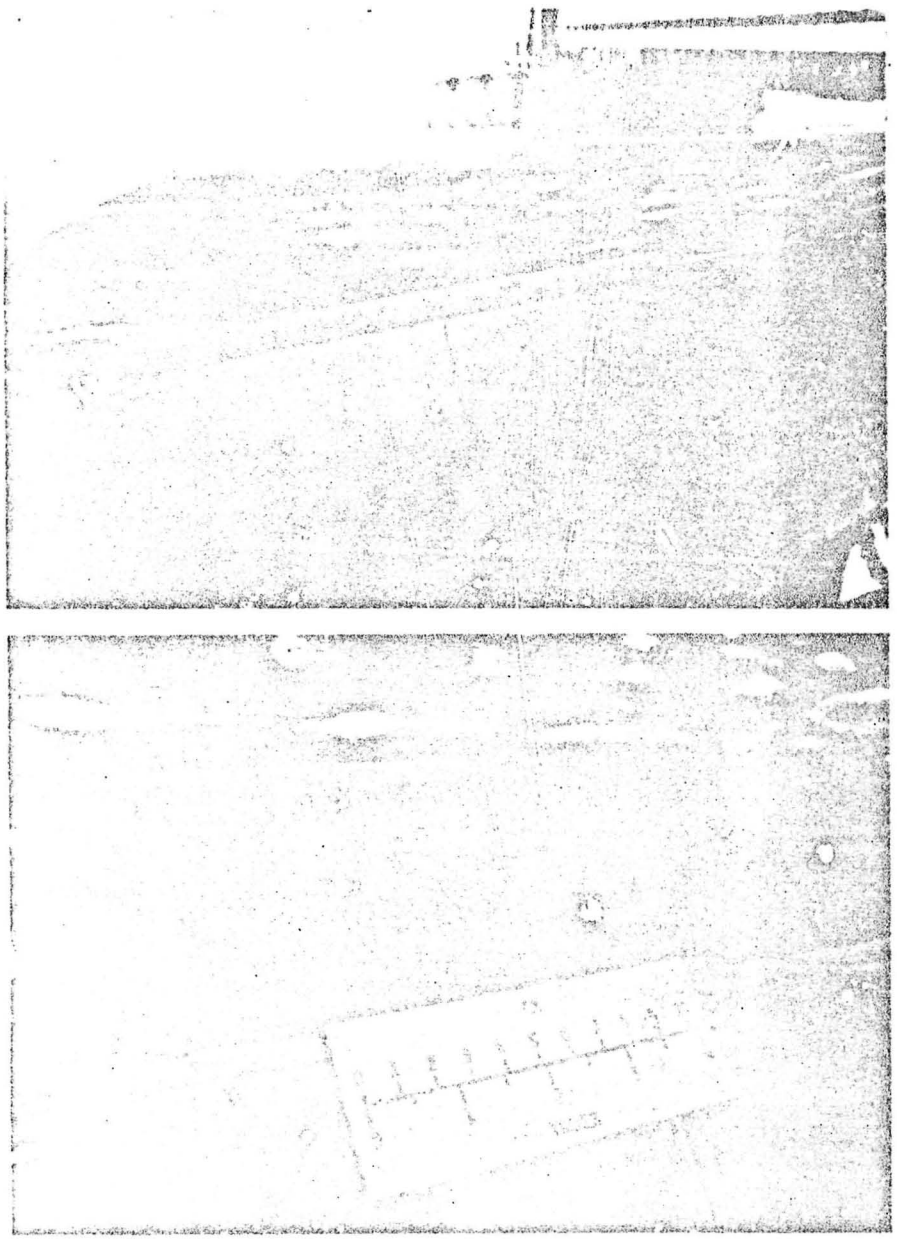

(b) Roughened Leading Edge

Figure 5. Test Surfaces (Continued)

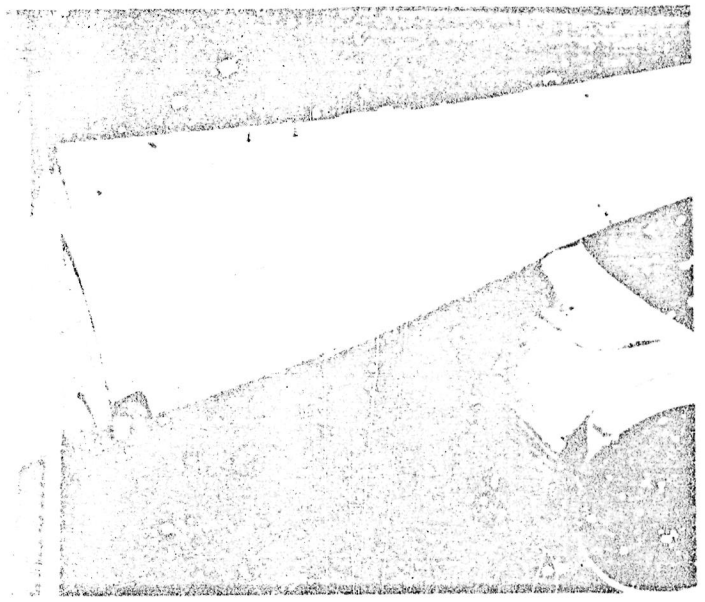

(c) Corogard Coated Surface

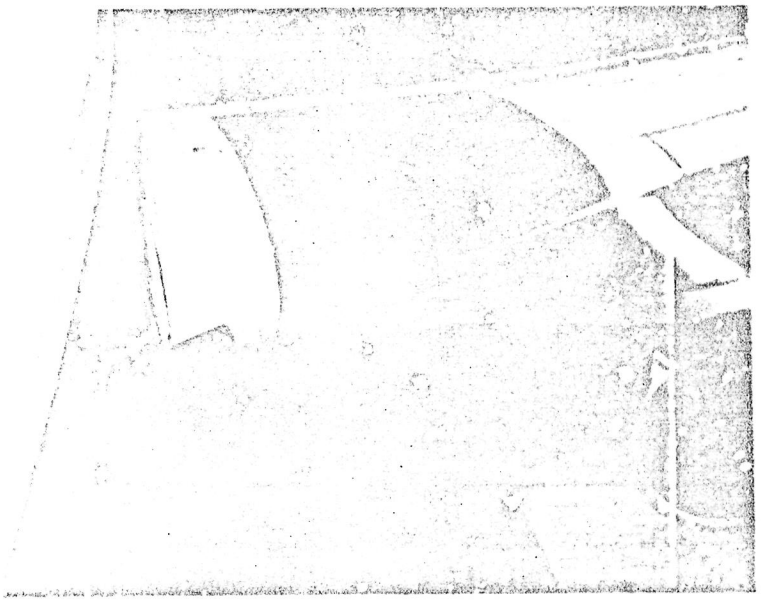

(d) CAAPCO B 274 Coated Surface

Figure 5. Test Surfaces (Concluded)

Corogard Paint--To obtain an additional reference to which the CAAPCO B-274 elastomeric polyurethane surface coating could be compared, Corogard was included in the test surfaces (fig. 5c). Corogard paint is widely used on large transport airplanes for its excellent corrosion protection characteristics; however, the surfaces painted with Corogard have a certain level of roughness that varies with application techniques and thus is, to some extent, controllable.

In this experiment, the intent was to test a Corogard-coated surface representative of the average roughness found on production airplanes. Usually the roughness is measured by a profilometer gage (Surtronic III), which follows the contour of the surface with a miniature stylus moved along a certain preset distance. Surveys of Corogard roughness on Boeing production airplanes indicated that a profilometer gage reading of about $r_a = 150 \pm 30$ μin is typical of the sampled cases. Duplication of this roughness level was intended for the present experiment; however, the coating ultimately was slightly rougher than desired, registering a mean value of about $r_a \approx 160$ μin on the profilometer gage.

Note that Corogard started at the front spar joint and continued back to the spoiler hinge line; i.e., past the boundary layer rakes. In a production airplane, the Corogard coating usually extends between the front and rear spar, but on the test airplane Corogard was extended further aft to avoid a change in surface conditions just ahead of the flow-measuring instrumentation.

CAAPCO Coating--This coating, the principal subject of this investigation, was applied in several layers following the procedure described in reference 2. Unlike the Corogard coating, the CAAPCO coating started at the leading edge (fig. 5d). Along the forward region of the wing (ahead of the front spar), five successive layers of CAAPCO B-274 were applied, resulting in an approximately 0.305 mm (12 mil) thick coating. Aft of the front spar, where erosion protection is not critical, a three-layer coating of approximately 0.127 mm (5 mil) thickness was applied. The resulting surface was fairly smooth, and to some extent the coating faired nonflush rivet heads and skin joints. The coating was applied under a protective enclosure that had a forced ventilation system. During coating application, the enclosure was opened and additional fans added to improve ventilation. This caused some dust and lint particles to be deposited on the wet surface during the curing period. It is believed that higher surface quality could be achieved under properly controlled application conditions.

The CAAPCO-coated test surface showed an average roughness level of about $'_a \approx$ 10 to 15 μin on the profilometer gage. Because of the resilient nature of the coating, the validity of this measurement is not certain.

A comparison of the average roughness of the three test surfaces, as measured by the profilometer, is:

- Bare metal 30 μin
- Corogard 160 μin
- CAAPCO 10 to 15 μin

4.3 INSTRUMENTATION

The instrumentation system consisted of four principal elements: (1) pressure sensors, including boundary layer rakes and static pressure survey belts; (2) scan/control module; (3) reference pressure/temperature transducers; and (4) onboard recording equipment of the test airplane.

Boundary Layer Rakes--The boundary layer rakes were the principal data sensors. Four rakes were used, two on each wing, as shown in figure 4. The general arrangement and principal dimensions of the rakes are shown in figure 6a, and a closeup photograph is presented in figure 6b. Each rake has 24 total pressure probes located at staggered heights up to 127 mm (5.0 in) above the base and one static pressure probe at the height of 38 mm (1.5 in) being displaced to the side by 38 mm (1.5 in). The total pressure probes are made of stainless steel tubing of about 1 mm (0.04 in) outside diameter with chamfered circular orifices. The static probe has a diameter of 2.36 mm (0.093 in) and a half-ellipsoid forebody. The installation of the rakes on the test airplane is shown in figure 6b and 6c.

Static Pressure Survey Belts--These belts served as supplementary data sensors used during only one flight. One belt was installed on each wing panel at the 25% semispan location (WBL 141) extending from the leading edge to the location of the inboard boundary layer rake (x/c = 73%). The belt was constructed, as shown in figure 7a, using two strips of 10-conduit plastic tubing (Strip-a-tube). Holes punched into the tubes at selected chordwise locations formed the static pressure sensors. Because the two outermost channels of the belts were not used, static pressures were measured at 18 locations along the test surface. Figure 7b shows photographs of the belt installation. Pressures from the boundary layer rakes and static pressure survey belts were transmitted by a bundle of Strip-a-tube conduits that ran through the flap cavity and led to the scan-control module installed in the cabin.

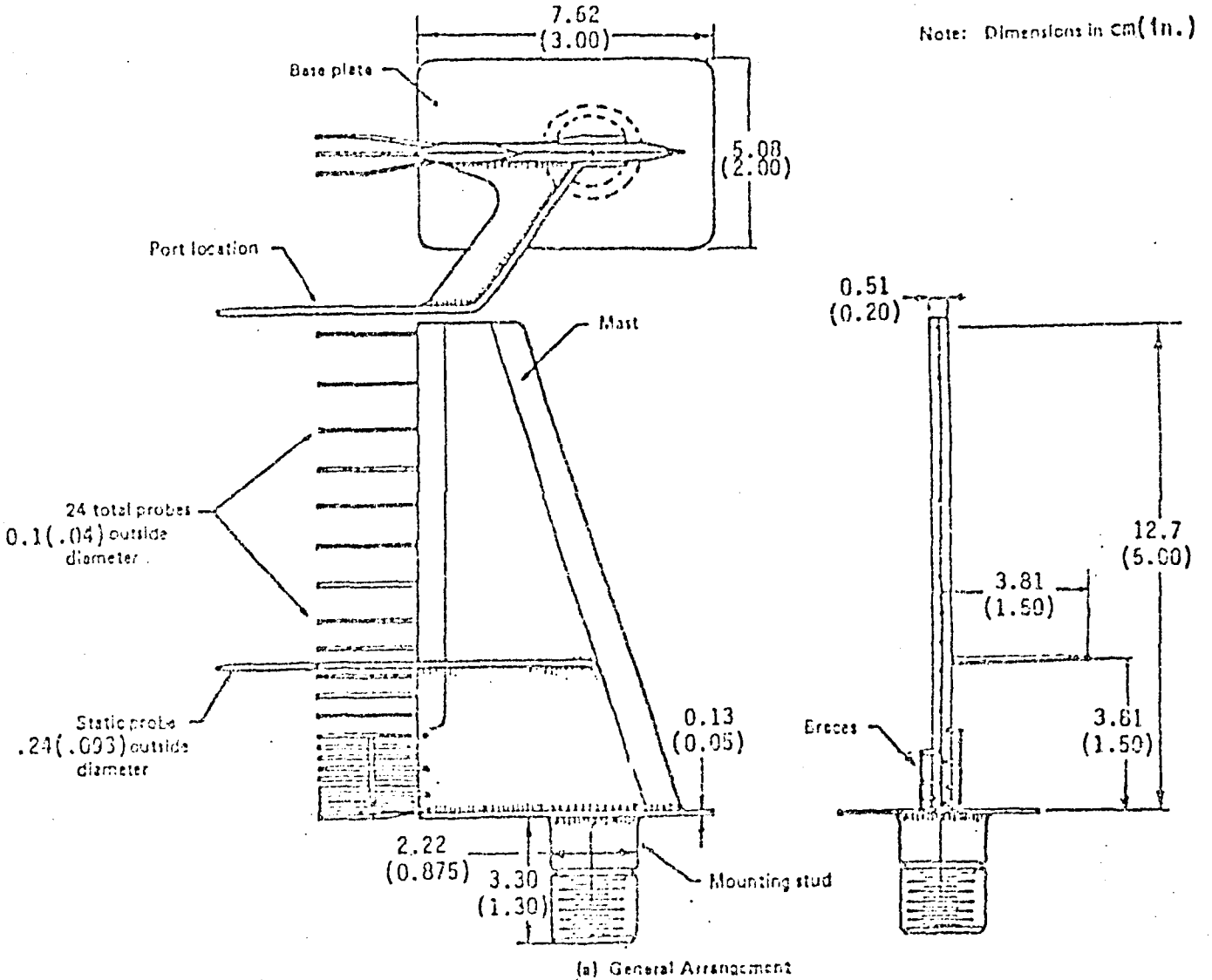

Figure 6. Boundary Layer Rakes

(b) Closeup of Rake

Figure 6. Boundary Layer Rakes (Continued)

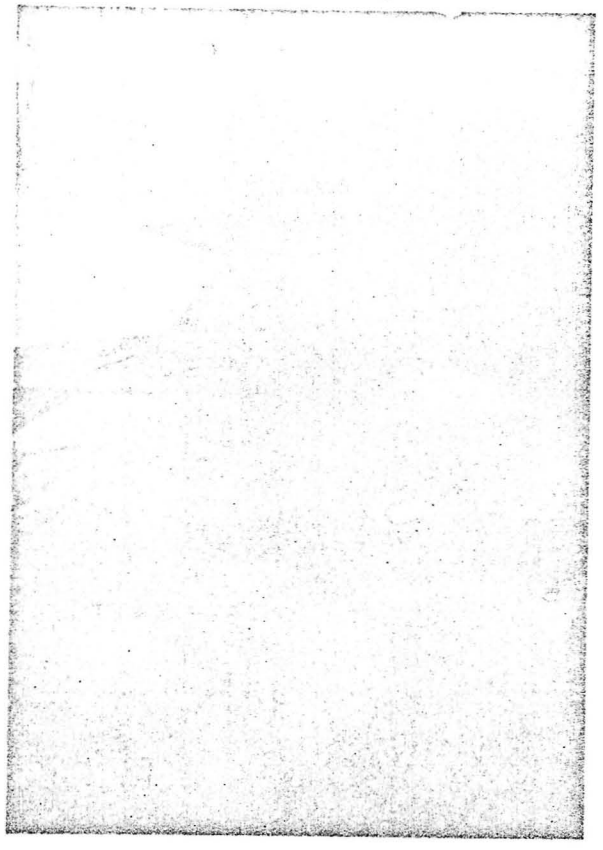

● Left wing

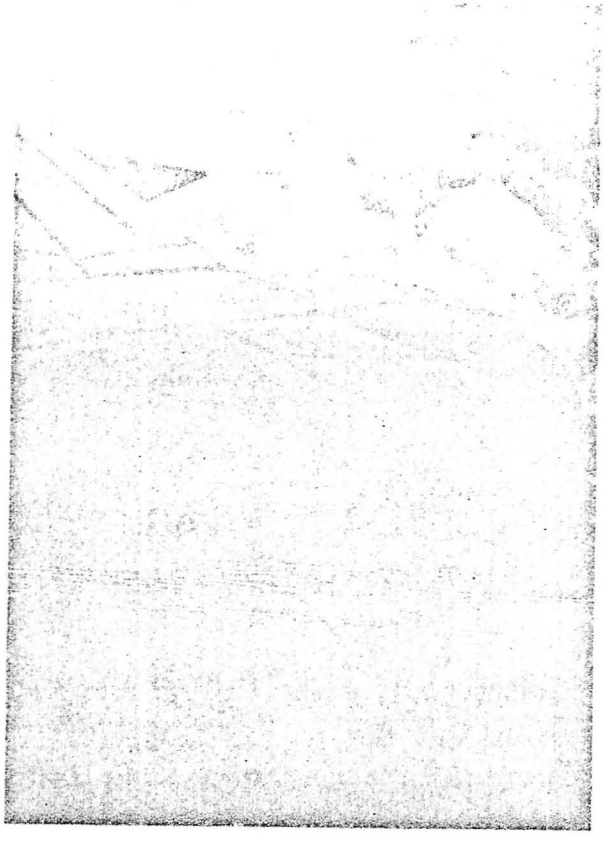

● Right wing

(c) Boundary Layer Rake Installations

Figure 6. Boundary Layer Rakes (Concluded)

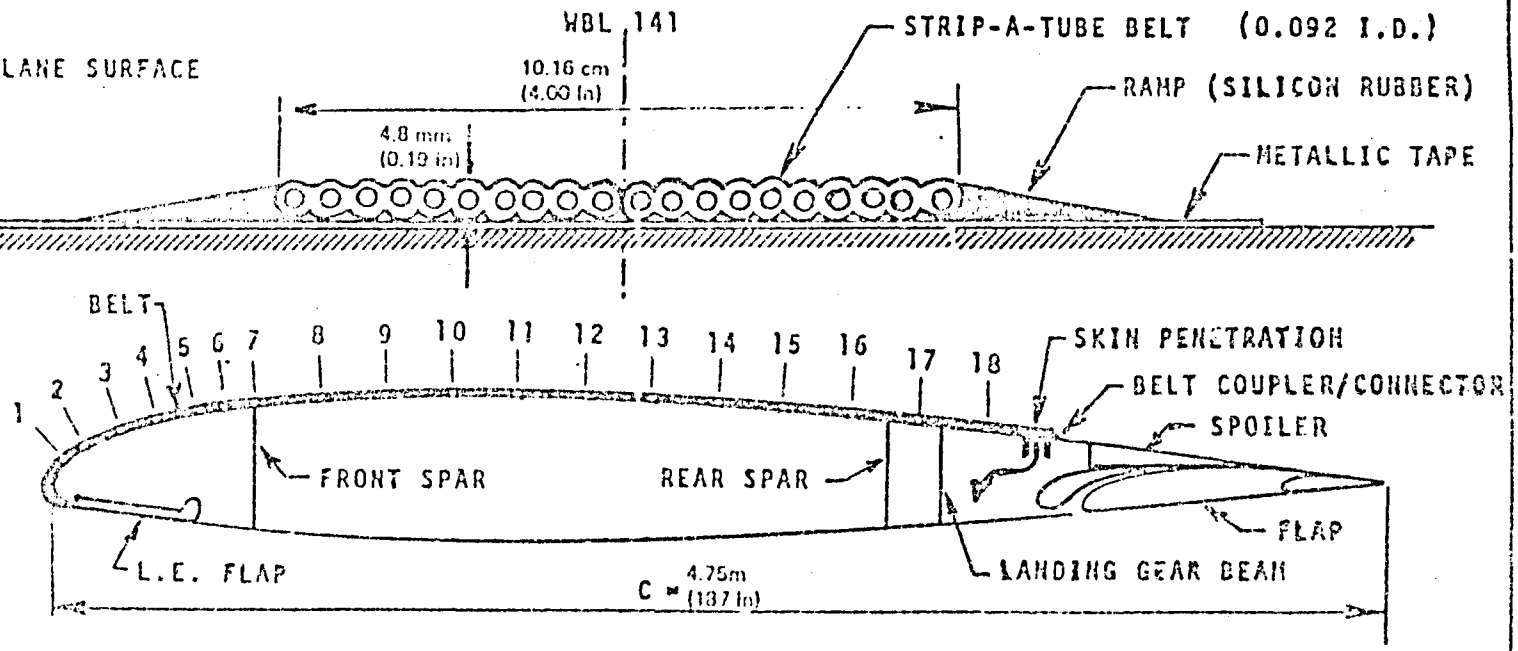

ORIFICE #	1	2	3	4	5	6	7	8	9	10	11	12	13	14	15	16	17	18
X/C X	1.5	2.5	5	7.5	10	12.5	15	20	25	30	35	40	45	50	55	60	65	70

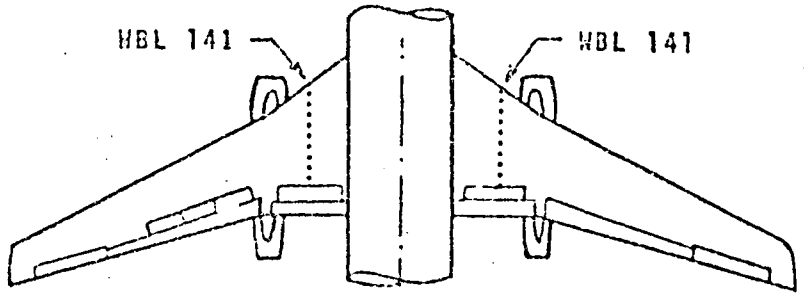

(e) Belt Installation Details

Figure 7. Static Pressure Survey Belts

0000076-33

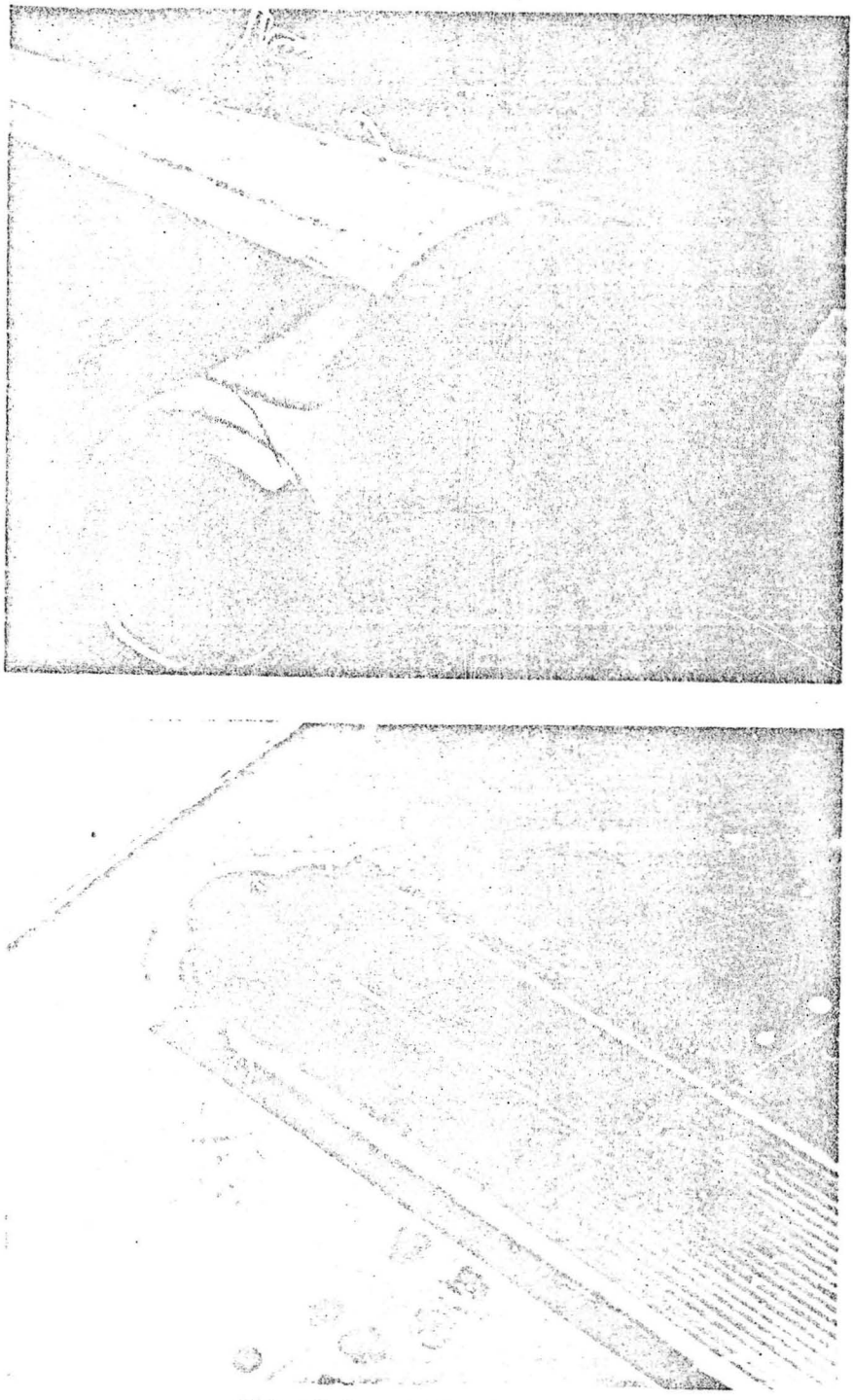

(b) Installation on Right Wing

Figure 7. Static Pressure Survey Belts (Concluded)

The Scan-Control Module--The scan-control module was the link between the pressure sensors and the airplane's data recording system. Its main functions were to activate and control the four pressure multiplexer valves (Scanivalves) and to supply excitation voltage and signal conditioning for the pressure transducers attached to each Scanivalve. The scan-control module also contained valving that allowed cabin air to flow out the measurement ports during nondata-taking periods. This purge function was provided to keep the pressure measurement tubes and probes clear of water or ice. Provision was made for manual control of purge/operate, initiate data sequence, and selection of scanning rate. Remote control and scanivalve position readout were also provided for preflight checkout. Details of the scan-control module assembly are described in reference 3.

Reference Pressure and Temperature Transducers--Four high-resolution Digiquartz-type transducers were used to measure the reference total, static, and impact pressures taken from the copilot's pitot static system and the freestream total temperature. These transducers are integral parts of the test airplane data acquisition system. The total and static pressures from these sources were transmitted to one channel of each Scanivalve and recorded with the scanned rake pressure data. Therefore, the system provided an updated recalibration at each scanning cycle.

Onboard Data Recording Equipment--The test airplane onboard data recording equipment consists of a 100-channel digital tape recorder and three 16-channel oscillographs for online data monitoring and quick-look data recording.

Of the 100 variables recorded by the onboard data acquisition system, only about 16 were pertinent to the present experiment. These included the four Scanivalve/transducer outputs and the Scanivalve position signal as well as the three reference pressures (total, static, and impact) from the airspeed system and the freestream total temperature. These variables were essential to the data analysis, but others, such as the airspeed, altitude, angle of attack, pitch and yaw angles, and fuel quantity were used only for the identification of flight conditions.

4.4 TEST PROCEDURE

The surface coatings drag evaluation tests were incorporated into the TCV flight test program on a "concurrent test" basis. The tests were usually performed after the test airplane completed its primary mission at the Wallops Island test site. All the tests were flown in tightly controlled corridors designated by Air Traffic Control.

There were five test flights, plus one supplementary test, during flight 3a when the roughened leading edge was tested. The following table lists the flights and test configurations chronologically.

Flight No.	Date	Test surfaces Left wing	Right wing	Data sources
1	12-11-80	Existing paint	Bare	Boundary layer rakes
2	1-20-81	Bare	Bare	Pressure belts
3a	1-23-81	Bare, L.E. grit	Bare	Boundary layer rakes
3	1-23-81	Bare	Bare	Boundary layer rakes
4	1-27-81	Corogard	Bare	Boundary layer rakes
5	2-03-81	CAAPCO	Bare	Boundary layer rakes

A total of 15 test conditions were flown during each test flight, except in the case of the roughened leading edge, which covered only four test conditions. The test conditions were selected to provide systematic variations of Mach number and lift coefficient throughout the cruise regime of the airplane. The following table lists the test conditions flown:

Test condition	C_L	M	W/δ, kg(lb)
1	0.75	0.55	149 180 (328 881)
2	0.55	0.65	152 983 (337 264)
3	0.45	0.70	145 165 (320 029)
4	0.35	0.75	129 611 (285 740)
5	0.65	0.55	129 447 (285 377)
6	0.45	0.65	125 167 (275 943)
7	0.35	0.70	112 906 (248 911)
8	0.55	0.55	109 532 (241 473)
9	0.35	0.65	97 352 (214 623)
10	0.25	0.75	92 579 (204 100)
11	0.45	0.55	89 616 (197 568)
12	0.25	0.70	80 647 (177 794)
13	0.25	0.65	69 537 (153 302)
14	0.35	0.55	69 702 (153 664)
15	0.25	0.55	49 787 (109 760)

To achieve a given combination of Mach number and lift coefficient, a test condition must be flown at a fixed value of W/δ. This is determined from the formula

$$W/\delta = 0.7\, P_o\, S_{REF}\, M^2 C_L$$

To establish a test condition, the momentary gross weight of the airplane is determined from onboard fuel gage readings. The appropriate pressure altitude that gives the required W/δ ratio is then calculated. Finally, engine thrust is set to establish the desired Mach number.

During each test condition, after the airspeed and altitude were stabilized, a minimum of 2 min was allowed for data taking. This permitted at least two full scanning cycles. Airspeed and altitude were held constant during the data recording; the maximum allowable deviations from the nominal values were $\pm$5.5 km/h ($\pm$3 kn) and $\pm$7.6m ($\pm$25 ft), respectively. There were about 3 to 5 min between test conditions to change and stabilize speed and altitude. The usual duration of the entire test sequence was about 1 hr 20 min.

Figures 8 through 10 show a typical set of data pertinent to the test conditions flown during one of the test flights (flight 3). The range of test conditions is depicted in terms of C_L and M in figure 8. It is evident that the actual flight conditions flown were very close to the preselected conditions. Figure 9 illustrates the time history of the flight, showing the altitude and airplane gross weight variation. The fuel burn rate during the early phase of the test sequence (at high altitudes) was approximately 2200 kg/h (4850 lb/h), and it increased to about 2900 kg/h (6390 lb/h) at the lower altitudes toward the end of the test. The average rate of fuel consumption was 230 kg (507 lb) per condition. Figure 10 shows the Reynolds number range covered by the selected sequence of test conditions. For the flight shown, the lowest value was R_1 = 5.1 million/m (1.55 million/ft) at condition 1, and the highest value was R_1 = 11.1 million/m (3.38 million/ft) at condition 15. Note that a unit Reynolds number of R_1 = 6.56 million/m (2 million/ft) is typical for jet transport airplanes during cruise.

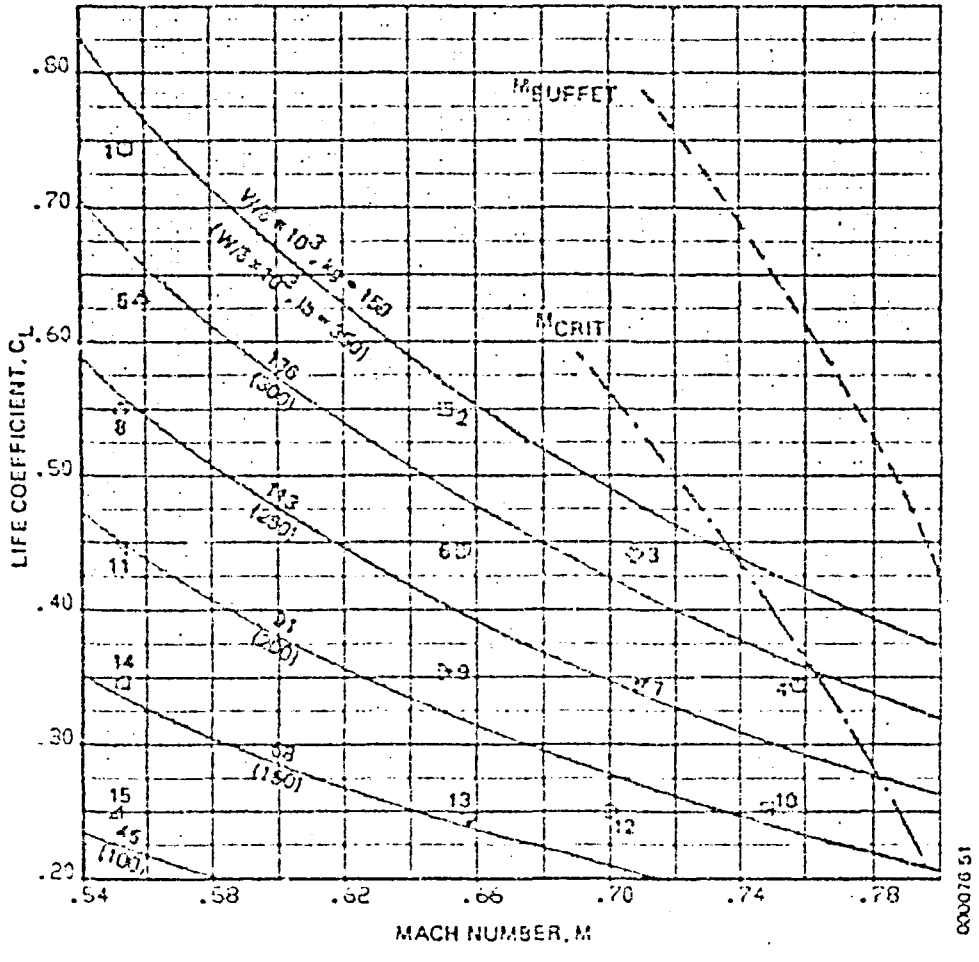

Figure 8. Range of Test Conditions

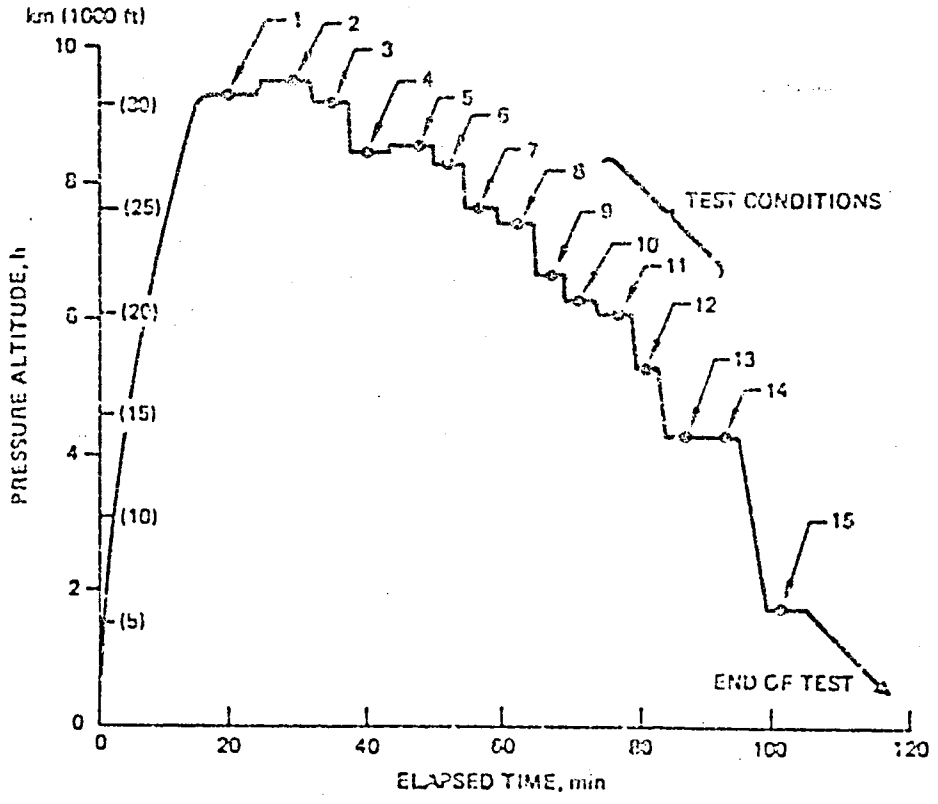

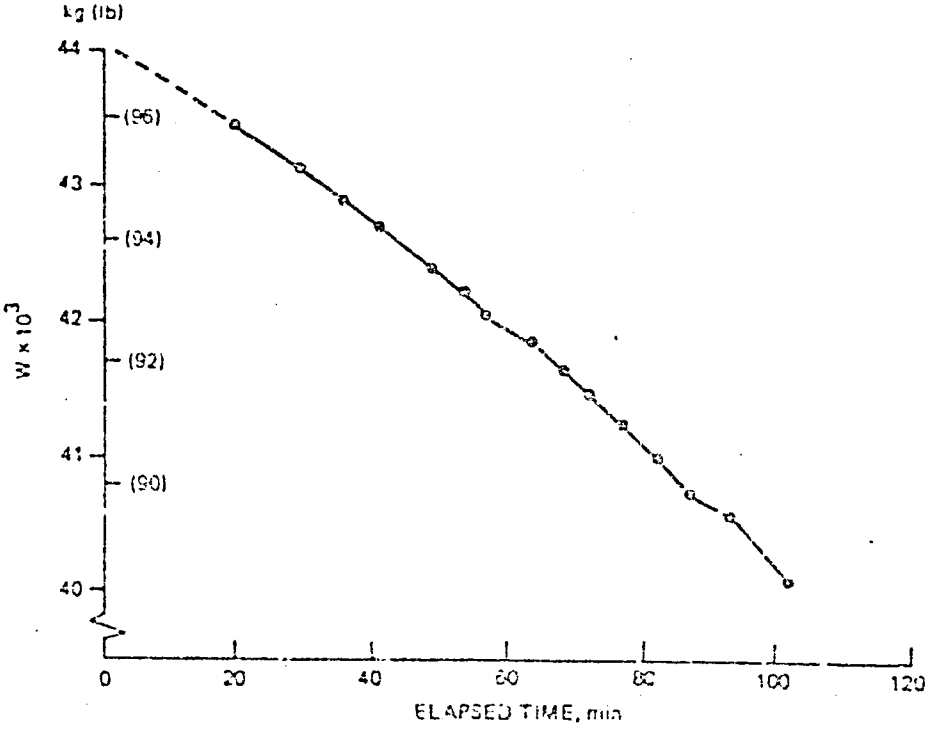

Figure 9. Time History of a Typical Test Flight (Flight 3)

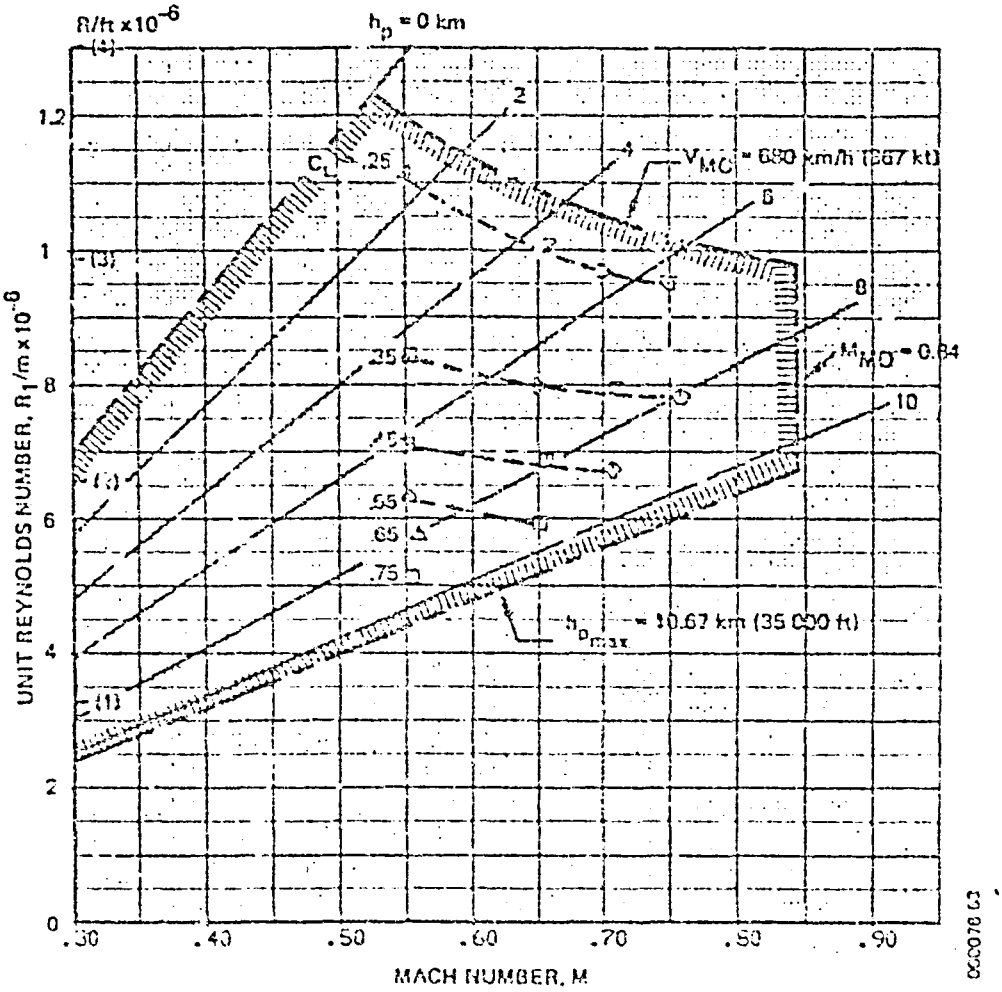

Figure 10. Reynolds Number Range of Tests

4.5 TEST ANALYSIS METHOD

The principal phases of the test analysis are illustrated in figure 11a through 11c. First, the boundary layer velocity profiles are determined from the measured total pressure loss within the boundary layer. Then, the momentum loss profile is calculated from which, by integration, the momentum thickness is evaluated (see fig. 11a). These calculations were performed by an existing Boeing computer program, A-55, entitled "Turbulent Boundary Layer Profile Analysis."

Because measurements were taken at an intermediate chordwise location, measured increments in momentum thickness must be extrapolated to the trailing edge to express the results in terms of section profile drag. This was done by calculating boundary layer growth along the test section from measured surface static pressure distributions and deriving a magnification factor that translates a given increment in momentum thickness, measured at the rake location, into a corresponding increment in section profile drag coefficient:

$$\Delta c_d = m \frac{\Delta \theta}{c}$$

where $\Delta\theta = \theta_{LEFT} - \theta_{RIGHT}$ is the momentum thickness difference between the left and right wing test sections, and m is the magnification factor as defined in figure 11b.

The boundary layer growth calculations were performed by another existing Boeing computer program, TEM 139, "A Finite Difference Method To Calculate the Boundary Layer Development on an Infinite Yawed Wing." The magnification factor was calculated following a method given by Nash and Bradshaw (ref. 5).

① MEASURE: TOTAL PRESSURE LOSS IN BOUNDARY LAYER

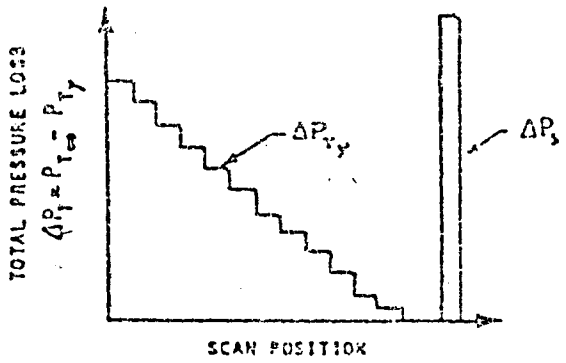

$$q_{c_y} = \Delta P_{t_y} - \Delta P_S$$

$$P_S = P_{T_\infty} - \Delta P_S$$

$$\Delta P_t = P_{T_\infty} - P_S$$

② COMPUTE: BOUNDARY LAYER VELOCITY AND MOMENTUM LOSS PROFILES (A-55)

$$\frac{u}{U_e} = \frac{M_y}{M_e}\sqrt{\frac{T_y}{T_e}}$$

where $$M_y = \sqrt{5\left[\left(\frac{q_{c\,y}}{P_S} + 1\right)^{2/7} - 1\right]}$$ and $$\frac{T_y}{T_e} = \frac{\rho_e}{\rho_y} = \frac{1+.2M_e^2}{1+.2M_y^2}$$

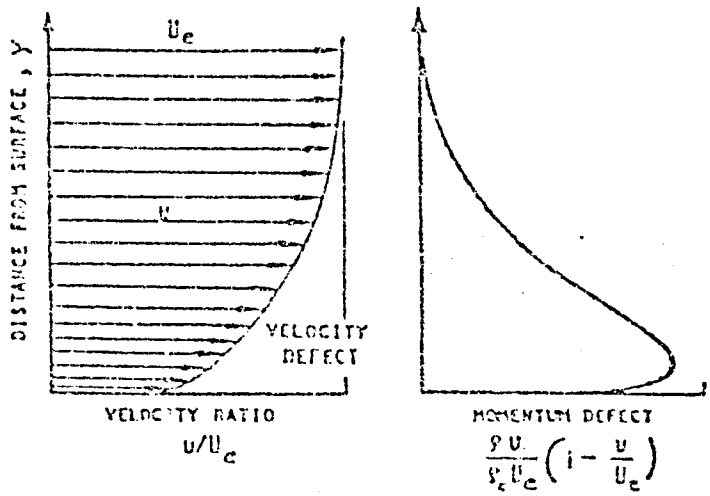

③ EVALUATE MOMENTUM THICKNESS $$\theta = \int_0^\delta \frac{\rho u}{\rho_e U_e}\left(1 - \frac{u}{U_e}\right) dy$$

(a) Boundary Layer Momentum Thickness Evaluation

Figure 11. Principles of Test Analysis

② MEASURE: CHORDWISE PRESSURE DISTRIBUTION

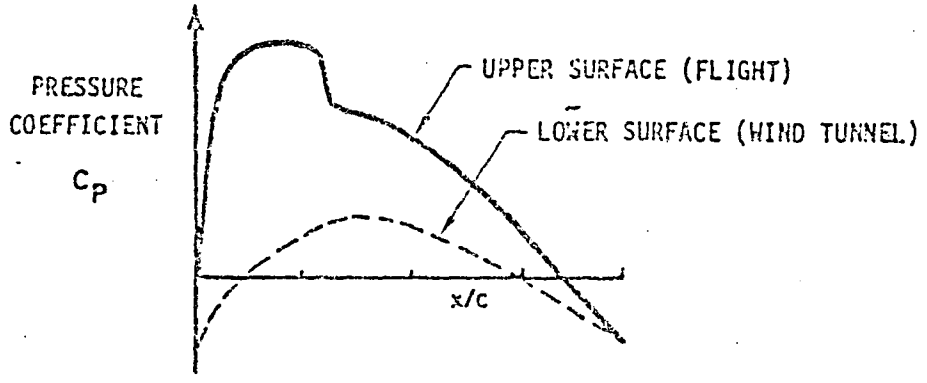

③ CALCULATE: BOUNDARY LAYER GROWTH (TEM-139)

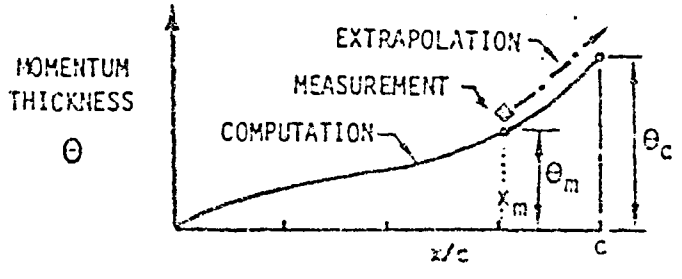

④ EVALUATE: SECTION PROFILE DRAG AND MAGNIFICATION FACTOR

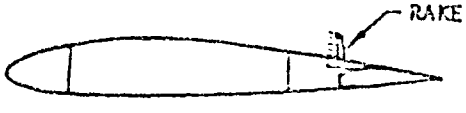

SECTION PROFILE DRAG (SMOOTH)

$$c_d = \frac{2\theta_c}{c}\left(\frac{U_{e_c}}{U_\infty}\right)^{\frac{H_c+5}{2}}$$ (SQUIRE & YOUNG)

MAGNIFICATION FACTOR

$$m = 2\left(\frac{\theta_m}{\theta_c}\right)^{1/5} \cdot \frac{U_\infty}{U_{e_c}} \cdot \left(\frac{U_{e_m}}{U_\infty}\right)^{1+(H_m+5)/2}$$

D00076-27

(b) Calculation of Upper Surface Boundary Layer Development

Figure 11. Principles of Test Analysis (Continued)

- EVALUATE UPPER SURFACE PROFILE DRAG INCREMENT :

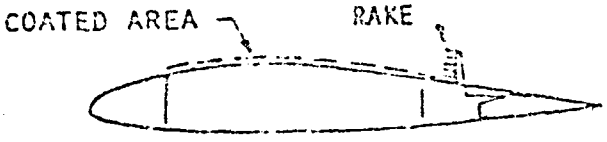

$$\Delta c_d = m \frac{\Delta \theta_m}{c}$$

WHERE $m = 2\left(\frac{\theta_m}{\theta_c}\right)^{1/5} \frac{U_{\infty}}{U_{e_c}} \cdot \left(\frac{U_{c_m}}{U_{\infty}}\right)^{1+\frac{H_{w}-5}{2}}$ (magnification factor)

and $\Delta\theta_m = \theta_{left} - \theta_{right}$ at $x/c = 73\,\%$

- ESTIMATE TOTAL AIRPLANE DRAG INCREMENT :

$$\Delta C_D = \frac{2}{S_{REF}} \int_{SOB}^{b/2} (\Delta c_d \cdot c)\, dz$$

$$\approx \Delta c_d \cdot \frac{A_{exp}}{S_{ref}} \cdot \xi$$

where $\frac{A_{exp}}{R_{ref}} = 0.84$ and

$\xi = \frac{\text{AVERAGE \% CHORD COATED}}{\text{TEST SECTION \% CHORD COATED}}$

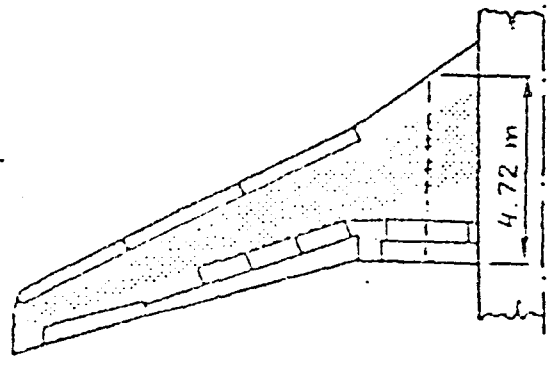

(c) Estimation of Airplane Drag Increment

Figure 11. Principles of Test Analysis (Concluded)

This calculation yields incremental drag coefficients based on the chord of the test section. The ultimate objective, of course, is to determine effects of the various surface configurations on total airplane drag. This, however, may be quite complicated because a number of factors must be taken into consideration, such as the chordwise extent of the coated area along the entire span as well as local flow conditions that also vary along the span. Furthermore, a surface coating may be applied only on the wing upper surface or on both surfaces, including the empennage. However, assuming that similar conditions and effects exist at all spanwise stations, conversion factors for airplane drag can be calculated. Figure 11c shows the method used in this analysis. While these factors are not exact, the error introduced is very small, considering the smallness of the basic drag increments, some of which are approaching the accuracy limits of the experiment.

4.6 DATA PROCESSING

The data processing and test analysis were accomplished in six steps, as shown in figure 12. NASA provided raw data tapes that contained time histories of 16 variables, including boundary layer rake pressures, reference total and static pressures, total temperature, remaining fuel weight, airspeed, altitude, and angle of attack. Figure 13a gives a complete listing of the recorded variables. Each measured quantity was recorded at the rate of 40 readings/sec. Because the data taking interval during each of the 15 test conditions lasted about 2 min (two scanning cycles), the basic tapes contained a large volume of data: some 1.2 million readouts per flight.

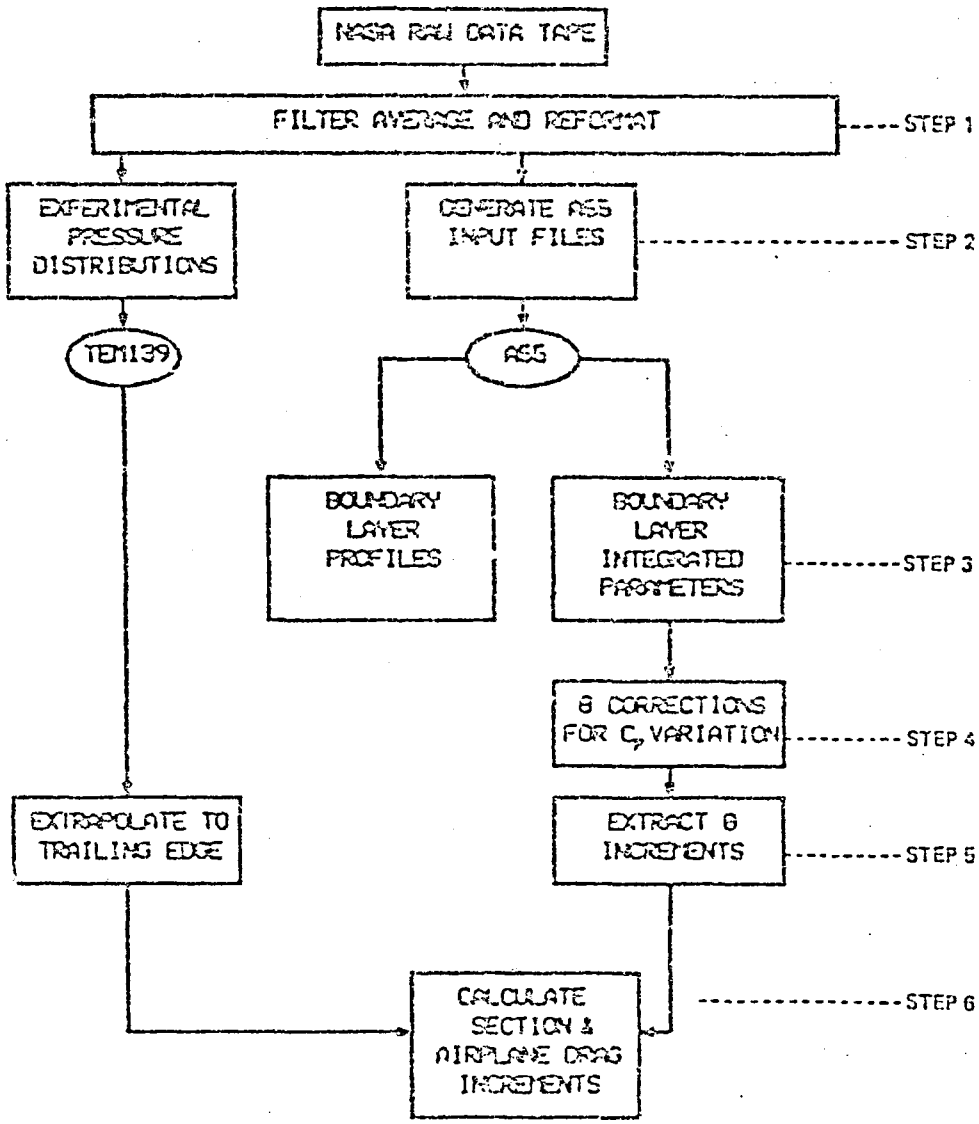

Figure 12. Data Processing Sequence

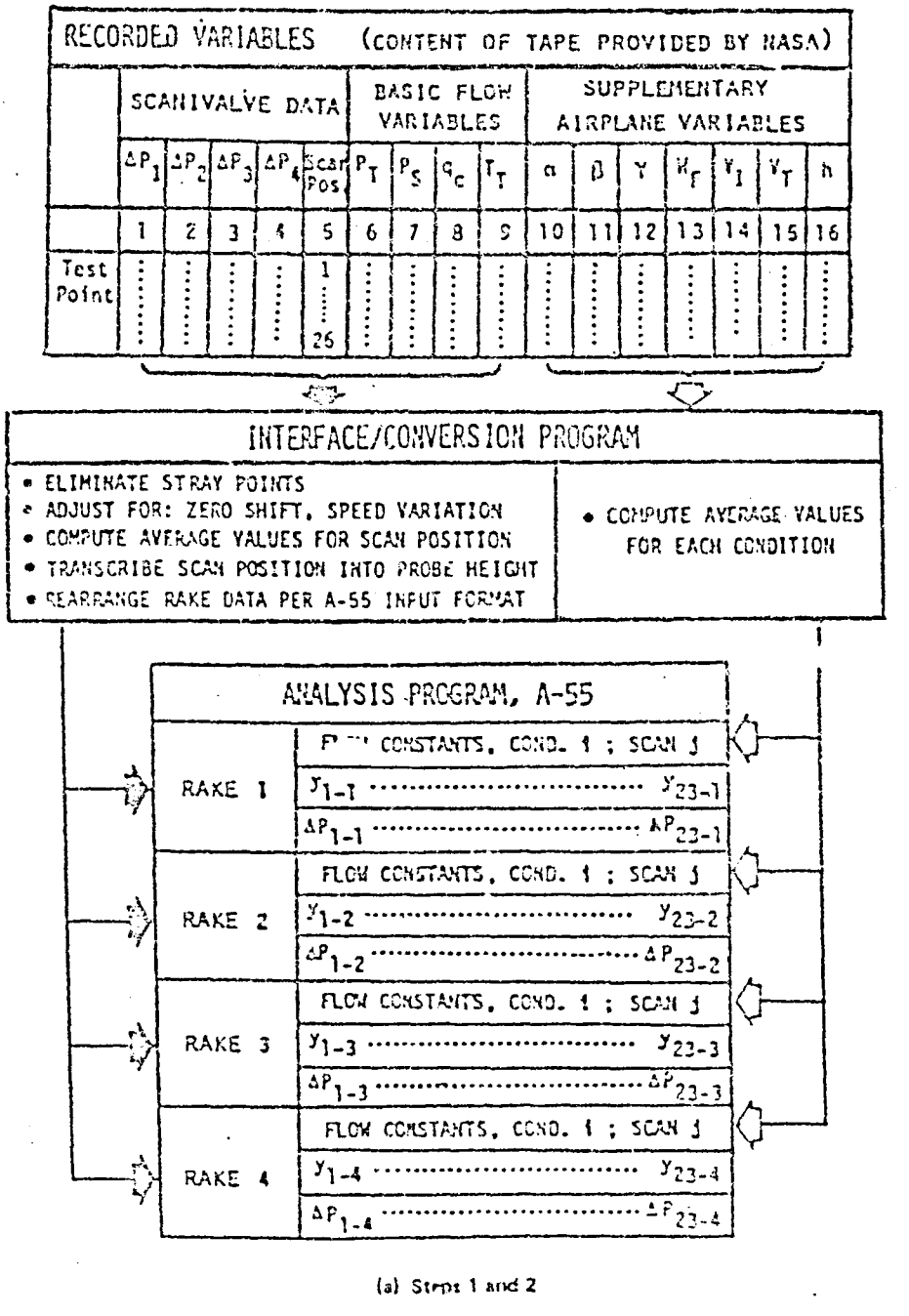

(a) Steps 1 and 2

000078 002

Figure 13. Data Processing Details

The first step of the data reduction process was to filter, average, and reformat the data contained in the raw data tapes. An auxiliary computer program was written to accomplish this task, which provided an interface between the recorded data and the computer programs used to analyze the data. The principal functions of the interface program are indicated in figure 13a. First, data that were unreasonably out of range (stray points) were deleted and then the mean and standard deviations were computed for each remaining data point. Based on the standard deviation, if the scatter in a set of data was too large, these data were to be deleted. Most of the data, however, fell within very narrow scatter bands ($\pm$0.1%); thus only very few data points were actually deleted. Another main function of the interface program was to generate average values of the test variables. The boundary layer rake data and the reference pressure data were averaged for each scan position, while those variables that were essentially constant during a given test condition (such as airspeed, altitude, temperature, etc.) were averaged for the entire scanning cycle. The averaged data, then, were adjusted for such small-scale perturbations as zero shift, amplifier sensitivity drift, or slight variations in airspeed during a scanning cycle.

In the second step of the data reduction process, input files were generated for the two principal computer programs used in the test analysis: the boundary layer profile analysis program (A-55) and the boundary layer growth analysis program (TEM 139). The input file format for A-55 is also shown in figure 13a.

The third step constituted processing the test data by the A-55 and TEM 139 computer programs. Data from flights 1, 3, 4, and 5 (i.e., the boundary layer survey data) were processed by A-55, while the surface pressure survey data from flight 2 were processed by TEM 139. A functional diagram of computer program A-55 is shown in figure 13b, illustrating the input/output variables and the computation sequence. From the output of A-55, two plot files were generated for the PDP 70-11 minicomputer, which allowed machine plotting of the test results. One

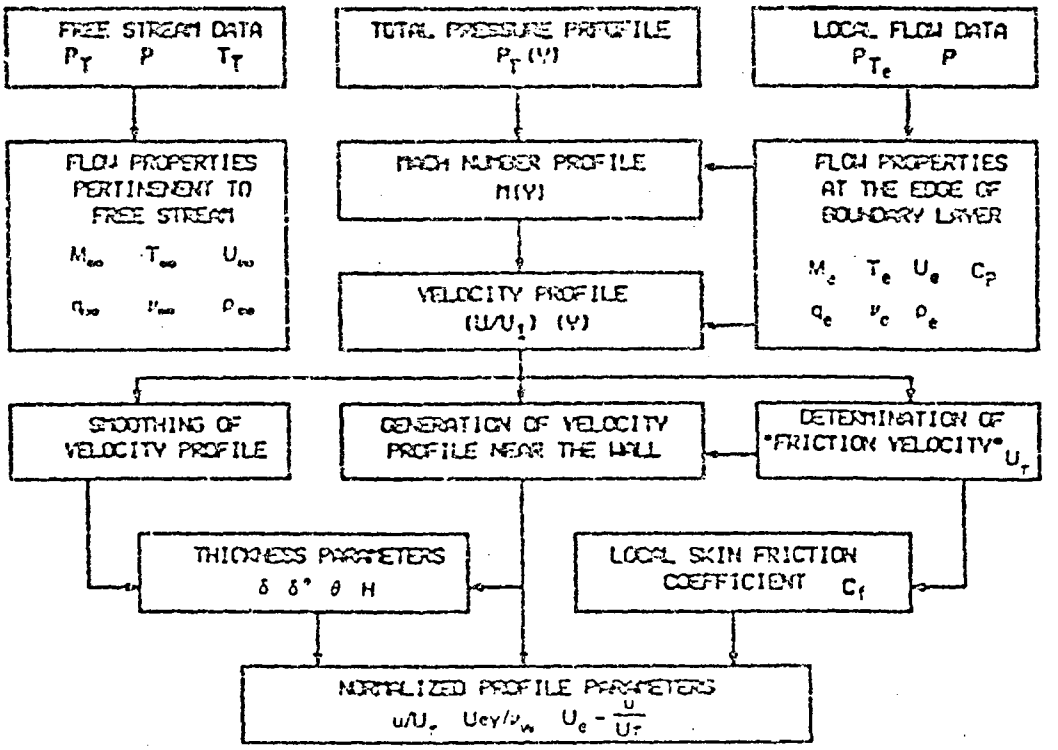

(b) Step 3

050078-003

Figure 13. Data Processing Details (Concluded)

file included the boundary layer profile parameters (i.e., those variables that are dependent on height), while the other contained the global or integrated parameters.

In the fourth step of data processing, a correction was applied to the boundary layer momentum thickness data to compensate for slight differences in the local static pressures (c_p's) between the left and right wing test sections.

During the fifth step, momentum thickness increments between the left and right wing test sections were extracted from the data. In parallel to this task, the applicable "magnification factors" were determined for each test condition based on results of the boundary layer calculations made by T&M 139.

The sixth step of the data reduction process constituted translation of the local momentum thickness increments measured at the rake location (73% test section chord) into section profile drag increments and, ultimately, extrapolation of the section profile drag increments in terms of total airplane drag increments.

5.0 TEST RESULTS

The test results are described in this section. In general, selected samples of the basic data are presented, and the results of the data analysis are discussed. The discussion begins with the static pressure surveys and subsequent boundary layer calculations. Finally, the results of the boundary layer surveys and drag evaluation are presented.

5.1 STATIC PRESSURE SURVEYS

Samples of the measured upper surface chordwise pressure distributions along the test section are shown in figure 14. The effect of lift coefficient variation at constant Mach number is shown in figure 14a; figure 14b shows the effect of Mach number variation at constant C_L. These measurements indicate orderly trends of static pressures except in the region around x/c = 10%, where a distinct aberration occurs. This is thought to be caused by waviness in the skin near the front spar. The aberration is amplified at higher Mach numbers (fig. 14b).

The pressure distributions measured on the two wing test panels were very similar. The right wing had slightly higher negative c_p's than the left wing, as shown in figure 15. The difference was about $\Delta c_p \approx$ 0.03 to 0.06 and, in general, larger along the forward region.

For calculating the boundary layer characteristics, corresponding c_p's between the two sides were averaged. Because the pressure belt was terminated at the x/c = 70% chord location, an extrapolation of pressure distributions back to the trailing edge was necessary to carry out calculations for the entire length of the airfoil upper surface. This, however, could be done with fairly high confidence knowing that the pressure variation over the aft end of the airfoil is nearly linear as long as the flow is not separated.

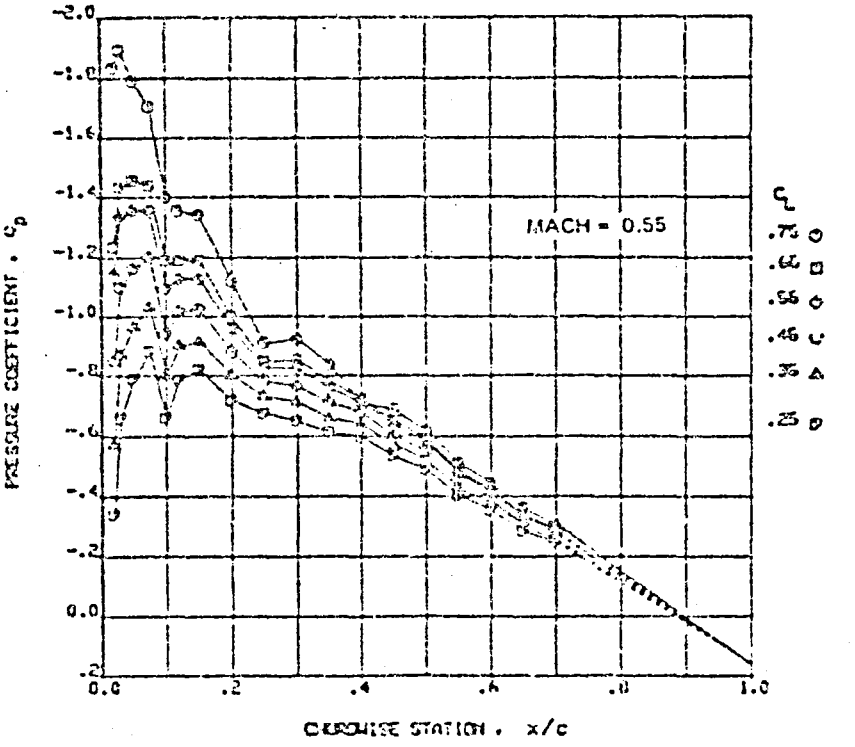

(a) Effect of Lift Coefficient at M = 0.55

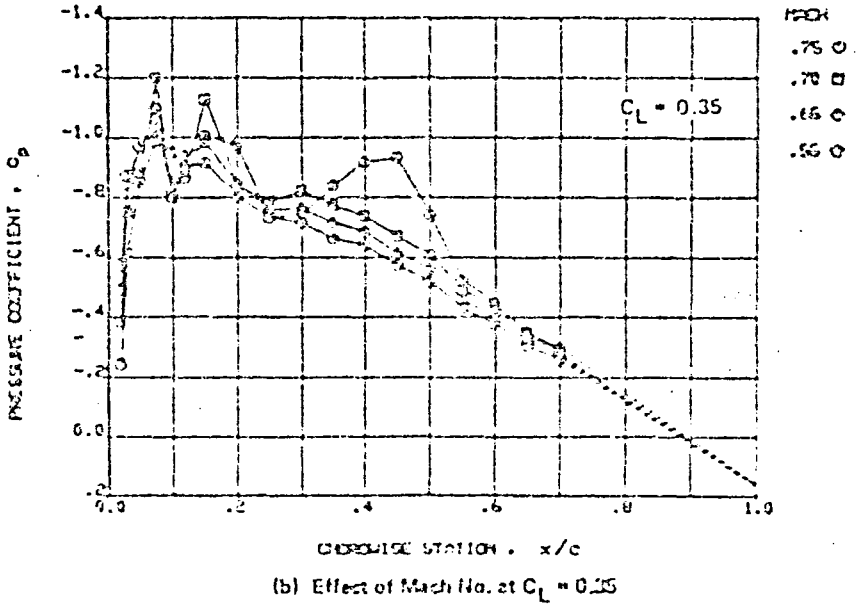

(b) Effect of Mach No. at C_L = 0.35

Figure 14. Typical Results of Static Pressure Surveys

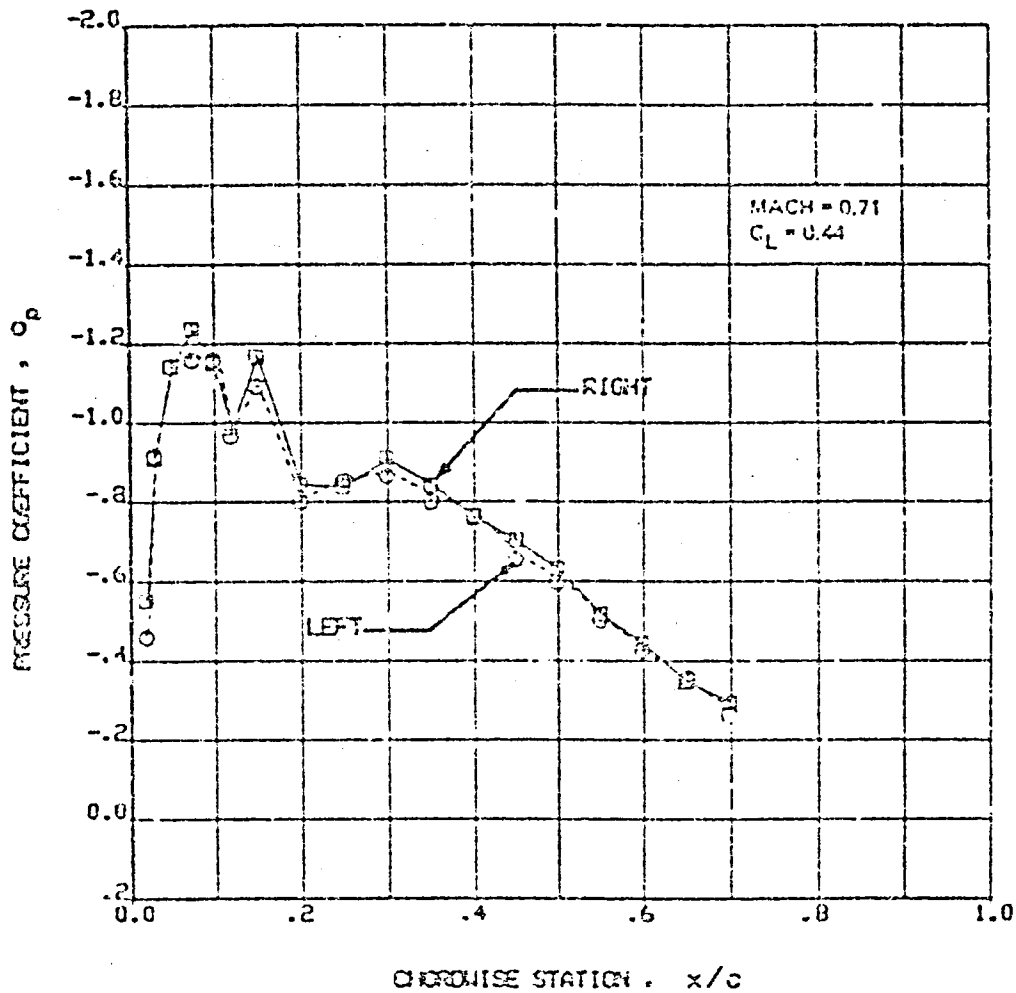

Figure 15. Comparison of Left and Right Test Section Pressure Distributions

Typical results of boundary layer calculations corresponding to the pressure distributions shown above are presented in figure 16a and 16b. These data were used for calculating the magnification factor (see fig. 11b), which is used for translating the measured momentum thickness differences into profile drag increments. The theoretical section profile drag was also determined based on these calculations following the approach outlined in figure 11b. The results are presented in figure 17, showing the profile drag variation with lift coefficient for the upper surface alone and for the entire airfoil section. The drag contribution of the lower surface was estimated on the basis of pressure distributions obtained in the wind tunnel. The calculated magnification factors are shown in figure 18.

5.2 BOUNDARY LAYER SURVEYS

It is more convenient to discuss the results of the boundary layer surveys in a different order than the sequence of test flights. The baseline data, obtained with bare surfaces on both sides (flight 3), are discussed first, followed by the results with Corogard (flight 4) and the CAMPCO coating (flight 5), respectively. The test results with the roughened leading edge (flight 3a) are then presented, followed by the test of existing paint (flight 1).

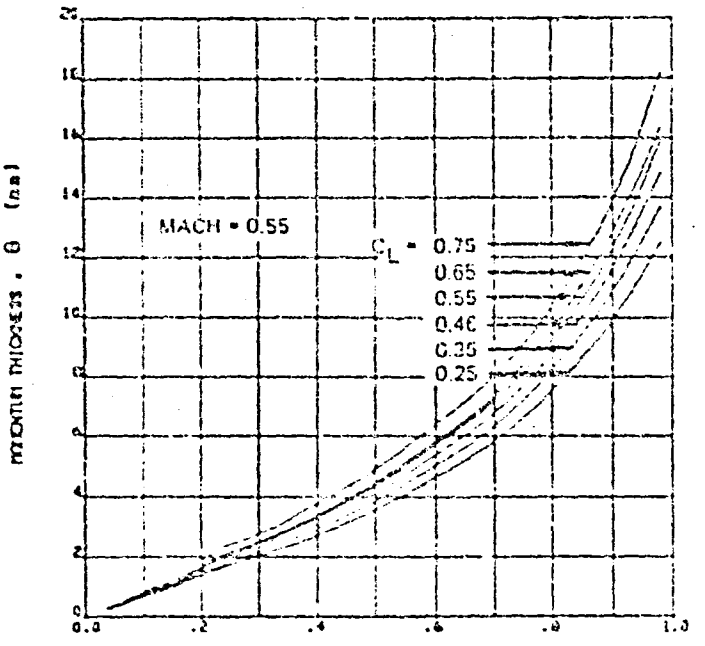

(a) Effect of Lift Coefficient at M = 0.55

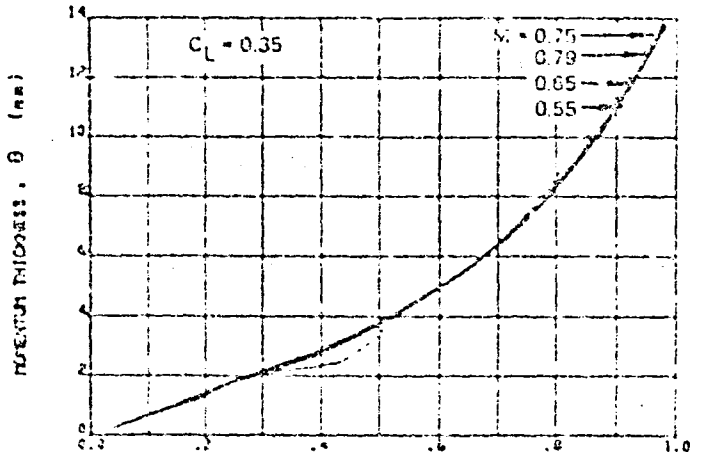

(b) Effect of Mach No. at C_L = 0.35

Figure 16. Calculated Boundary Layer Growth

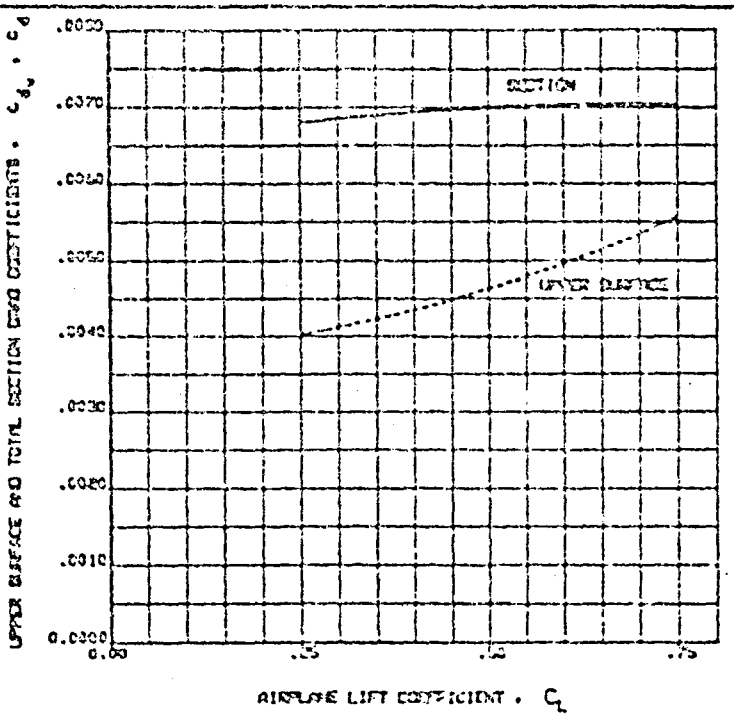

AIRPLANE LIFT COEFFICIENT , C_L

Figure 17. Calculated Section Profile Drag Characteristics

$$m = 2\left(\frac{\theta_m}{\theta_c}\right)^{0.2} \cdot \frac{U_m}{U_{e_c}} \cdot \left(\frac{U_{e_m}}{U_m}\right)^{1+\frac{H_m+5}{2}}$$

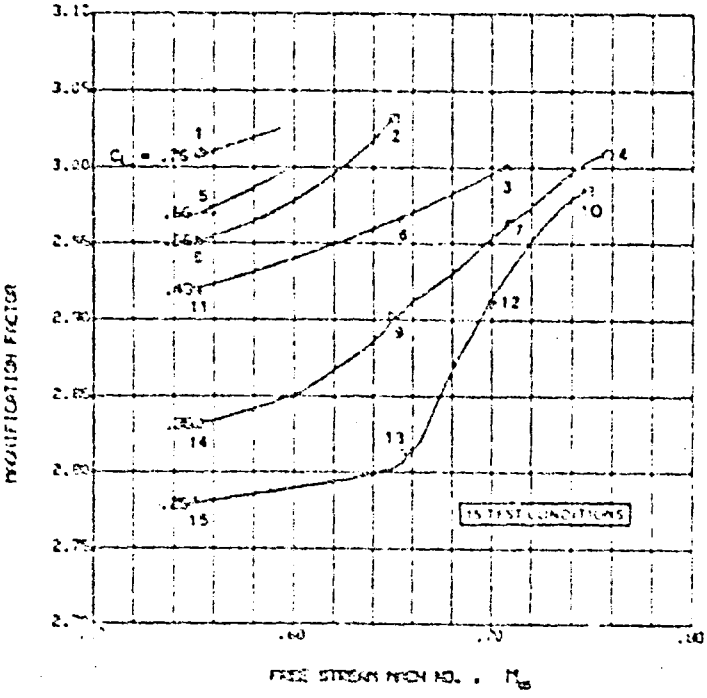

FREE STREAM MACH NO. , M_∞

Figure 18. Calculated Magnification Factors

5.2.1 Bare-to-Bare Surface Comparison

A typical set of measured boundary layer profiles is presented in figure 19, showing velocity variations (fig. 19a) and momentum loss variations (fig. 19b) across the boundary layer for varying lift coefficient and constant Mach number. The measurements indicate a very orderly behavior of the boundary layer, with steady increase in the velocity defect and momentum loss as lift coefficient increases. The thickness of the boundary layer at the measurement station varies from about δ = 50 to 80 mm (2 to 3 in). Figure 20 shows a comparison between the boundary layer profiles measured on the left and right wing panels (rake 2 is on the left side and rake 3 is on the right side). The profiles appear to be nearly identical, both in terms of velocity defect (fig. 20a) and momentum defect (fig. 20b). There is, however, a slight difference in the value of momentum thickness (derived by integration of momentum loss profile). It was first assumed that this difference was well within the accuracy limits of the measurement, but a closer look at all these data revealed that the small difference between the two sides was consistent and, therefore, not a random error.

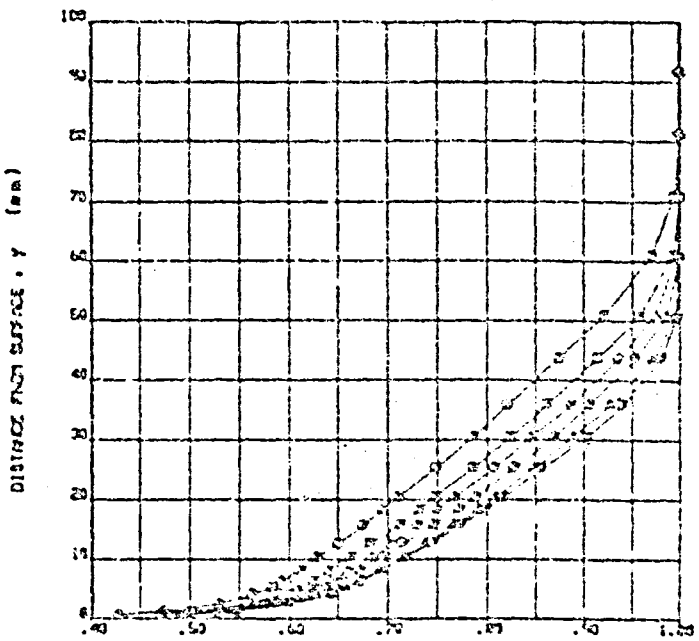

(a) Velocity Profiles

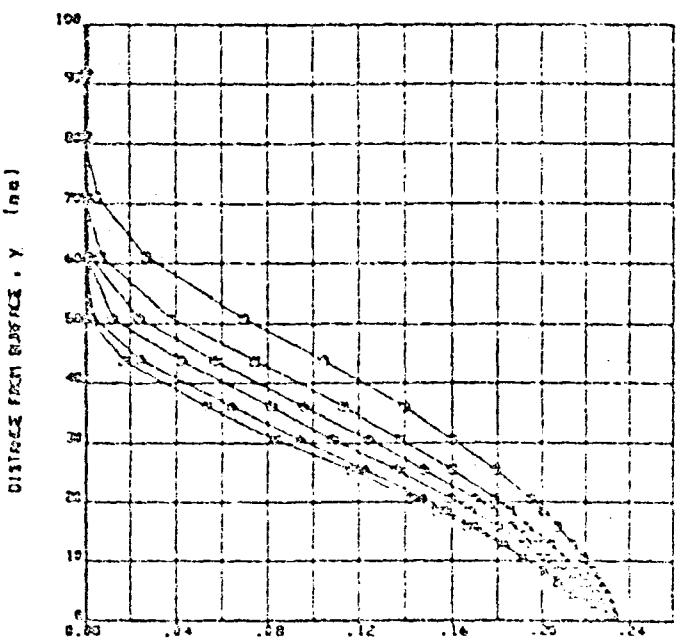

(b) Momentum Loss Profiles

Figure 19. Typical Measured Boundary Layer Profiles--Bare Surface, M = 0.55

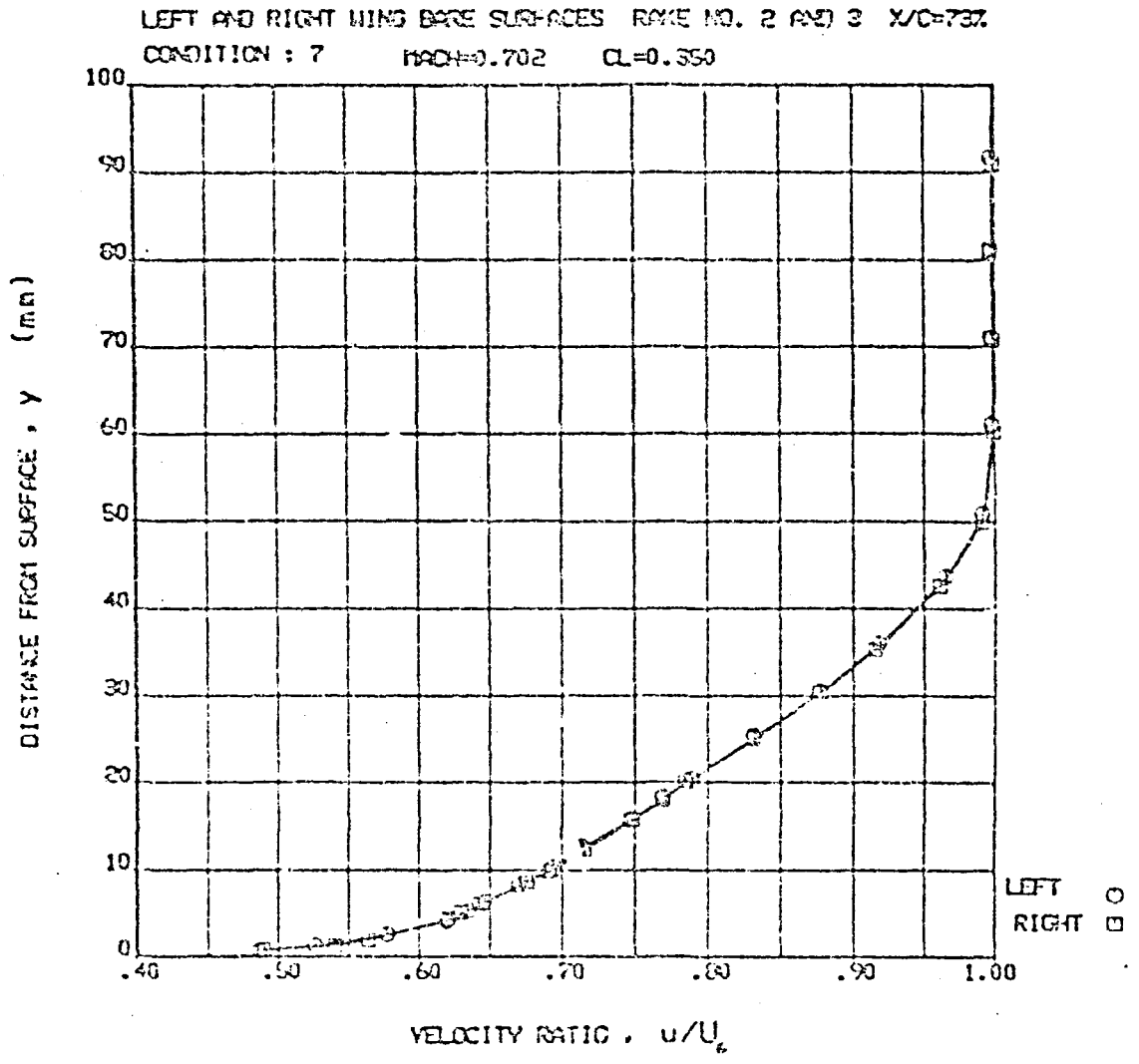

(a) Velocity Profiles

Figure 20. Comparison of Boundary Layer Profiles—Bare Left and Right Wings (Flight 3); M = 0.702, C_L = 0.35

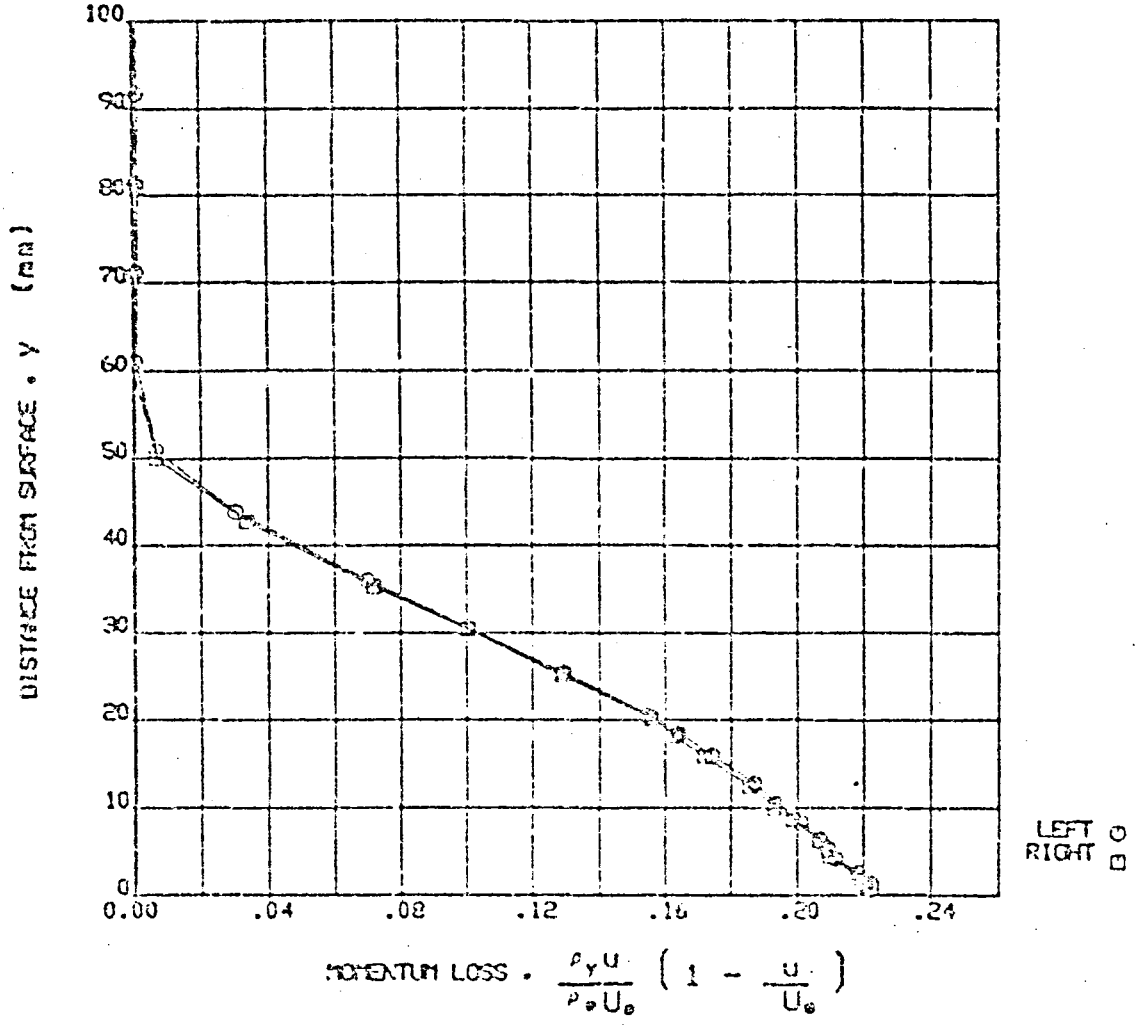

(b) Momentum Loss Profiles

Figure 20. Comparison of Boundary Layer Profiles--Bare Left and Right Wings (Flight 3); M = 0.702, C_L = 0.35

A further look into possible reasons for the slight differences between the two sides indicated that the momentum thickness difference can be linked to differences in pressure coefficients measured by the static port of the boundary layer rakes. This is illustrated in figure 21, where measured momentum thickness data are plotted against pressure coefficient for three selected flight conditions. (Note that two data points are shown for each rake corresponding to the two data scans performed during each test condition.) Reasons for the differences in local pressure coefficients between the left and right wing test stations are not certain. No leaks or plugs in rake static pressure lines or obvious errors in data recording were discovered during a post-test recheck of the instrumentation system. The most likely explanations for the differences in local c_p measurements are that the geometry of the two sides is slightly different, which could be caused by rigging of the trailing-edge flaps, or a slight asymmetrical deflection, under airloads, of the inboard spoilers. Note that the static pressure surveys also indicated slight differences in c_p between the two sides. As the test results showed a fairly distinct pattern regarding the effect of c_p variations on the measured momentum thickness, a convention was adopted for the data analysis according to which measured $\Delta\theta$ values were adjusted to variations in c_p. The adjusted value of the momentum thickness was derived as

$$\theta_{corr} = \theta_{meas} + \frac{d\theta}{dc_p}\left(c_{p_{meas}} - c_{p_{nom}}\right)$$

where the gradient $\frac{d\theta}{dc_p}$ determined, as indicated in figure 21, and $c_{p_{nom}}$ was obtained by extrapolating the measured pressure distribution data to the rake location. This adjustment further reduced the small differences in momentum thickness observed between the two sides in the bare-to-bare condition and rendered these data more amenable to machine processing for evaluation of the extremely small $\Delta\theta$ differences. This same adjustment procedure was also applied for all the other test surface evaluations.

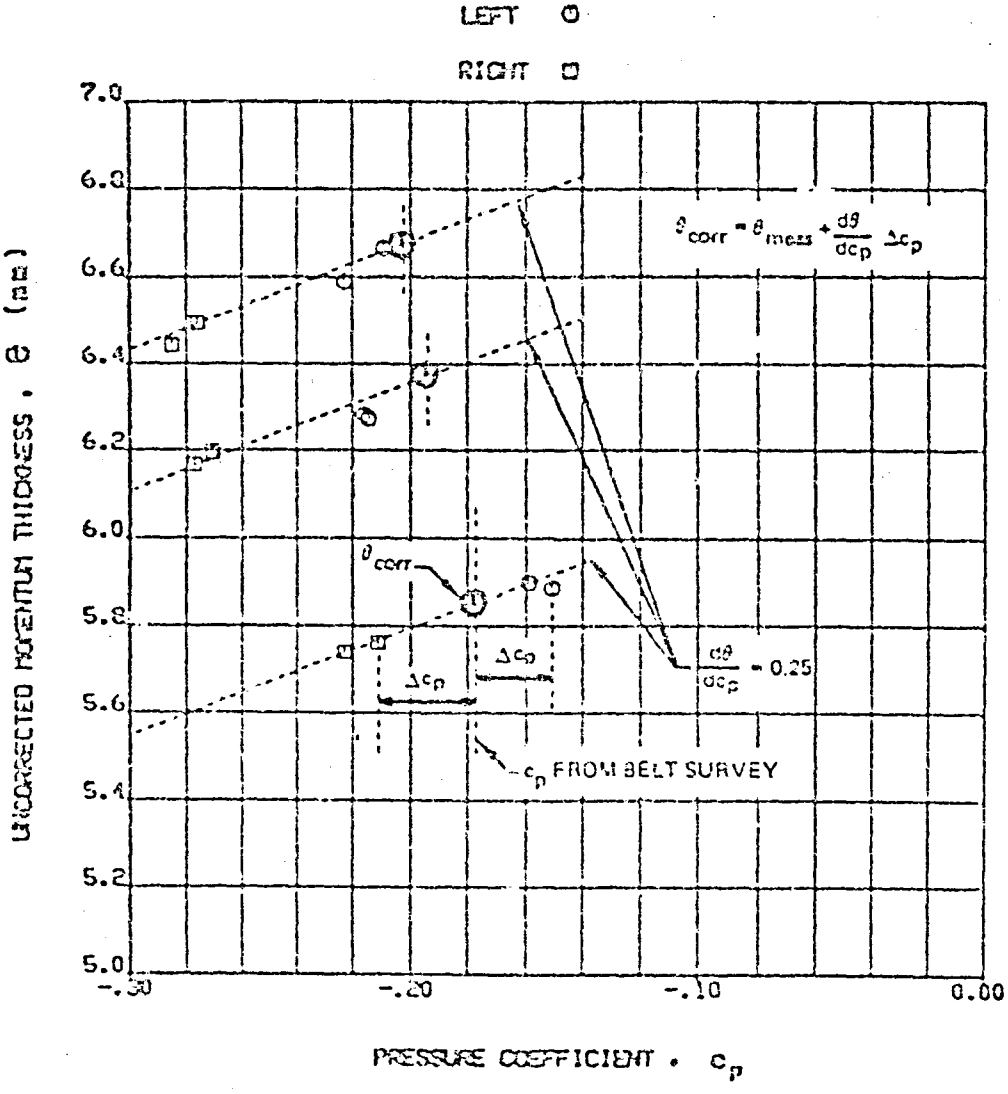

Figure 21. Momentum Thickness Corrections for Variations in Local Static Pressure (Left and Right Wing Bare Surfaces)

Figure 22 shows the adjusted momentum thickness data comparing left and right sides. Considering the greatly expanded θ scale, differences between the two sides appear to be very small, although at high lift coefficients the right side tends to show slightly higher values of θ than the left side. The $\Delta\theta$ increments are shown in figure 23.

5.2.2 Corogard-to-Bare Surface Comparison

Figure 24 illustrates a typical set of measured boundary layer profiles, indicating both the velocity defect (fig. 24a) and the momentum defect (fig. 24b) across the boundary layer for the Corogard-coated surface and the bare reference surface. The effect of Corogard is obvious--increased velocity deflect and momentum loss throughout the boundary layer and slightly increased local velocity (i.e., shear) next to the surface. For the case shown, the increment in measured momentum thickness is 0.36 mm (0.014 in), or about 6% of θ for the bare surface. This value, however, is subject to adjustment (fig. 25). After the adjustment, the increment is reduced to $\Delta\theta$ = 0.30 mm (0.012 in). This is about 4.8% of θ for the bare surface. The case shown represents an average flight condition. At lower lift coefficients (i.e., higher Reynolds numbers) the increments are higher, whereas at higher C_L's (i.e., lower Reynolds numbers) the Corogard surface shows little or no increment in momentum thickness relative to the bare surface. The results, in terms of adjusted momentum thickness, are shown in figure 26. Momentum thickness increments and corresponding section drag coefficient increments, derived from the adjusted momentum thickness data, are presented in figure 27. Distinct trends of increasing $\Delta\theta$ or Δc_d with decreasing C_L are evident. This apparent dependency on C_L, however, mainly reflects Reynolds number effects as shown in Section 5.3.

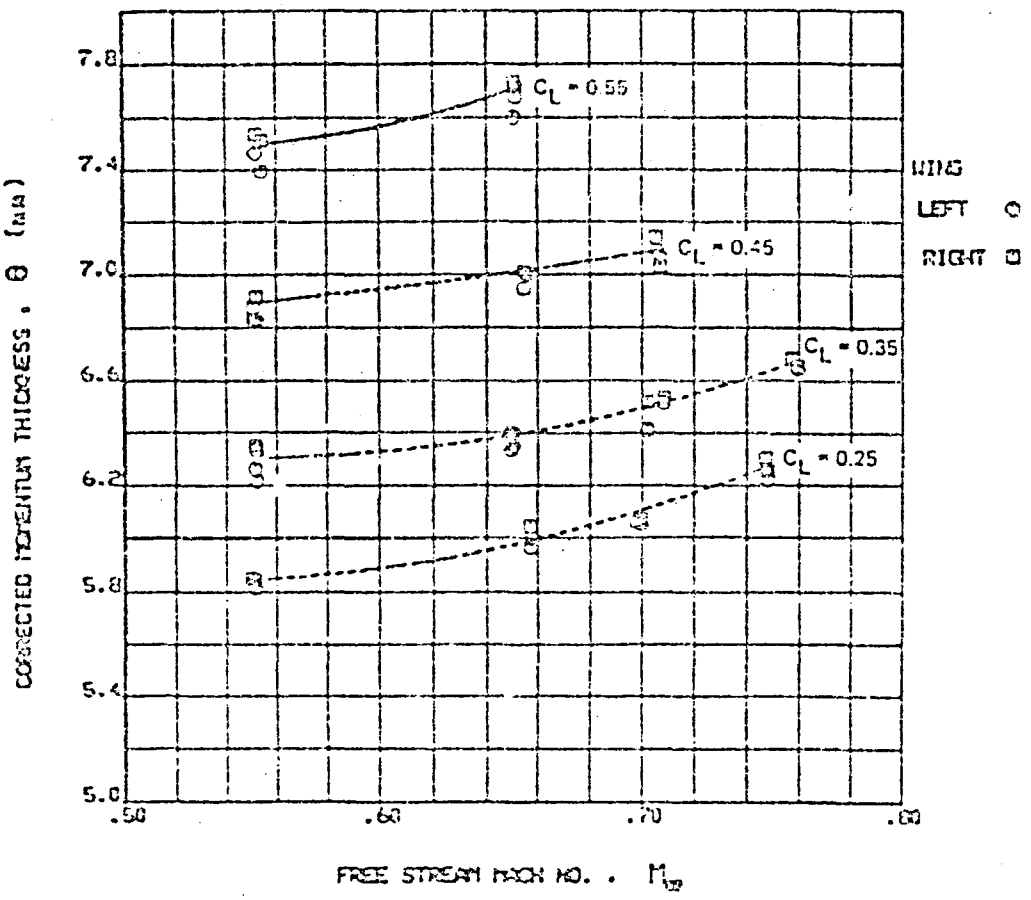

Figure 22. Corrected Momentum Thickness—Bare Surfaces

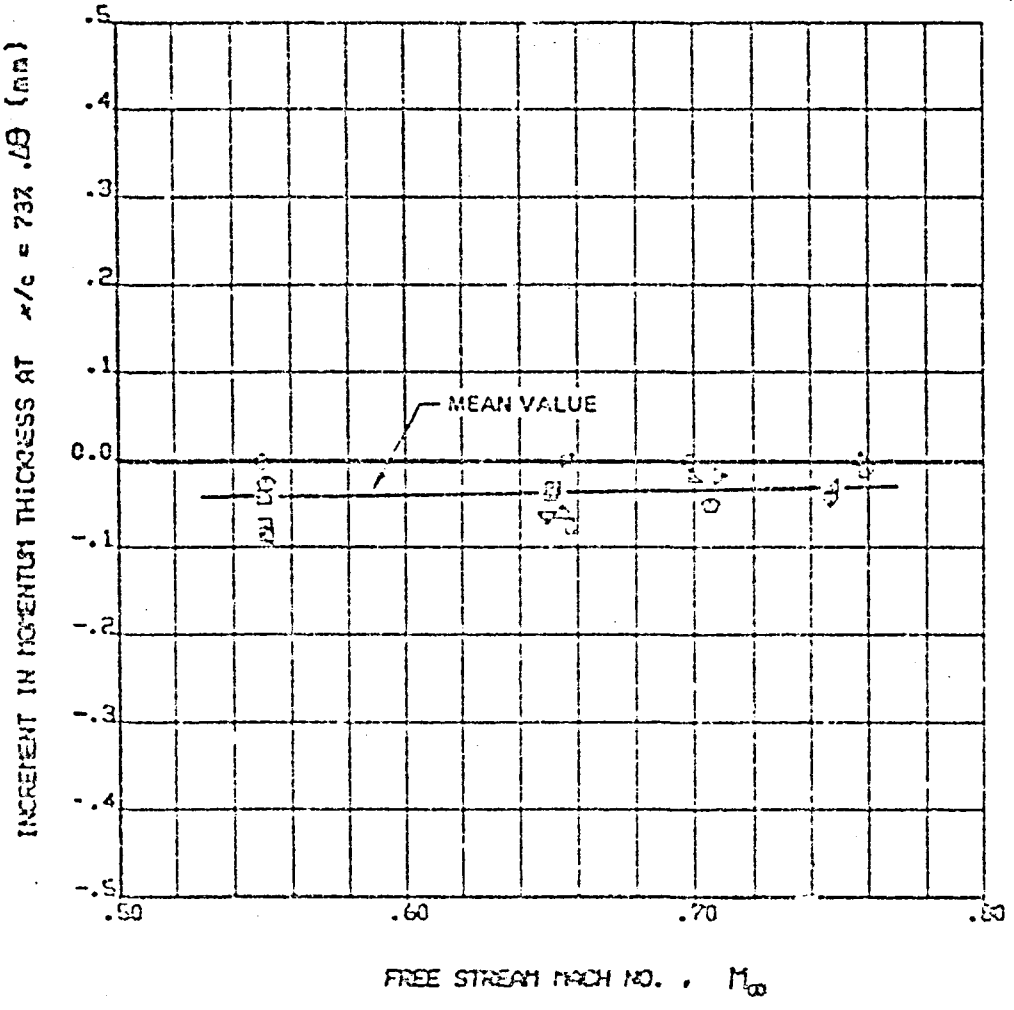

Figure 23. Momentum Thickness Comparison—Left and Right Wings (Bare Surface)

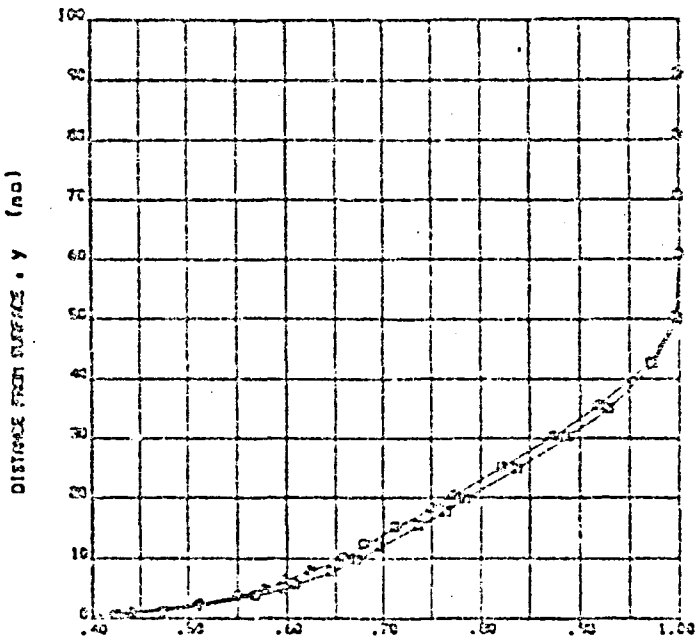

(a) Velocity Profiles

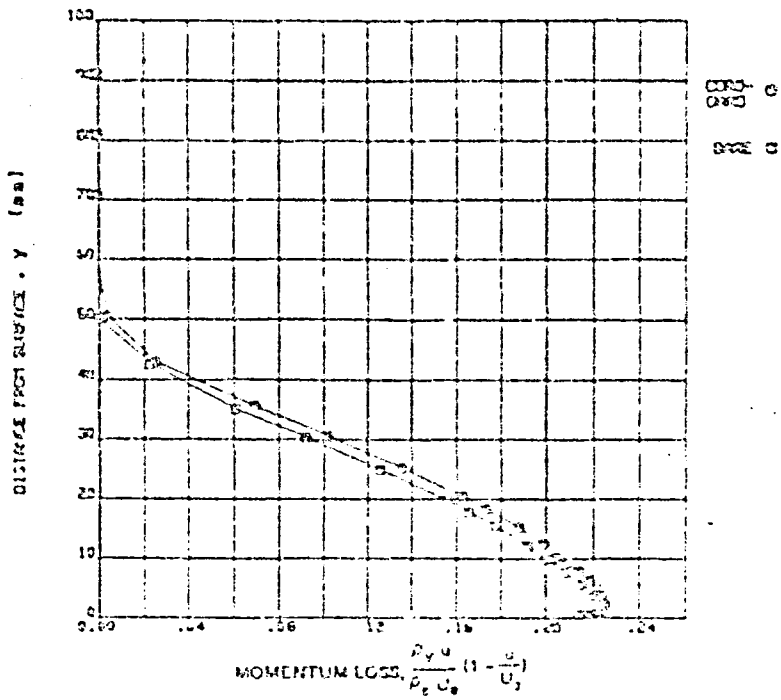

(b) Momentum Loss Profiles

Figure 24. Comparison of Boundary Layer Profiles—Corrugated and Bare Surface (Flight 4); M = 0.716, C_L = 0.251

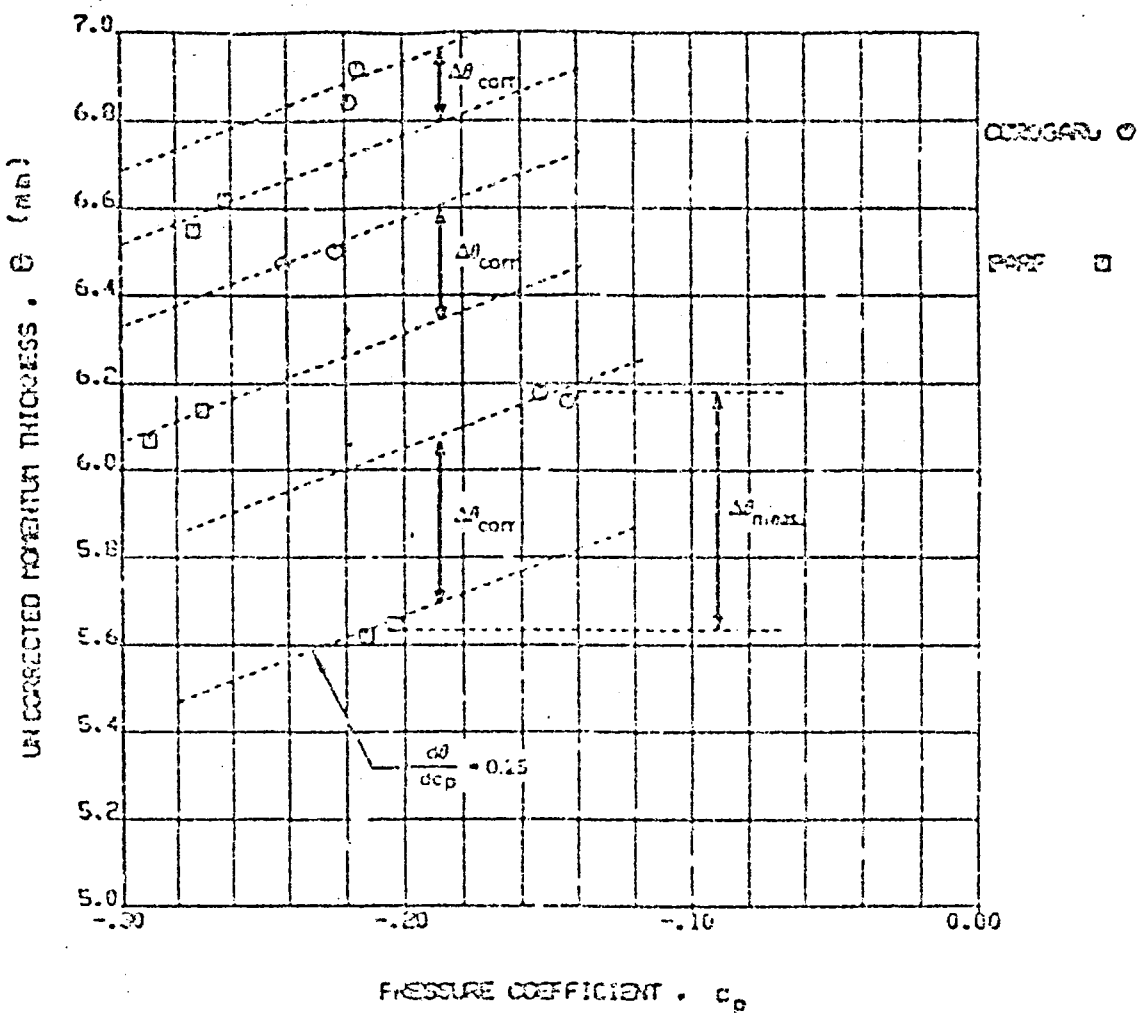

Figure 25. Momentum Thickness Corrections for Variations in Local Static Pressures (Corrugated and Bore Surface)

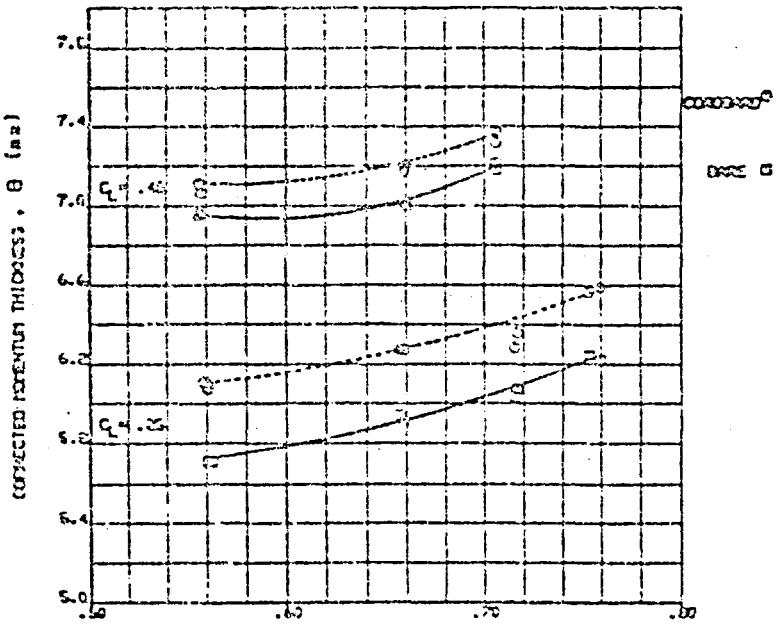

(a) At C_L = 0.25 and 0.45

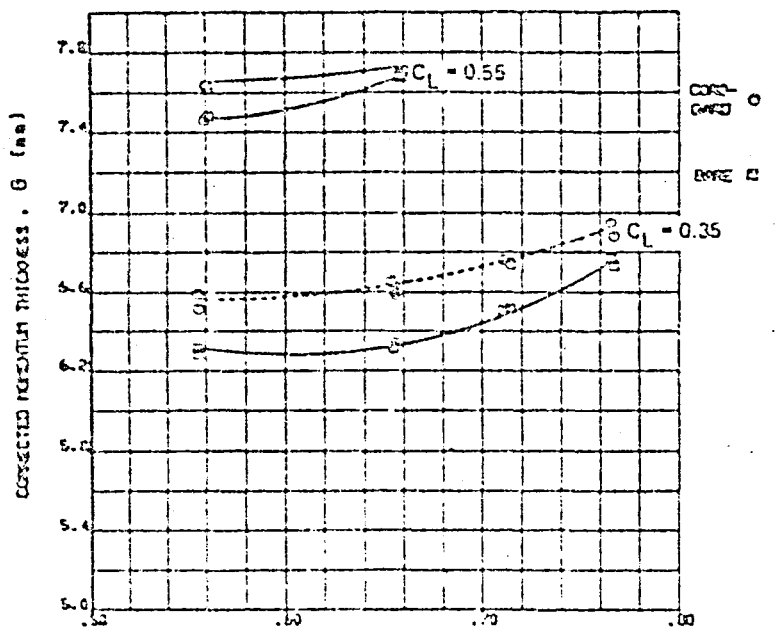

(b) At C_L = 0.35 and 0.55

Figure 26. Corrected Momentum Thickness—Corogard Versus Bare Surface (Flight 4)

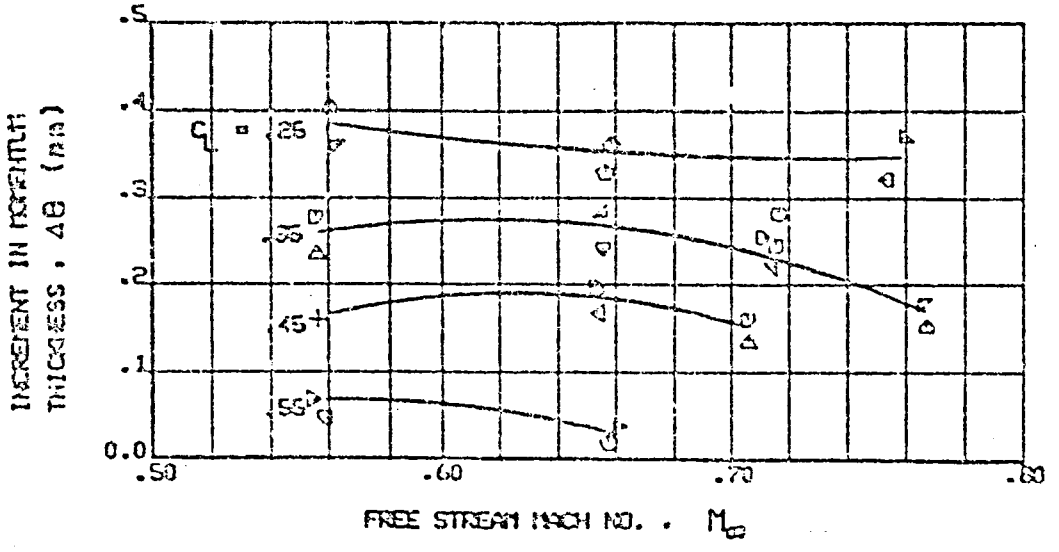

(a) Momentum Thickness Increment at x/c = 75%

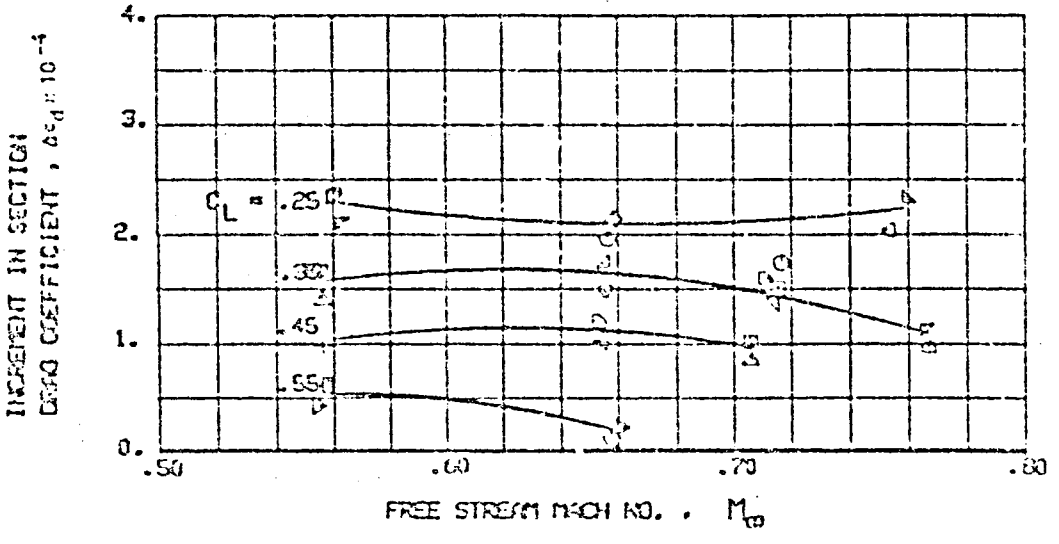

(b) Section Profile Drag Increment

Figure 27. Incremental Effect of Corrugard Paint Relative to Bare Surface (Flight 4)

5.2.3 CAAPCO-to-Bare Surface Comparison

A typical set of measured boundary layer profiles is shown in figure 28, where the CAAPCO-coated surface is compared with the bare reference surface. The measurements show very small difference in the velocity profiles (fig. 28a) or in the momentum loss profiles (fig. 28b) between the two sides. Consequently, the momentum thickness values evaluated from the boundary layer profiles are nearly the same. The differences in the c_p values, however, are also present in this set of data, as illustrated in figure 29; and when the measured momentum thickness is adjusted for this effect, the CAAPCO coating exhibits slightly lower momentum thickness than the bare surface. The adjusted momentum thickness data for the CAAPCO-to-bare comparison are shown in figure 30. A small decrement in momentum thickness for the CAAPCO-coated surface is present throughout the entire range of test conditions. The decrements in θ, as extracted from the data by a test-point-to-test-point comparison, and the corresponding decrements in section drag coefficient are shown in figure 31. Accordingly, the drag reduction due to the CAAPCO coating ranges from $\Delta c_d = 0.00005$ to 0.00012 (0.5 to 1.2 drag counts). This is discussed in terms of percent section profile drag and percent airplane drag in Section 5.3.

5.2.4 Bare Surface With Rough Leading Edge

A typical set of boundary layer profiles showing the effect of rough leading edge is presented in figure 32. The lower portions of the boundary layer velocity profiles are essentially identical, but throughout the outer region there is a small but definite difference where the rough leading edge shows a larger velocity defect. Considering that the two surfaces are not different at the measurement station (both sides being in bare condition), this difference in the outer region of the boundary layer is logical because the inner region, where local flow conditions have a dominant effect, is unchanged. The effect of leading-edge roughness mainly shows in the outer region of the profile, which is largely determined by the upstream flow conditions.

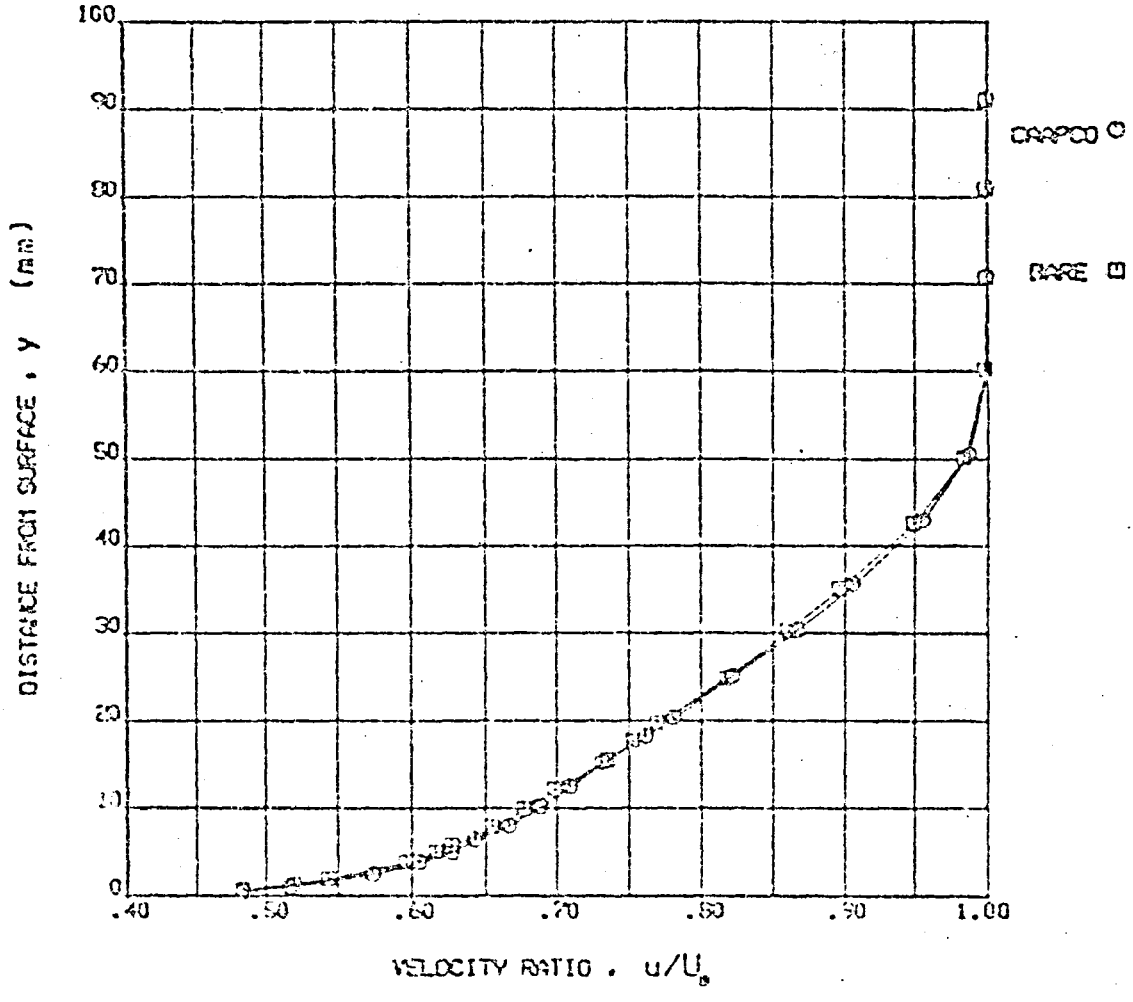

(a) Velocity Profiles

Figure 28. Comparison of Boundary Layer Profiles–CAAFCO Versus Bare Surface (Flight 5); M = 0.661, C_L = 0.445

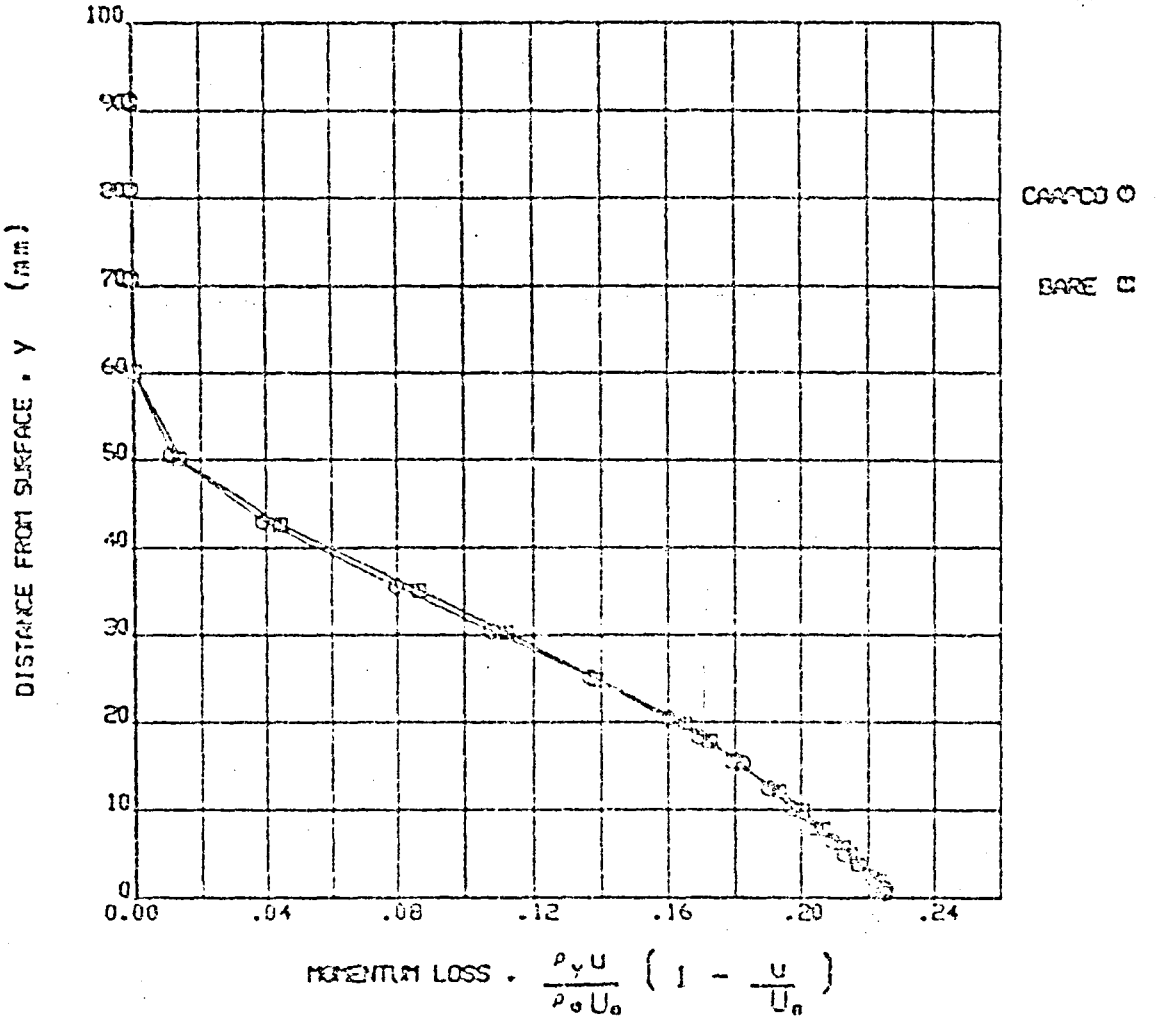

(b) Momentum Loss Profiles

Figure 28. Comparison of Boundary Layer Profiles—CAAPCO Versus Bare Surface (Flight 5); M = 0.661, C_L = 0.445

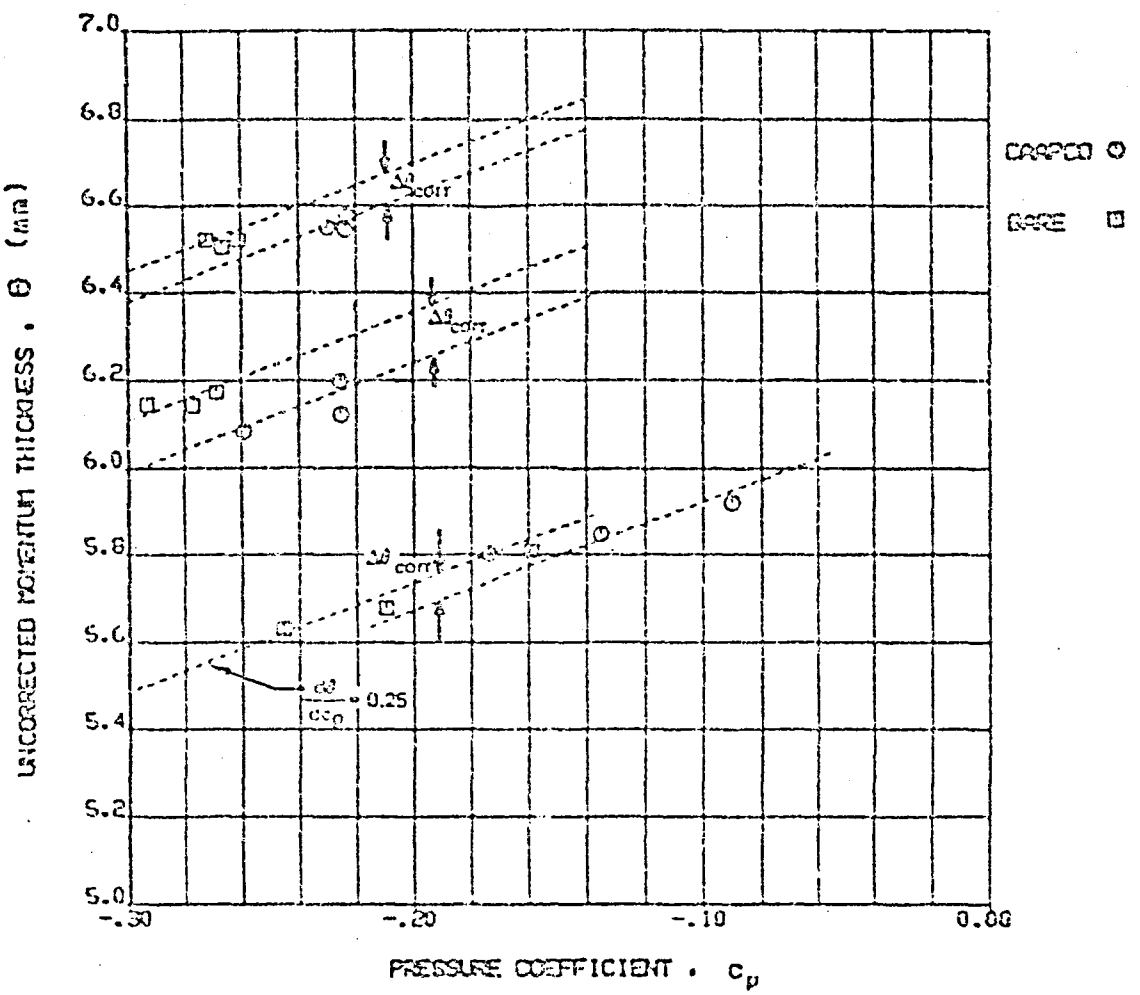

Figure 29. Momentum Thickness Corrections for Variations in Local Static Pressures (CAAPCO and Bare Surface)

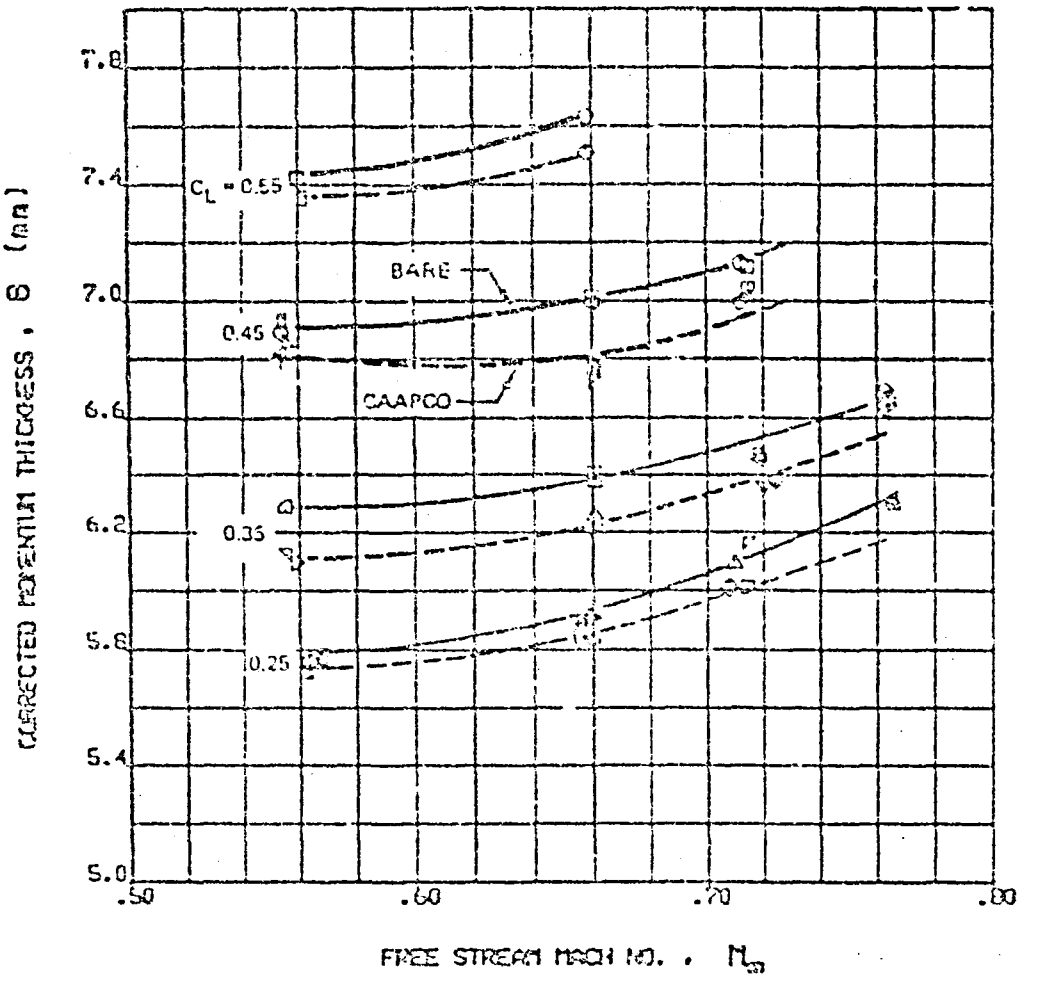

Figure 30. Corrected Momentum Thickness, CAAPCO Versus Bare Surface (Flight 5)

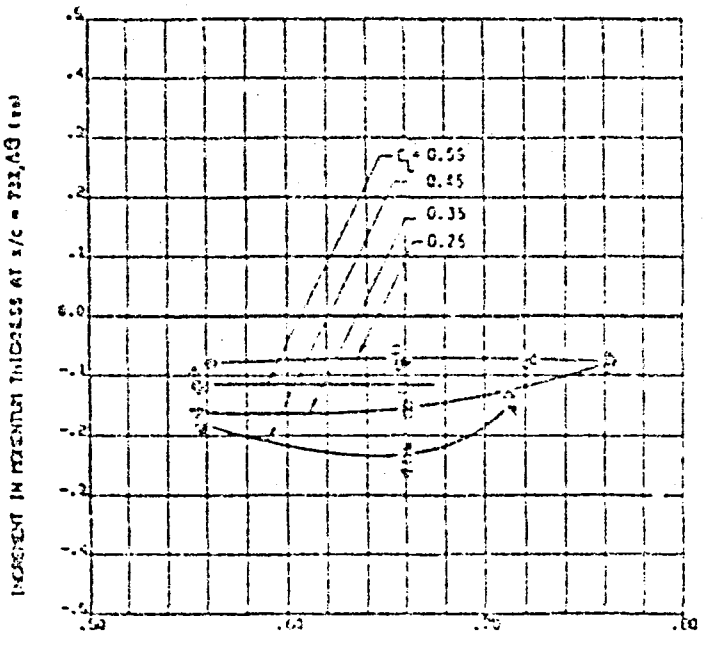

(a) Momentum Thickness Decrement

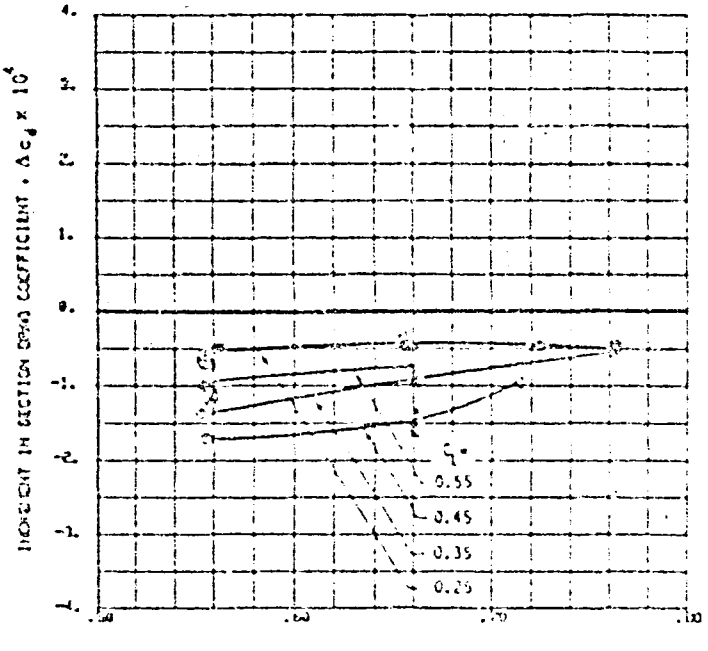

(b) Section Profile Drag Decrement

Figure 31. Effect of CAAPCO Relative to Bare Surface (Flight 5)

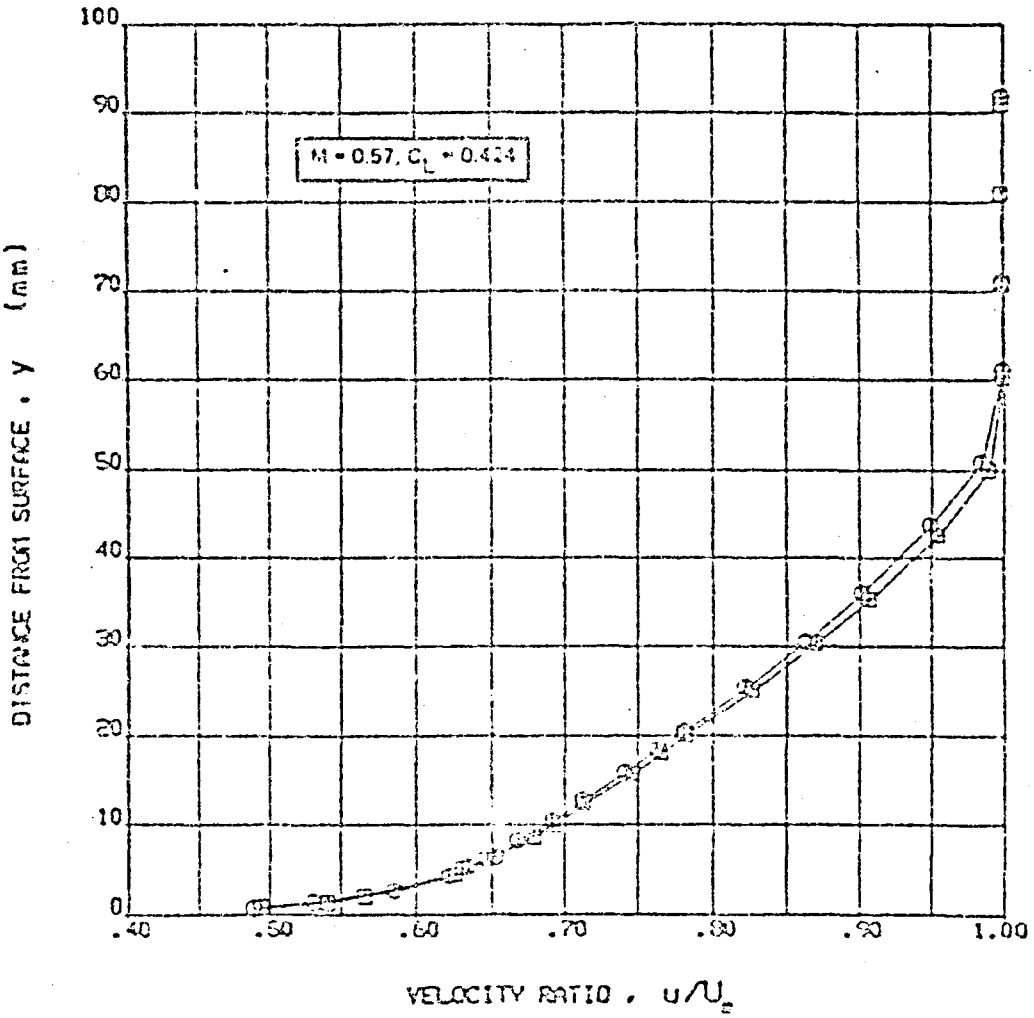

Figure 32. Typical Boundary Layer Profiles—Effect of Rough Leading Edge

Momentum thickness data derived from the measurements were subjected to the same adjustment procedure as described previously. The resulting θ's are shown in figure 33. The rough leading edge was tested only at four of the 15 selected flight conditions during a ferry flight from Langley Field to the Wallops Island test site. These four test conditions were all below altitudes of 6000m ($\approx$ 20 000 ft).

Incremental effects of the rough leading edge relative to the bare surface are shown in figure 34. Three data points acquired at C_L = 0.25 indicate a momentum thickness increment of about $\Delta\theta$ = 0.08 mm ($\approx$ 0.003 in) and a corresponding section profile drag increment of Δc_d = 0.00005 (0.5 drag count). The fourth data point, taken at C_L = 0.45, indicates a $\Delta\theta$ = 0.18 mm (0.007 in) and a Δc_d = 0.00011 (1.1 drag count). The larger effect of leading-edge roughness at the higher lift coefficient is expected.

5.2.5 Existing Paint-to-Bare Surface Comparison

Testing of the existing painted surface took place during the first flight, which also served as a shake-down experiment for checking out the instrumentation and data recording systems. The functioning of the data acquisition system was demonstrated, but there were some problems with the data recording. The reference pressure readings (e.g., from the Digiquartz transducers) were not recorded during the first half of the test due to a faulty power supply; and at some conditions the rake pressures exceeded the preset scales of the recorders. For these reasons not all of the 15 test conditions flown yielded valid data, so the evaluation of this surface is not as accurate as those of the subsequent flights.

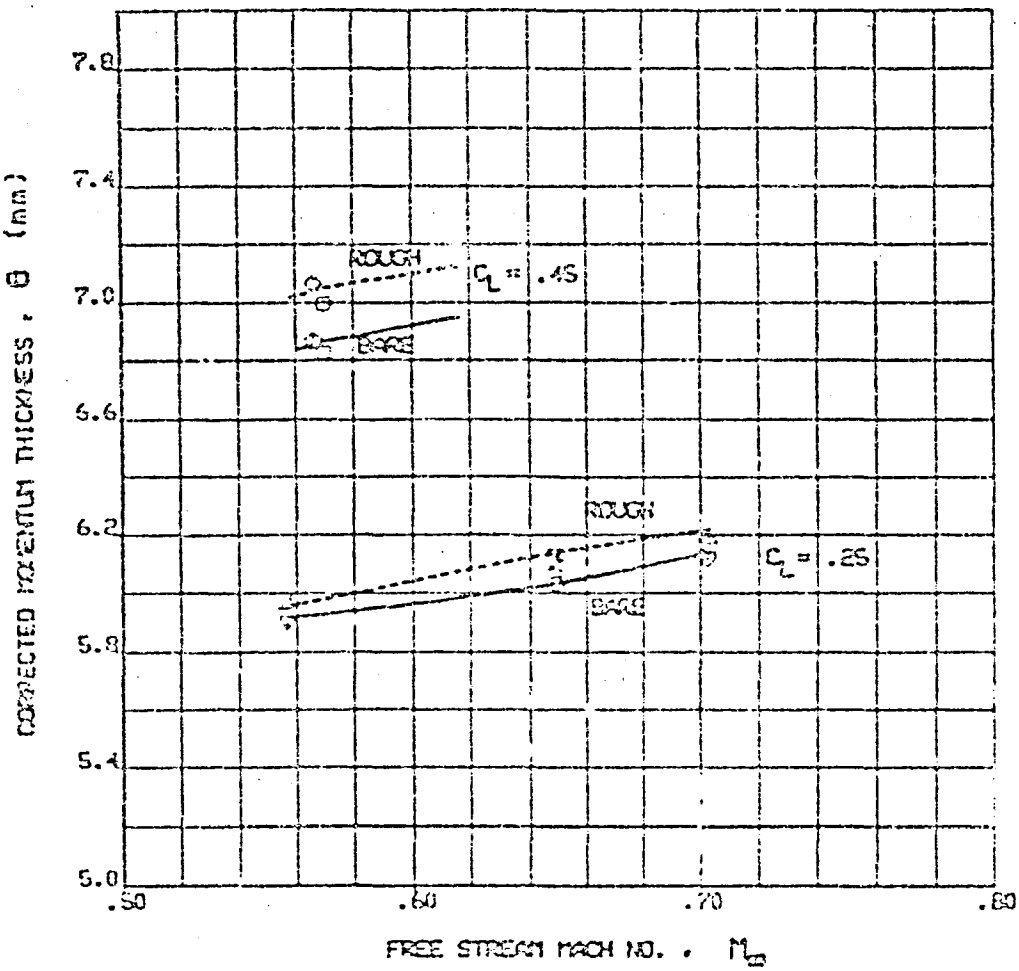

Figure 33. Corrected Momentum Thickness—Rough Leading Edge Versus Bare Surface (Flight 3a)

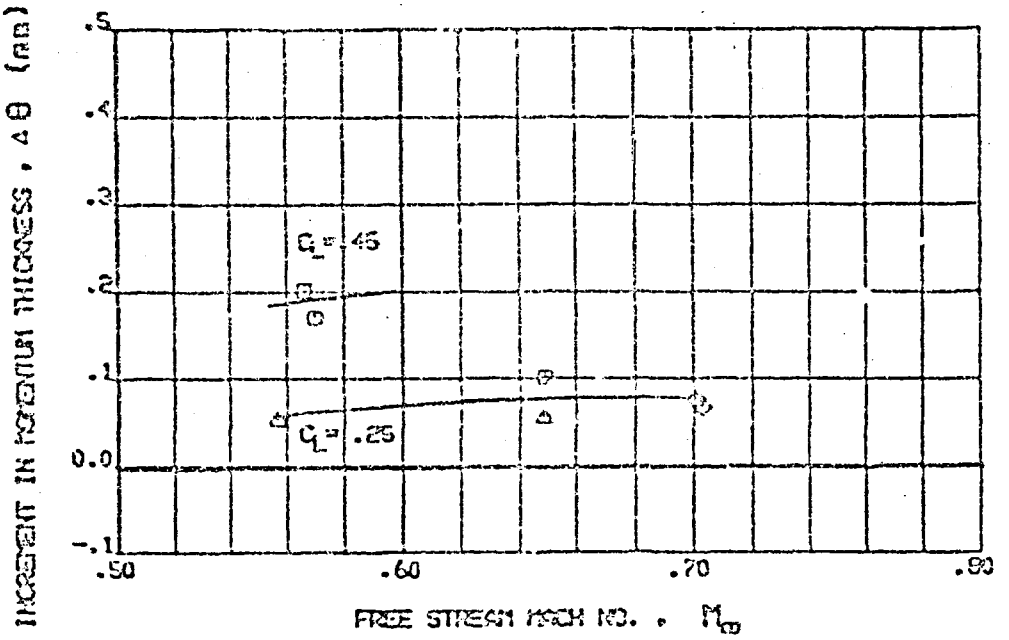

(a) Increment in Momentum Thickness

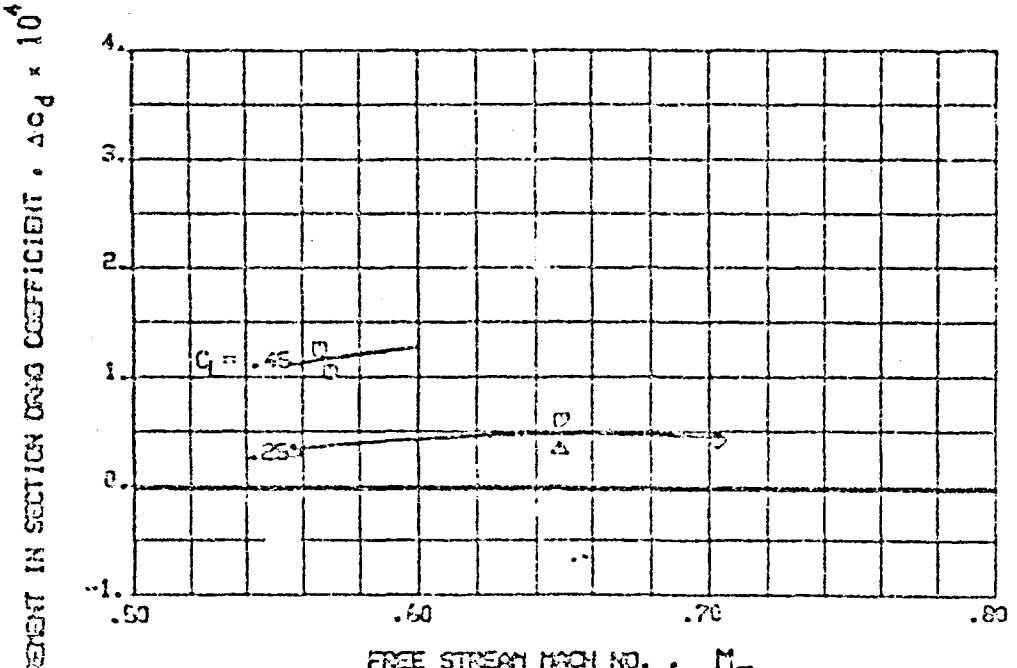

(b) Increment in Section Drag Coefficient

Figure 34. Effect of Rough Leading Edge (Flight 3a)

A typical set of boundary layer profiles, showing the effect of the existing paint in comparison with the bare reference surface, is presented in figure 35. A small increase in velocity defect due to the painted surface is clearly noticeable. The momentum thickness data derived from the measurements indicated that the increments between the two test surfaces were not always consistent, as shown in figure 36 for a typical set of test conditions (C_L = 0.35). The painted surface appeared to have slightly higher drag than the bare surface; the increments, however, are about the same magnitude as the experimental data scatter.

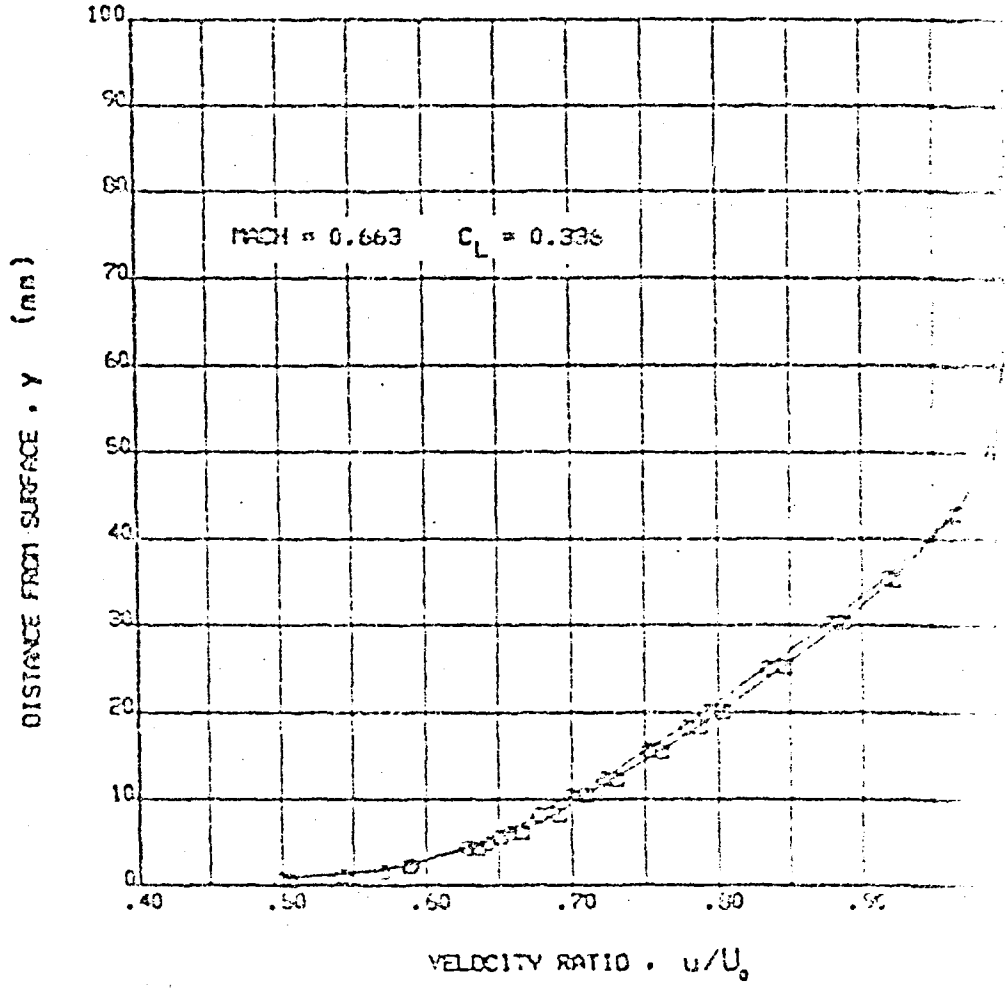

Figure 35. Velocity Profiles—Original Paint and Bare Surface

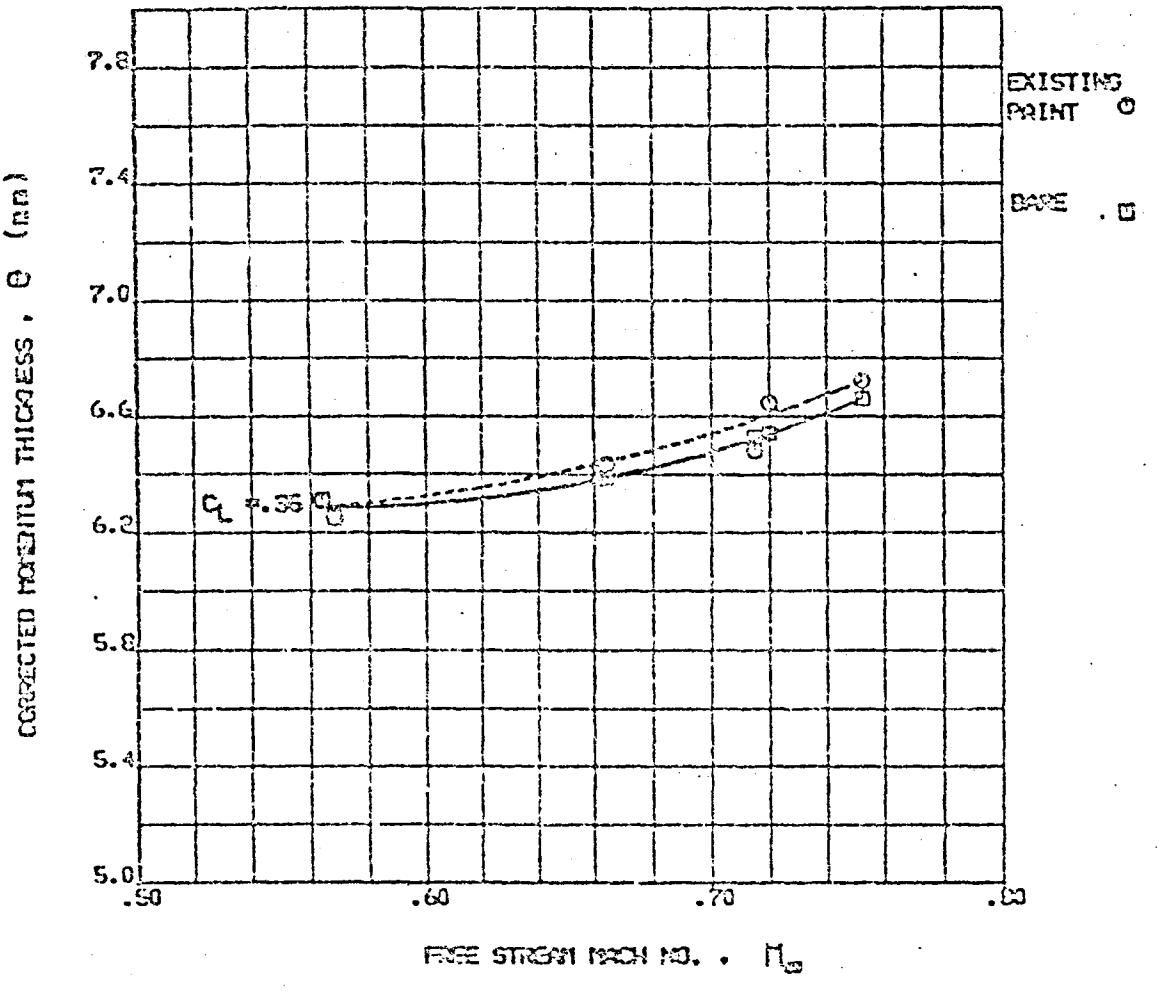

Figure 36. Corrected Momentum Thickness, Existing Point Versus Bare Surface (Flight 1)

5.3 SUMMARY OF DRAG EVALUATION

5.3.1 Section Drag

Final drag evaluation results for each test surface are presented in figure 37 as section profile drag increments plotted as a function of freestream unit Reynolds number. The data have been plotted in this form because classic experiments indicate that unit Reynolds number is the primary factor in distributed roughness effects.

CAAPCO Coating (fig. 37a)--This surface produced a lower drag than the bare reference surface, about 0.75% to 2% of the section profile drag. The 2% decrement is applicable to lower Reynolds numbers or higher lift coefficients. The relationship could be better defined with additional test data. At a typical cruise Reynolds number of 6.5 million/m (2 million/ft), the section drag decrement is 1.4%.

Corogard Surface (fig. 37a)--This surface showed a clear trend of increasing drag with increasing unit Reynolds number when the latter exceeded a certain limit below which the surface was indicated to be hydraulically smooth. As shown, this critical Reynolds number is about 4.9 million/m (1.5 million/ft) for the particular surface tested. At the highest Reynolds numbers of this test, the increment is seen to be about 3.5%. At a typical cruise Reynolds number of 6.5 million/m (2.0 x 10 million/ft), the increment is 1.2%.

Bare-to-Bare Surface (fig. 37b)--These comparisons indicate a small difference in section profile drag between the left and right wing test sections, which amounts to an average of about 0.35%. No definite trends are discernible with Reynolds number, Mach number, or lift coefficient. This drag difference found on the baseline configuration was accounted for when assessing effects of the other surface coatings tested.

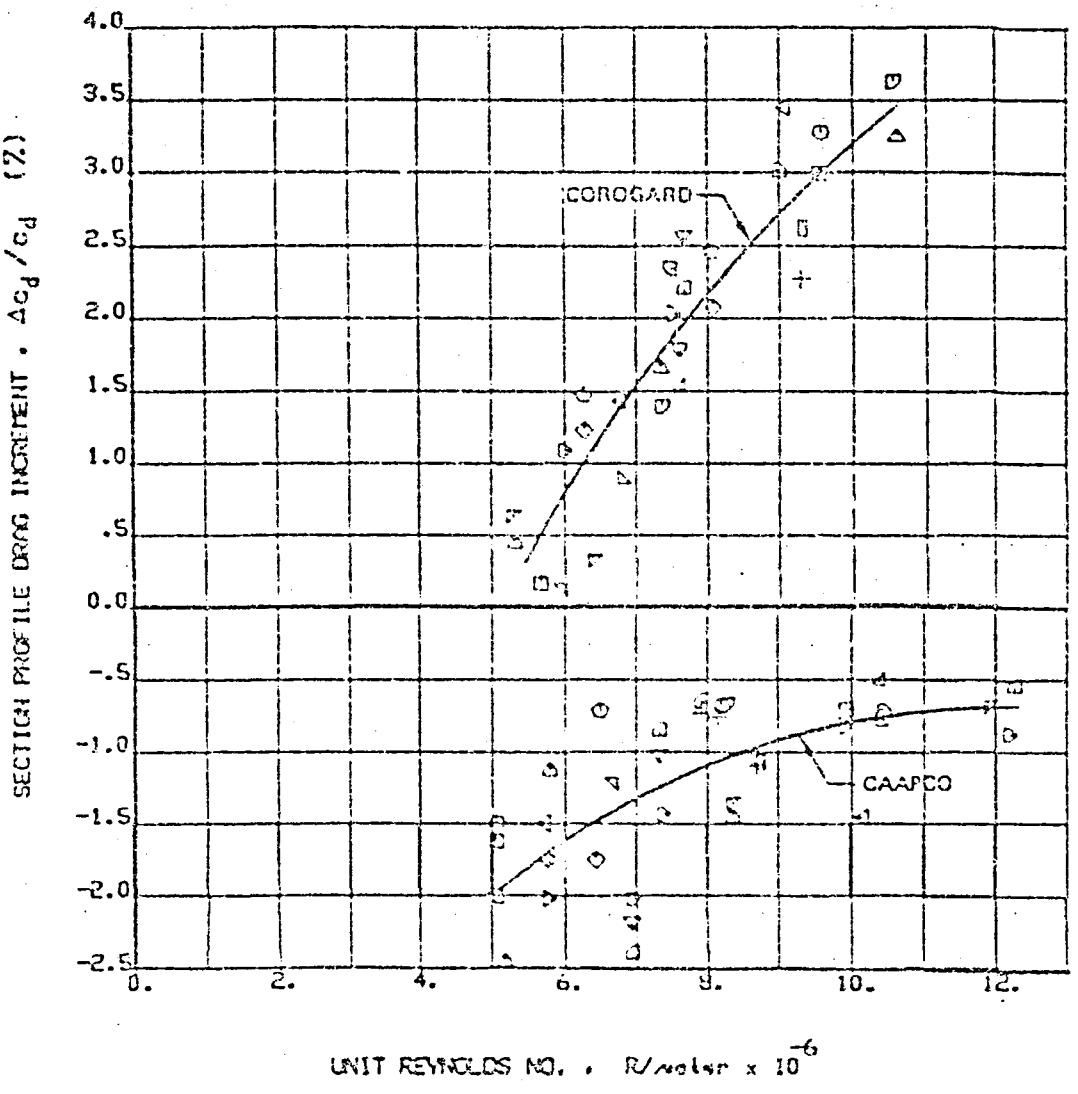

(a) CAAPCO and Corogard Relative to Bare Surface

Figure 37. Effect of Surface Coatings on Test Section Profile Drag

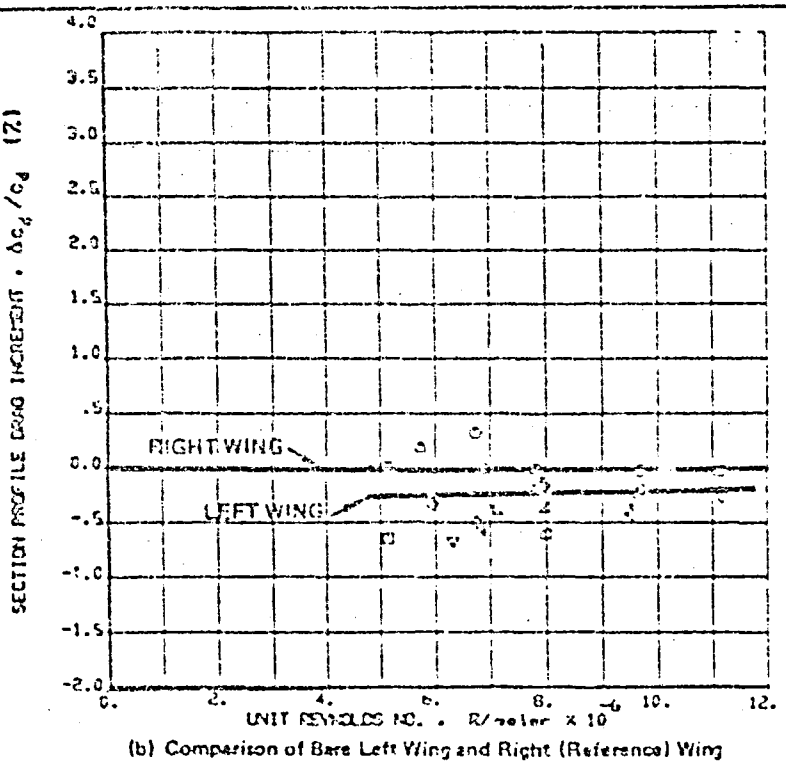

(b) Comparison of Bare Left Wing and Right (Reference) Wing

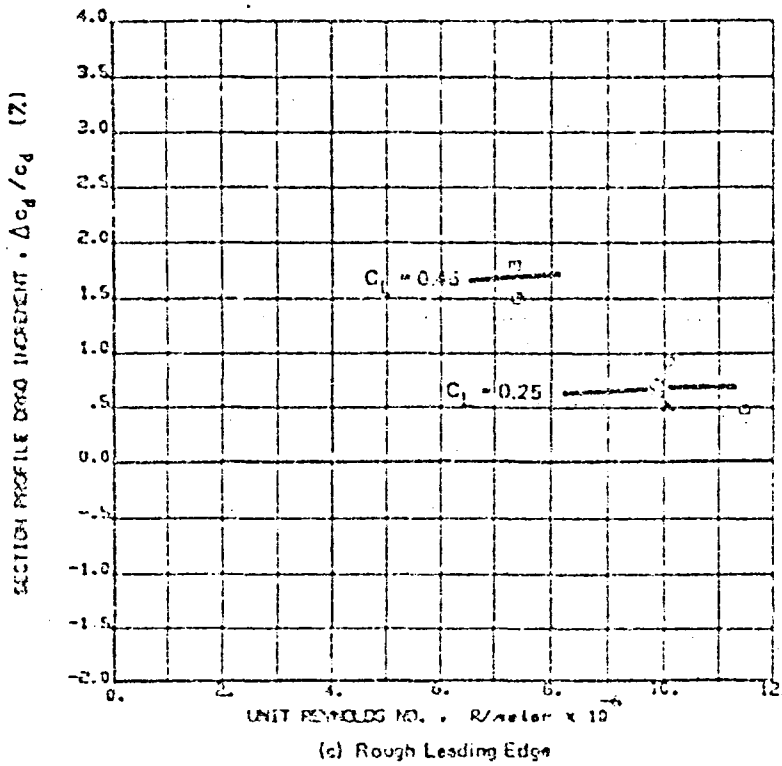

(c) Rough Leading Edge

000015 47b

Figure 37. Effect of Surface Coatings on Test Section Profile Drag (Concluded)

Rough Leading Edge (fig. 37c)--This test showed a drag increment amounting to about 0.65% of the section profile drag at three test conditions flown at C_L = 0.25, and about 1.6% at one condition flown at C_L = 0.45. The trend is plausible; however, additional data are required to firmly establish the effects of lift coefficient on drag increment.

The existing painted surface showed a slightly higher drag level than the bare surface. The increments, however, are of the same magnitude as the experimental scatter band, and so these results are not conclusive.

5.3.2 Conversion to Airplane Drag

To accurately determine the effect on total airplane drag, additional measurements would have to be made at enough spanwise stations to permit integration over the entire wingspan. If, however, it is assumed that the same section drag coefficient increments occur at all spanwise stations, the total airplane drag increments can be estimated as described in figure 11c. Results of such calculations are presented in figure 38. For the Corogard data only, an adjustment was made for differences in the amount of Corogard at various stations on production 737 airplanes. For the test airplane, 57.5% chord was covered with Corogard at the test station, while 42% is an appropriate average for production airplanes, giving ξ= 0.73 (see fig. 11c). This adjustment is considered appropriate because the Corogard data exhibit typical distributed roughness characteristics. For CAAPCO and the roughened leading edge, however, the data behave as if discrete roughness elements are involved. Hence the effects may not vary in a simple manner with coated areas, and the drag coefficient increments were assumed to be independent of spanwise location (i.e., ξ= 1.0).

At a typical cruise condition, C_L = 0.45 and R_1 = 6.5 million/m (2.0 million/ft); the total airplane drag increments are shown in figure 38 to be:

CAAPCO	0.2% decrease
Corogard	0.2% increase
Rough L. E.	0.3% increase

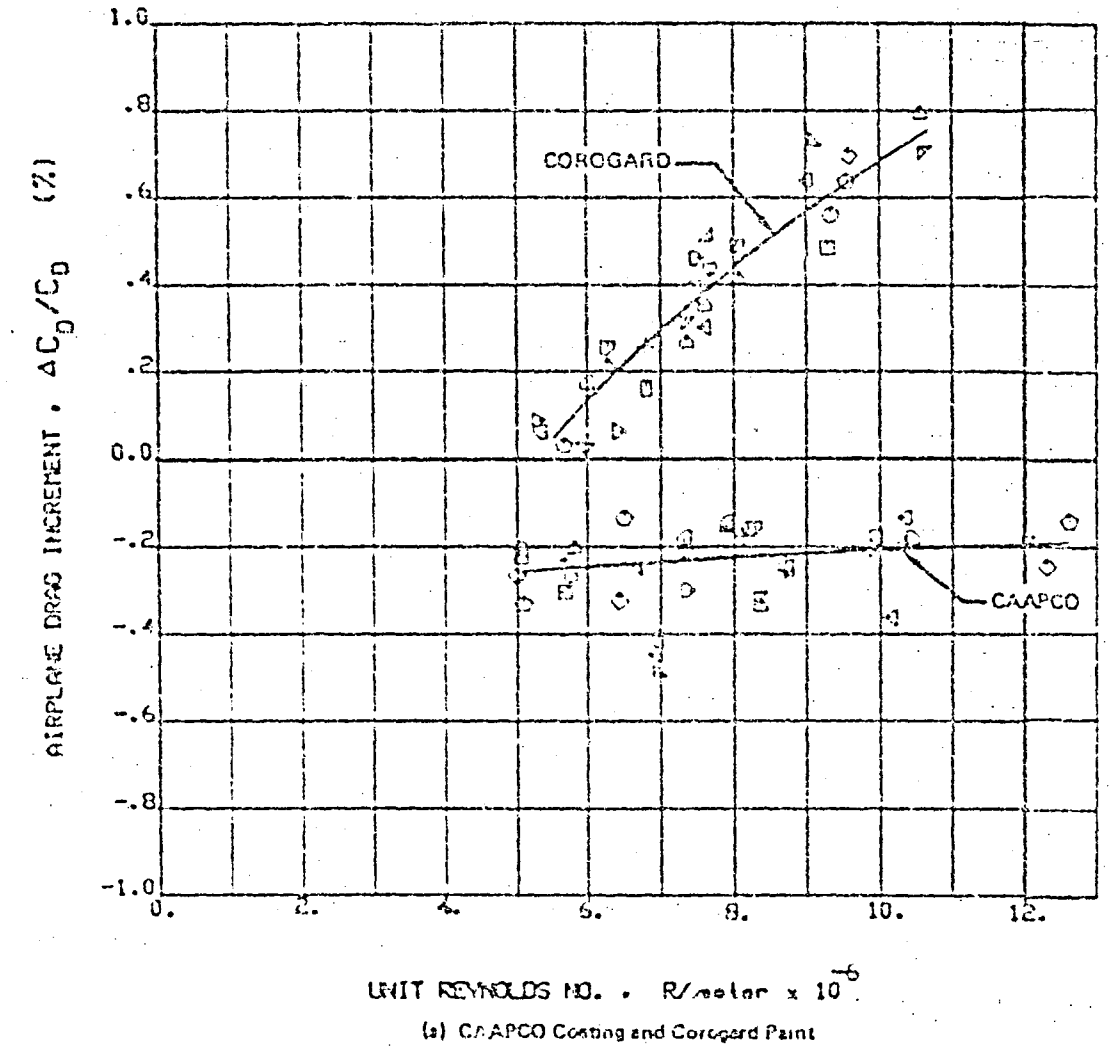

(a) CAAPCO Coating and Corogard Paint

Figure 38. Effect of Surface Coatings on Total Airplane Drag

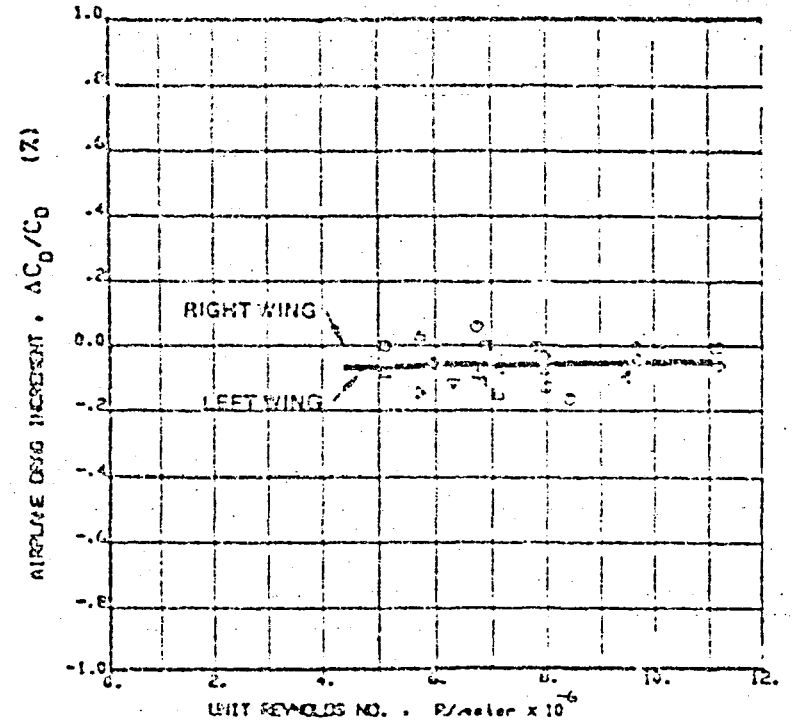

(b) Comparison of Bare Left Wing and Right (Reference) Wing

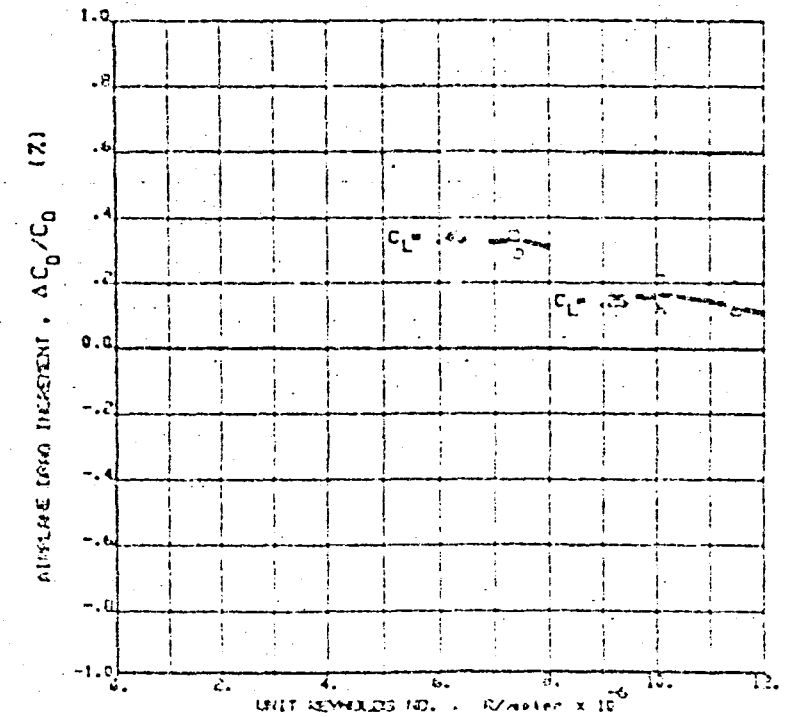

(c) Rough Leading Edge

Figure 38. Effect of Surface Coatings on Total Airplane Drag (Concluded)

6.0 CONCLUSIONS

The test has provided a set of highly accurate basic data showing the effects of various surface finishes such as bare metal, Corogard, CAAPCO, polyurethane enamel, and leading-edge roughness on boundary layer properties. Corogard was applied at the test site and was slightly rougher than is typical of factory applications. A severely eroded leading edge was simulated with No. 50 grit.

Evaluation of the effects of various surface configurations was based on measured differences in boundary layer momentum thickness, $\Delta\theta$, between the left and right wing test sections (side-to-side comparison). The right side, being retained in the bare metal condition throughout the test, served as a baseline.

Flight-to-flight comparisons between the respective test surfaces were also made to cross check results obtained from the side-to-side comparisons. The two sets of data were in qualitative agreement; however, the flight-to-flight comparisons require more corrections for variations in flight conditions (particularly Reynolds number) and thus are considered not as definitive as the side-to-side comparisons.

Small differences between the left and right test sections were observed when both sides were in the bare metal configuration. These differences appeared in both the boundary layer and the surface static pressure measurements. The difference was less than 1% in momentum thickness and was accounted for in the data analysis. The cause is not known, but there are several possible explanations such as slight differences in the rigging of the trailing-edge flaps or asymmetric movement of spoilers under airloads.

The principal conclusions are as follows:

1. The test surfaces showed the following differences in measured momentum thickness relative to the bare metal reference surface:

   - CAAPCO ~ 1.5% to 3% decrease in θ_m
   - Corogard (r_a = 160 μin) ~ 0% to 7.5% increase in θ_m
   - Roughened leading edge ~ 1.5% to 3% increase in θ_m

   The existing paint also showed increases in momentum thickness. The increments, however, were of the same magnitude as the experimental data scatter.

2. The measured momentum thickness increments ($\Delta\theta$) were converted into section drag increments (Δc_d), using the method given by Nash and Bradshaw (ref. 5). The section profile drag for the baseline configuration was calculated, using the measured chordwise pressure distributions and available empirical data. Thus, effects of the various surface configurations could be expressed in terms of section profile drag:

   - CAAPCO ~ 0.75% to 1.5% decrease in c_d
   - Corogard ~ 0% to 3.75% increase in c_d
   - Roughened leading edge ~ 0.75% to 1.5% increase in c_d

3. The test results for Corogard show a strong variation of the drag increment with unit Reynolds number, which is consistent with the trends in classical sand-grain roughness drag data. The other data show no large Reynolds number effects, consistent with classical data for discrete excrescences. Roughened leading-edge data show a variation with lift coefficient that is plausible, but the data are too limited for firm conclusions.

4. To determine airplane drag increments accurately, similar measurements and analyses would have to be carried out at several locations along the wingspan. If it is assumed that similar conditions prevail at all spanwise locations, the preceding section profile drag increments would be roughly equivalent to the following airplane drag increments:

o	CAAPCO	0.2% decrease in C_D
o	Corogard	0.2% increase in C_D
o	roughened leading edge	0.3% increase in C_D

These increments apply for the test airplane at typical cruise conditions (unit Reynolds number approximately 6.5 million/m). The Corogard drag increments observed at higher Reynolds numbers are equivalent to as much as 0.75% airplane drag. An assessment of the effects of these drag increments on the fuel consumption of an airplane in airline operation would require a complete mission analysis to be performed, which is outside the scope of this document.

5. As indicated by this test, CAAPCO has a small drag benefit. The benefit is thought to result from smoothing fasteners and joints in the bare metal; therefore, this benefit may vary considerably at other span stations or for other airplanes. Before CAAPCO could be used in the inspar region, corrosion protection equivalent to Corogard would have to be demonstrated.

7.0 REFERENCES

1. William D. Beasley and Robert J. McGhee, "An Exploratory Investigation of the Effects of a Thin Plastic Film Cover on the Profile Drag of an Aircraft Wing Panel." NASA Technical Memorandum 74073, October 1977.

2. Aircraft Surface Coatings Study--Verification of Selected Materials. NASA CR-159288, Boeing Commercial Airplane Company, September 1980.

3. Task Data Package No. 1., Rev. A--Surface Coatings Drag Measurement Test. Boeing Document D6-48670, Boeing Commercial Airplane Company, September 1980.

4. Surface Coatings Drag Measurement Test--Test Plans and Procedures. Boeing Document D6-48675, Boeing Commercial Airplane Company, September 1980.

5. J. F. Nash and P. Bradshaw. "The Magnification of Roughness Drag by Pressure Gradients." Journal of the Royal Aeronautical Society, Vol. 71, January 1967.

APPENDIX

SURFACE ROUGHNESS MEASUREMENT

The method used to measure surface roughness is briefly described, and some roughness readings and traces are shown.

The instrument used to measure roughness was the Surtronic III profilometer, represented in figure A-1. The battery-operated display-traverse unit contains electronic circuitry and a motor that drives the pickup arm. Surface roughness is transmitted from a diamond stylus on the pickup arm through a variable reluctance transducer to the averaging circuitry. The traverse of the stylus is divided into five segments (cutoffs), and the roughness of each cutoff is averaged. The summation average of the five cutoffs is presented in a digital readout as the roughness number for that traverse.

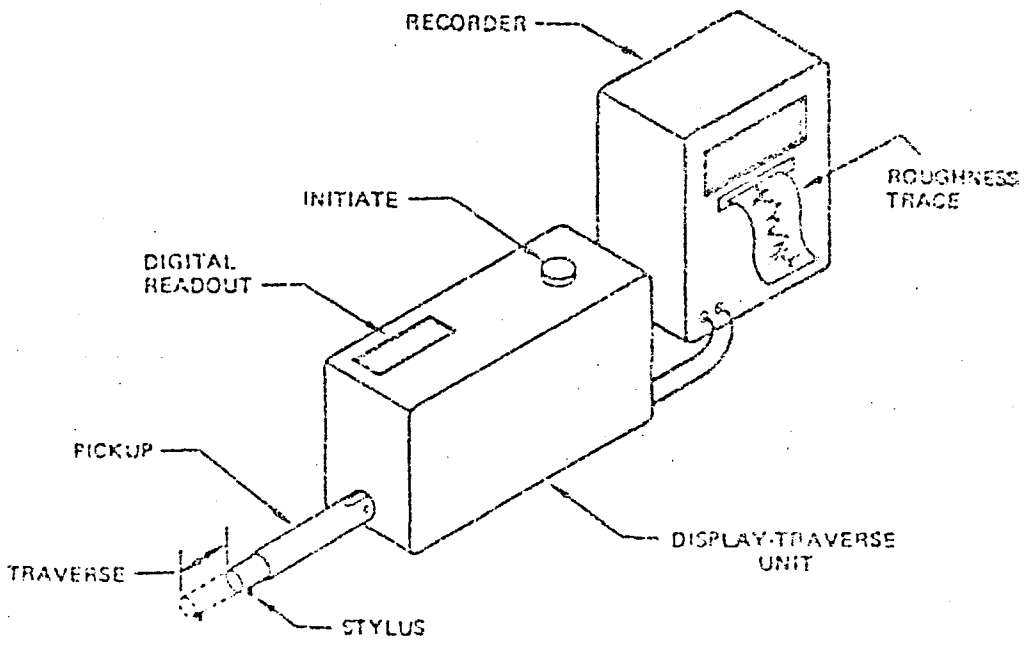

Figure A-1. Surtronic III and Recorder

The customary cutoff of 0.76 mm (0.03 in) was selected for roughness measurements on the NASA TCV airplane test panels. Figures A-2, A-3, and A-4 show measurement locations and roughness values for the bare surface, CAAPCO coating, and Corogard paint, respectively. Measurements were taken at 80 to 90 locations for each surface, with emphasis on the wing stations where boundary layer rakes (R_1, R_2, R_3, R_4) were located.

The 0.76 mm (0.03 in) cutoff was selected to obtain readings that characterized roughness rather than surface waviness. Figure A-5 shows typical characteristics of the various surfaces as traced by the recorder. The profilometer was located where the 0.76 mm (0.03 in) cutoff gave the r_a values noted above each trace. Then the profilometer was set to a long traverse of approximately 12.7 mm (0.5 in), and the traces were made. The traces show surface waviness as well as roughness. Waviness can be caused by "orange peel effect" in the coating, nonuniformities in the paint solvent, or can be transmitted from the substrate surface. It should be noted that the Corogard trace was "borrowed" from another airplane. It shows, however, typical surface characteristics corresponding to a r_a = 107 μin reading on a 0.76 mm (0.03 in) cutoff.

RIGHT-HAND WING

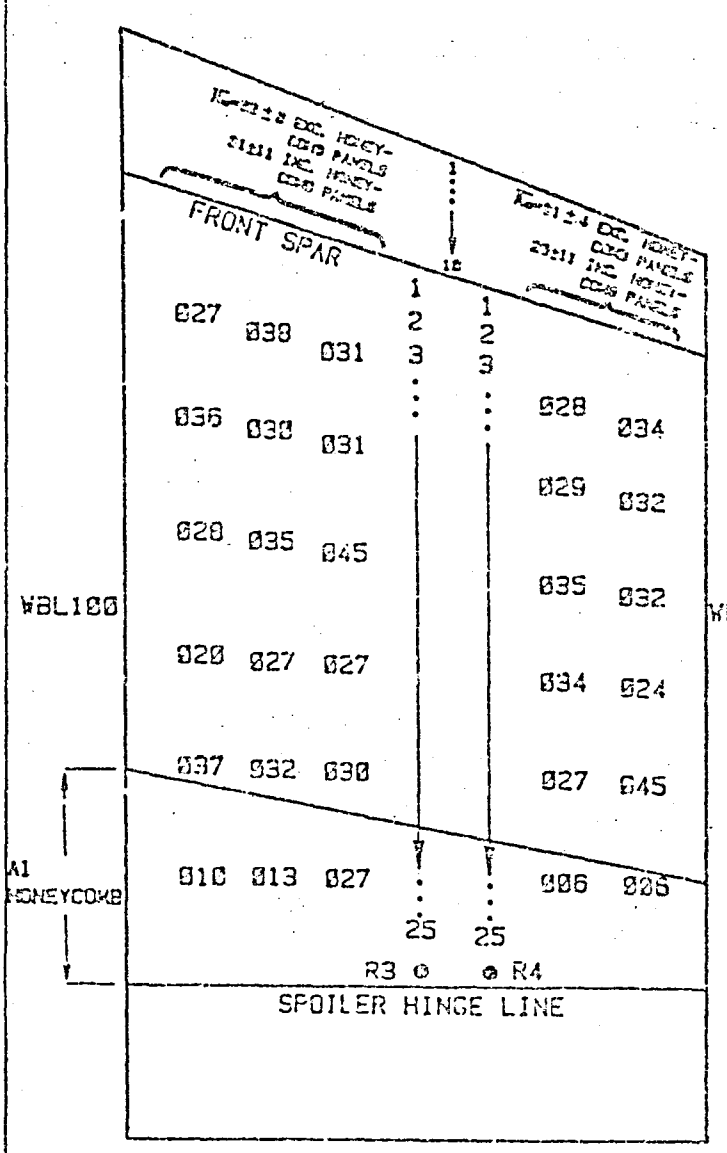

LEADING EDGE	
POS	Ra-µi
1	013
2	033
3	022
4	019
5	014
6	012
7	017
8	039
9	019
10	013
Ra±SD	20±9

	Ra-µi	
POS	R3	R4
1	031	039
2	035	034
3	032	036
4	040	025
5	036	032
6	029	032
7	040	028
8	026	033
9	021	030
10	039	025
11	026	029
12	033	027
13	023	031
14	031	024
15	037	025
16	028	032
17	023	027
18	027	034
19	032	037
20	034	025
21	012	021
22	009	018
23	011	008
24	022	016
25	010	014
$\overline{Ra}$=	27	27
SD	±9	±7
$\overline{Ra}$=	31	30
SD	±6	±4

A1 HONEYCOMB

INC. HONEYCOMB

EXC. HONEYCOMB

CUT-OFF = .03"

C-2 *Figure A-2. Roughness Average Survey, Bare Metal*

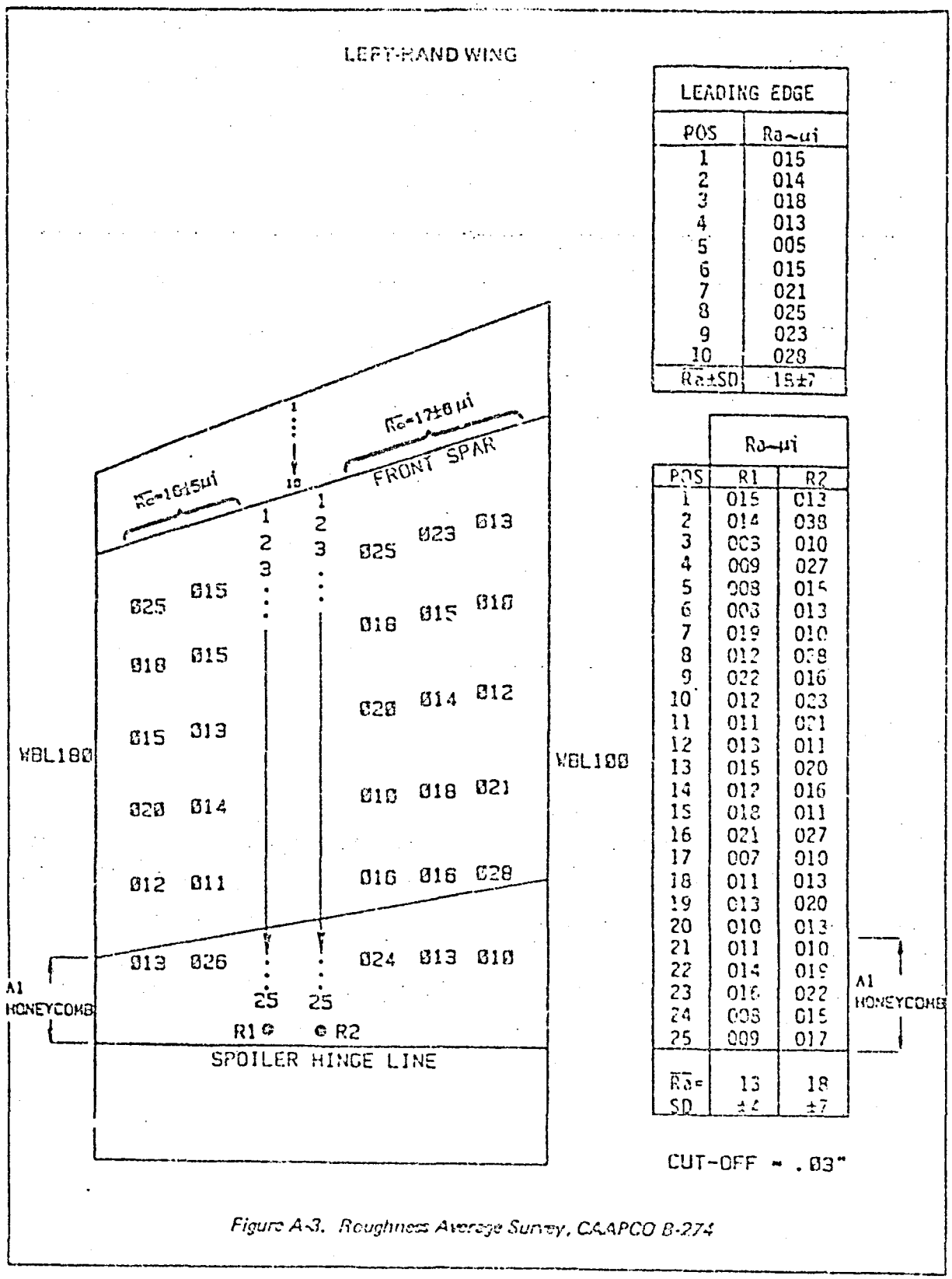

LEADING EDGE	
POS	Ra~µi
1	015
2	014
3	018
4	013
5	005
6	015
7	021
8	025
9	023
10	028
$\overline{Ra}$±SD	15±7

	Ra~µi	
POS	R1	R2
1	015	013
2	014	038
3	003	010
4	009	027
5	008	015
6	003	013
7	019	010
8	012	038
9	022	016
10	012	023
11	011	021
12	013	011
13	015	020
14	012	016
15	018	011
16	021	027
17	007	010
18	011	013
19	013	020
20	010	013
21	011	010
22	014	019
23	016	022
24	008	015
25	009	017
$\overline{Ra}$=	13	18
SD	±4	±7

CUT-OFF = .03"

Figure A-3. Roughness Average Survey, CASPCO B-274

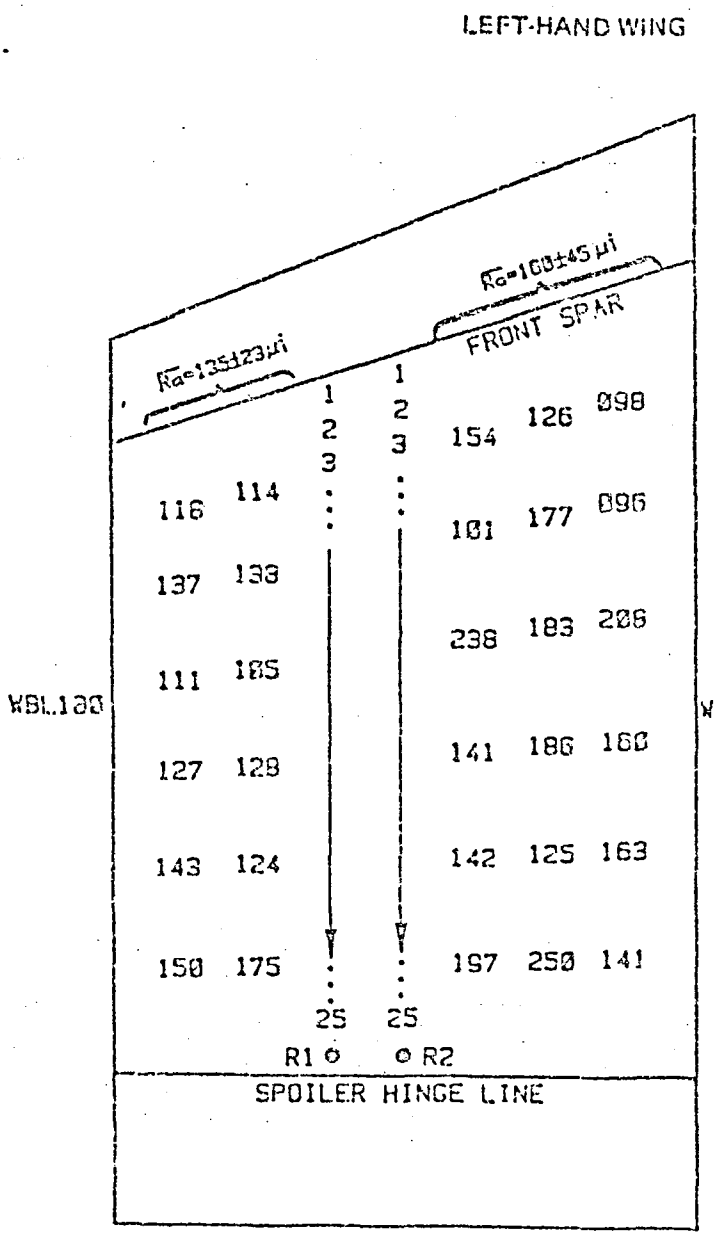

POS	Ra-µi R1	R2
1	158	157
2	158	156
3	192	140
4	154	175
5	129	166
6	114	103
7	151	173
8	180	137
9	195	173
10	139	142
11	200	113
12	193	147
13	158	149
14	122	159
15	217	168
16	111	200
17	147	172
18	170	121
19	159	210
20	135	124
21	181	133
22	151	126
23	198	153
24	176	170
25	125	157
$\overline{Ra}$=	161	153
SD	±29	±25

CUT-OFF = .03"

Figure A-4. Roughness Average Survey, Corogard (After Flight Test)

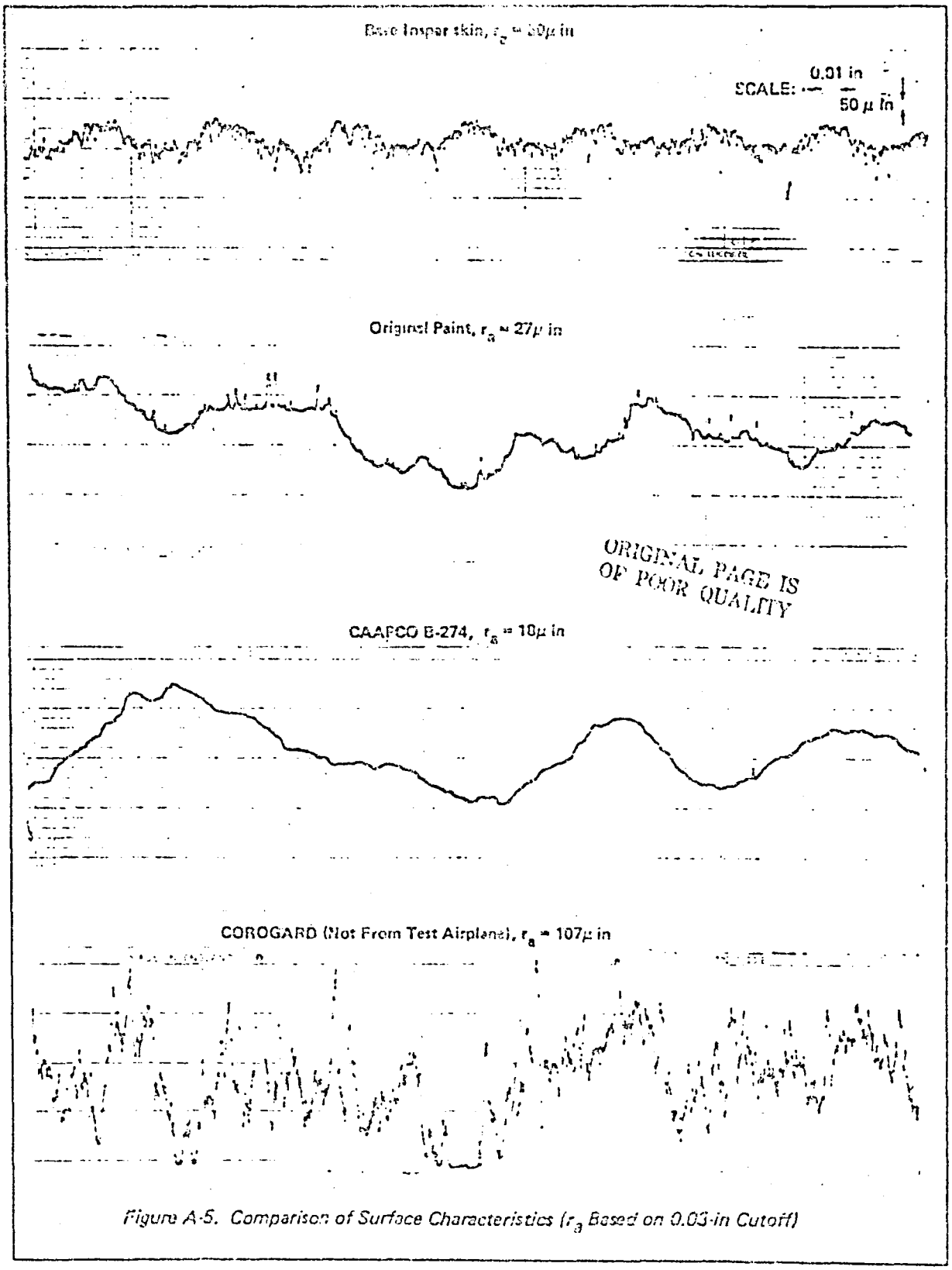

Figure A-5. Comparison of Surface Characteristics (r_a Based on 0.03-in Cutoff)